UNIVERSIDADE DE SÃO PAULO
INSTITUTO DE GEOSCIÊNCIAS

Paleoclimate reconstruction based on high-resolution multiproxy geochemistry of speleothems from Paraná and São Paulo states, Brazil

JULIO CAUHY RODRIGUES

Orientador: Prof. Dr. Francisco William da Cruz Junior

São Paulo

2020

UNIVERSIDADE DE SÃO PAULO
INSTITUTO DE GEOSCIÊNCIAS

Paleoclimate reconstruction based on high-resolution multiproxy geochemistry of speleothems from Paraná and São Paulo states, Brazil

JULIO CAUHY RODRIGUES

Orientador: Prof. Dr. Francisco William da Cruz Junior

Dissertação de Mestrado

Nº 864

COMISSÃO JULGADORA

Dr. Francisco William da Cruz Junior

Dr. Juan Pablo Bernal Uruchurtu

Drª. Marília Harumi Shimizu

São Paulo
2020

AGRADECIMENTOS

A realização deste trabalho foi possível graças ao financiamento da FAPESP através de bolsa de mestrado vinculado ao processo número 2019/02791-1 e ao estágio de pesquisa no exterior (BEPE-FAPESP) processo número 2019/23364-4. Agradeço ao Prof. Dr. Francisco William da Cruz Junior (Chico Bill) por me orientar durante a realização deste trabalho e por incentivar ativamente a colaboração com outros pesquisadores e laboratórios essenciais para o desenvolvimento desta pesquisa. Agradeço também ao Prof. Dr. Nicolás Stríkis que igualmente me orientou e por me auxiliar nas discussões e no tratamento dos dados essenciais para o desenvolvimento deste trabalho.

Sou muito grato à Alyne Barros pela ajuda e trabalho no Laboratório de Isótopos Estáveis (LES-CPGEO) que permitiu a aquisição dos dados isotópicos, à Hellen Cristine pelo apoio com as análises de PIXE no Laboratório de Análises de Materiais por Feixes Iônicos (LAMFI-USP), ao Prof. Dr. Juan Pablo pelo apoio e colaboração com as análises de elementos traços no Laboratório de ELA-ICP-MS do Centro de Geociências da Universidade Nacional Autonoma do México, ao Prof. Dr. Hai Cheng pelo apoio do Instituto de Mudanças Ambientais Globais da Universidade de Xi'na Jiaotong (China) que possibilitou a realização de parte das análises geocronológicas realizadas pelo aluno Vitor Azevedo através de colaboração, ao Prof. Dr. R. Lawrence Edwards pelo apoio do Laboratório de Geocronologia da Universidade de Minnesota (EUA) que possibilitou a realização das análises geocronológicas durante meu estágio de pesquisa.

Este trabalho também me proporcionou a primeira experiencia de vivência fora do Brasil a qual sou muito grato pelo Prof. Chico Bill e Prof. Larry Edwards que através de colaboração permitiram a realização do estágio de pesquisa no Laboratório de Geocronologia da Universidade de Minnesota (EUA). Agradeço ao Jon e Lydia Orson por me receber tão bem em sua casa e oferecer toda ajuda que necessitei e por me mostrar um pouco de Minneapolis. Agradeço novamente ao Prof. Dr. Larry Edwards por me auxiliar durante o estágio de pesquisa e aos pesquisadores Xianglei Li e Peter Schroedl por ensinarem detalhadamente todas as etapas necessárias para a aquisição de dados e por estarem sempre à disposição para resolver qualquer dúvida ou problema. Agradeço também aos pesquisadores Peter Chutcharavan, Yijia Liang, Dylan Parmenter pela ajuda e pela companhia durante as longas jornadas no laboratório. Por fim, mas não menos importante, agradeço ao meu

amigo Plínio Jaqueto pela ajuda e colaboração durante as longas jornadas de laboratório, pela ajuda com o tratamento dos dados, por apresentar a UMN, pelos tubings e tombos no snow, e por todos Orange Chickens e cervejas artesanais.

Gostaria de agradecer também aos meus colegas de laboratório e de sala no IGC-USP: Plácido Buarque, Lucas Godinho (Rejeitto), Veronica Ramires, Valdir Novello, Melissa Martinez, Giselle Utida, Suellyn Emerik, Vitor Azevedo, Tom Morita, Janine Carmo, Ybiatã, que me ajudaram durante esses dois anos através de discussões, análises ou mesmo pela companhia e risadas. Também agradeço aos meus primos Brenda Rocha, Caue Cioff e João Zambrini pelos conselhos e ajuda na vida acadêmica.

Um agradecimento especial para Suellyn por toda ajuda com a amostragem, companhia e pelo trabalho no acervo de espeleotemas do Laboratório de Sistema Cársticos. Também agradeço especialmente a Dr. Giselle Utida pela imensa ajuda com burocracias, documentações, relatórios, eventos, conselhos e por sempre se fazer disponível para qualquer problema ou dúvida, me ajudando muito (MUITO) durante todo meu mestrado.

Agradeço à diretora do PETAR Juliana Conrado, pela autorização para realizar as atividades de campo na Gruta Lage Branca e ao Jurandir e Ditinho pelo auxílio durante os trabalhos de campo. Agradeço também à Leda Zogbi pela confecção do perfil utilizado para as coletas na Lage Branca e pela amizade e cavernadas. Agradeço também ao Rejeitto pelo auxílio na segurança e instalação das vias de escalada essenciais para a coleta na gruta.

Aos meus amigos Gabriel Rangel, João Garbelim, Anderson Pires, Cauê Moara, Everton Lima, Bruno Cirilo, Gustavo Ribeiro, Bruno Italalong, pela parceria de muitos anos que sempre me ajudou (ou atrapalhou) em minha vida. Aos meus companheiros de tatame de longa data Leandro Goulart, Vinicius Nobre, Daniel do Vale (Banana), Lucas Milani, Adriano Santos, Igor Schneider, Julio Moraes, Raphael Oliveira por sempre estarem presentes e por me ajudarem ao longo desses anos. Agradeço também ao Prof. Enrique Muniz por me receber muito bem em sua academia em Minneapolis e pelos treinos entre as densas jornadas de laboratório.

Agradeço à minha parceira de cavernada, perrengues, laboratório, escritório, tatame e sonhos Marcela Eduarda Della Libera de Godoy pela ajuda em todas as etapas deste trabalho (campo,

análises, discussões, revisão etc.), por sempre me incentivar a ir atrás do que quero, pelas aulas de inglês e pela parceria durante esses anos.

Um agradecimento especial à minha mãe Ana Paula Cauhy e meu pai Cesarvinicius S. Rodrigues por sempre me apoiarem e sempre estarem a disposição para me ajudar em tudo.

AKNOWLEDGES

This work was possible thanks to FAPESP funding through a master's grant linked to process number 2019/02791-1 and to the research internship abroad (BEPE-FAPESP) process number 2019/23364-4. I thank Prof. Dr. Francisco William da Cruz Junior (Chico Bill) for guiding me during this work and for actively encouraging collaboration with other researchers and laboratories essential for the development of this research. I also thank Prof. Dr. Nicolás Stríkis, who also guided me and dedicated his time to help me with the discussions and data treatment essential for the development of this work.

I am very grateful to Alyne Barros for the help and work at the Stable Isotope Laboratory (LES-CPGEO) that allowed the acquisition of the isotopic data, to Hellen Cristine for the support with the PIXE analyzes at the Ion Beam Material Analysis Laboratory (LAMFI USP), to Prof. Dr. Juan Pablo for the support and collaboration with the analysis of trace elements at the ELA-ICP-MS laboratory of the Center for Geosciences of the Universidad Nacional Autonoma de México, to Prof. Dr. Hai Cheng for the support of the Institute of Global Environmental Changes at the University of Xi'na Jiaotong (China) which made it possible to carry out part of the geochronological analyzes performed by the student Vitor Azevedo through collaboration, to Prof. Dr. R. Lawrence Edwards for the support at the Geochronology Laboratory at the University of Minnesota (USA) that made it possible to carry out geochronological analyzes during my research internship.

This work also gave me the first experience of living outside Brazil, for which I am incredibly grateful for Prof. Chico Bill and Prof. Larry Edwards, who through collaboration allowed the research internship to be carried out at the Geochronology Laboratory at the University of Minnesota (USA). I thank Jon and Lydia Orson for welcoming me so well in their home, for the conversations, company, for offering all the help I needed and for showing me a little bit of Minneapolis. Thanks again to Prof. Dr. Larry Edwards for helping me during the research internship and the researchers Xianglei Li and Peter Schroedl for teaching in details all the necessary steps for data acquisition and for always being available to resolve any questions or problems. I am also grateful to the researchers Peter Chutcharavan, Yijia Liang, Dylan Parmenter for their help and the company in the lab. Finally, I would like to thank my friend Plínio Jaqueto

for the help and collaboration during the long lab days, for the help with data processing, for the walks through Minneapolis, tubings, snowboard falls, and for all Orange Chickens and Craft beers.

I would also like to thank my laboratory and classmates at IGC-USP: Plácido Buarque, Lucas Godinho (Rejeitto), Veronica Ramires, Valdir Novello, Melissa Martinez, Giselle Utida, Suellyn Emerik, Vitor Azevedo, Tom Morita, Janine Carmo, Ybiatã, who helped me during these two years through discussions, analyzes or even by the company and laughter. I also thank my cousins Brenda Rocha, Caue Cioff and João Zambrini for their advice and help in academic life.

Special thanks to Suellyn for all the help with sampling, companionship and for working on the collection of speleothems at the Karst System Laboratory. I also especially thank Dr. Giselle Utida for the immense help with bureaucracies, documentation, reports, events, advice and for always being available for any problem or question, helping me a lot (GREATLY) throughout my master's degree.

I thank the director of PETAR Juliana Conrado, for the authorization to carry out the field activities in Lage Branca cave and to Jurandir and Ditinho for their assistance during the field work. I also thank Leda Zogbi for making the cave profile used for the collections at Lage Branca and for the friendship and cave expeditions. I would also like to thank Rejeitto for his assistance in the safety and installation of the climbing routes essential for the work in the cave.

To my friends Gabriel Rangel, João Garbelim, Anderson Pires, Cauê Moara, Everton Lima, Bruno Cirilo, Gustavo Ribeiro, Bruno Italalong, for the partnership of many years that has always helped (or hindered) me in my life. To my longtime dojo mates Leandro Goulart, Vinicius Nobre, Daniel do Vale (Banana), Lucas Milani, Adriano Santos, Igor Schneider, Julio Moraes and Raphael Oliveira for always being there and for helping me over the years. I also thank Prof. Enrique Muniz for welcoming me very well at his gym in Minneapolis and for training between the dense lab days.

I am grateful to my partner in the cave, wrenches, laboratory, office, dojo, and dreams Marcela Eduarda Della Libera de Godoy for the help in all stages of this work (field, analysis, discussions, review etc.), for always encouraging me to go after what I want, for the English classes and the partnership during those years.

Special thanks to my mother Ana Paula Cauhy and my father Cesarvinicius S. Rodrigues for always supporting me and always being available to help me with everything.

RESUMO

RODRIGUES, J.C., 2020, Reconstrução Paleoclimática baseada na geoquímica multiproxy de alta resolução de espeleotemas dos estados do Paraná e São Paulo, Brasil [Dissertação de Mestrado], São Paulo, Instituto de Geociências, Universidade de São Paulo, 115p.

Uma das maiores dificuldades na avaliação do impacto das mudanças climáticas na ocorrência de eventos extremos de precipitação reside na limitação dos dados históricos. Neste contexto, registros de espeleotemas de cavernas sujeitas a eventos recorrentes de inundação são utilizados para avaliar a frequência com que eles vêm ocorrendo nos últimos sete mil anos. Para isto, foi avaliada a ocorrência de camadas detríticas depositadas sobre os espeleotemas, indicativas de eventos de inundações em espeleotemas coletados nas cavernas Lage Branca e Malfazido. Estas formações foram precisamente datadas pelo método U/Th e apresentam altas taxas de crescimento, o que torna possível a reconstituição de eventos de alta frequência de inundação de cavernas no Leste do Paraná e Sul de São Paulo. A análise química pelo método PIXEs foi utilizado para auxiliar na identificação das camadas detríticas visíveis nos espeleotemas. Os dados isotópicos de $\delta^{18}O$ dos espeleotemas refletem mudanças no regime de chuvas monção de verão vs. extratropical de inverno. Os espeleotemas foram analisados quimicamente pele técnica de LA-ICP-MS e sugerem que a incorporação de elementos traços é controlado por mecanismos de PCP (*prior-calcite precipitation)* e PAP (*prior-aragonite precipitation*) nos espeleotemas CR-1 e MFZ-N-1, respectivamente. As análises de componentes principais (*PCA*) permitiram reduzir os conjuntos de dados multivariados de elementos traços, a ponto de facilitar a avaliação das condições hidrológicas na área de estudo através de suas relações com PCP e PAP. Análises estatísticas dos proxies juntamente com índices paleoclimáticos indicaram possíveis ligações entre a área de estudo e anomalias de TSMs dos Oceanos Atlânticos e Pacífico. Comparações com índices paleoclimáticos sugerem que períodos de alta frequência de eventos de inundação na caverna Malfazido podem estar relacionados a anomalias de TSM associadas ao aumento da atividade da SMSA sobre sudeste da América do Sul ou às condições similares ao El Niño. Além disso foi levantada uma possível ligação entre eventos extremos de precipitação e forçante vulcânica. As reconstituições das paleoinundações da caverna Lage Branca indicam que a transição entre o Holoceno Médio e Tardio é marcada pela mudança na circulação atmosférica para condições de maior atividade do Sistema de Monção da América do Sul (SMAS) juntamente com o aumento da chuva de verão indicados pelos registros de espeleotemas do Sudeste do Brasil. Essas mudanças são relacionadas a um aumento abrupto na frequência de paleoinundações na caverna após o ano de 4200 A.P., com uma tendência observada para os registros de $\delta^{18}O$ e elementos traços indicando maior atividade da SMAS e a condições mais úmidas até o período mais anômalo em 2000 A.P. Após este período, um hiato nos espeleotemas da Lage Branca marcado por uma camada detrítica grossa indica que os espeleotemas podem ter ficado mais sujeitos a condições de inundação devido ao aumento da precipitação de verão. Em resumo, novos registros de alta resolução contribuem de forma inédita no entendimento da frequência de eventos extremos de precipitação relacionados a inundações em cavernas, e em quais condições hidrológicas e de circulação atmosférica essas mudanças de frequência estão relacionadas. O novo registro de paleoinundação de espeleotemas da Lage Branca contribuem para entender como os eventos de inundações em cavernas podem ser afetados por mudanças na circulação atmosférica em resposta à mudança no estado médio do clima associado às alterações da SMAS pelas mudanças de insolação de verão.

Palavras-chave: paleoinundação, espeleotemas, inundação em caverna, extremos de precipitação

ABSTRACT

RODRIGUES, J.C., 2020, Paleoclimate reconstruction based on high-resolution multiproxy geochemistry of speleothems from Paraná and São Paulo states, Brazil [Master's Thesis], São Paulo, Instituto de Geociências, Universidade de São Paulo, 115p.

One of the greatest limitations on evaluating climate changes impact and the occurrence of the extremes events resides in the limitation of historical data. In this context, speleothems records from cave galleries subjected to recurrent flood events are used to assess past frequency of extreme events. Detrital layers within speleothems deposited during flood recession are used here to reconstruct the occurrence of cave flood events for the last seven thousand years, allowing the study of these events beyond the pre-industrial period. Speleothems from Lage Branca and Malfazido caves are used here to reconstruct the frequency of cave paleo floods for the Mid-Late Holocene and for the last millennium, respectively. Well-resolved chronology for the speleothems were obtained by U/Th age method. Visual methods associated with PIXEs analysis were used to identify detrital layers associated with floods within the speleothems. Stable isotopes analyses were performed to access atmospheric-circulation conditions. Trace elements analysis (LA-ICP-MS) were performed for Malfazido' speleothem and a previous record of trace element from Cristal cave are used. Correlation between the trace element ratios suggest that PCP and PAP are the main control in trace elements concentrations. Therefore, a novel high-resolution record is presented using principal component analysis for each speleothem that can account for most of the variance observed in the multivariate dataset. These PCs are used here as proxies for assess hydrological conditions in the cave sites by its relations with PCP and PAP. Statistical analysis of $\delta^{18}O$ with paleoclimate indices showed a possible link between the study area and SSTs anomalies from Atlantic and Pacific Ocean. Comparisons with paleoclimatic indices suggest that periods of high cave flood frequency in Malfazido cave may be related to SSTs anomalies associated with enhancement in SAMS activity over SESA or to El Niño-conditions and a possible link between extreme precipitation events and volcanic forcing is commented. Also, the paleoclimate reconstructions indicates that the transition between Middle and Late Holocene is marked by changing in the atmospheric circulation for conditions with higher South America Monsoon System (SAMS) activity and enhancement of summer rainfall as indicated by $\delta^{18}O$ and trace elements of speleothems from PETAR site. These changes are related to an abrupt increase in the paleoflood cave frequency after 4200 B.P., with a trend in $\delta^{18}O$ and trace elements indicating higher SAMS activity and wetter conditions. After 2000 B.P., Lage Branca cave may have been more susceptible to flood events due to increased summer precipitation, as showed by a hiatus in both speleothems characterized by a thick detrital layer. In summary, novel high resolution records of Malfazido and Cristal cave contribute in an unprecedented manner to understand the frequency of extreme precipitation events related to cave floods, and in which atmospheric-circulation and hydrological conditions that these changes in frequency; and the novel Lage Branca speleothems paleoflood record contribute to understand how low frequency cave flood can be affected by changes in the atmospheric circulation in response to change in the mean climate state associated with the modulations by insolation on the SAMS.

Keywords: speleothems, paleoflood, climate reconstruction, paleoclimate, cave floods, extreme precipitation events.

SUMMARY

LIST OF FIGURES

1. INTRODUCTION

Extreme precipitation events represent the largest source of risk to societies around the globe and have become more frequent and intense in the last decades, being responsible for 74% of the deaths related to natural disasters between 1991-2010. The Intergovernmental Panel on Climate Change (IPCC) scientific reports have indicated through climate change projections and observational analyses an increase in the frequency and intensity of extreme rainfall events (Debortoli et al., 2017).

Several studies have been assessing the frequency and magnitude of extreme precipitation events in southeast Brazil based on rainfall monitoring stations and climate models. For instance, in São Paulo state Carvalho et al. (2002) investigated the relationship between summertime extreme precipitations events with intense convective activity of the South Atlantic Convergence Zone (SACZ), and for those events Liebmann (2001) showed that they are correlated with sea surface temperature (SST) anomalies. Also, Pedron et al. (2017) identified significant trends on several indices of climate extremes based on daily rainfall data since 1889 in Curitiba city, located 100 km away from the study area of this project.

One of the greatest struggles on evaluating the impact of climate changes in the occurrence of the extremes events resides in the limitation of historical data to beyond the pre-industrial time period, when humankind didn't exert a remarkable influence on Earth's climate. Regarding that, reconstituting the frequency of extreme events beyond the instrumental data becomes essential to understand how the current warming trend affects the frequency and the magnitude of those events (Denniston & Luetscher, 2017)

In order to produce proxy records for extreme precipitation variability, here we present a novel geochemistry and sedimentary approaches have been used in speleothems to evaluate cave floods caused by those events. Speleothem from flooded galleries are ideal recorders of past frequency of extreme events, providing robust evidence of large amplitude changes in the local water table thorough the deposition and preservation of mud layers (Dasgupta et al., 2010; Denniston et al., 2015; Frappier et al., 2014; Gázquez et al., 2014; González-Lemos, 2014; González-Lemos et al., 2015).

Cave floods events can be preserved in speleothems as fine sediments such as clay and silt present in the flood water deposit on the speleothem surface during the flood recession, resulting in a clay-rich layer that may be trapped by the resumption of the speleothem growth, preserving

the sediment from subsequent erosion (Gázquez et al., 2014; González-Lemos, 2014; González-Lemos et al., 2015) If the speleothem grows continuously for a long period, it may preserve a detailed flood record for thousands of years (Dorale et al., 2005).

Thereafter, this new approach is promising due to several basic stalagmites characteristics, such as its simple stratigraphy based on a precise U/Th dating method and the potential to record cave flood events from thousand or hundreds of thousands years. Several methods have been used to recognize and characterize the detrital layers within speleothems with a series of visual methods, including optical and scanning electron microscopy for visual identification (González-Lemos et al., 2015) as well as various geochemical analyses such as ultra-violet fluorescent analyses (Dasgupta et al., 2010) and trace elements analysis using Laser-ablation mass-spectrometry analyses (LA-ICP-MS) (González-Lemos et al., 2015) and XRF- scanning (Finné et al., 2015).

Speleothems subject to flooding are generally avoided for paleoclimate studies because the formation might have been corroded or abraded. Furthermore, the occurrence of detrital sediments, such as clay and silt are major source of detrital ^{232}Th, which can preclude precise U/Th dating (Frappier et al., 2014). However, in some cases a high-resolution flooding chronology can be provided by high-precision U-Th dating, allowing an annual-solved chronology of flood events when combined with speleothem lamination counting (Dasgupta et al., 2010).

If a flood chronology is archived, the frequency of cave floods is obtained by the observed number of events in a given time (Dasgupta et al., 2010). The frequency of floods can be compared with others records, and combined with stable isotopes and trace elements data, in order to access hydrological and environmental conditions related to changes in the flood frequency. Despite the potential of speleothems on provide reliable record of past changes in extreme events, so far, few studies have been dedicated to this issue.

An important step to link cave floods to extreme precipitation events involves integrating the climate and the cave hydrology data. To test this link, rainfall and river flow from surface monitoring stations can be compared with cave monitoring as water level data from divers, cave stream flow or speleothems flood record (Dasgupta et al., 2010; Denniston & Luetscher, 2017; Wilhelm et al., 2019).

In light of the above, this research aims to reconstruct the flood frequency from Laje Branca cave, in the south of São Paulo state, based on precise dated speleothems subjected to lower frequency cave floods during the Middle and Late Holocene; for the Last Millenia, a speleothem

from Malfazido cave, in northeast of Paraná state, is used to reconstitute a high-resolution record of flood activity for higher frequency flood events. Stable isotopes and trace elements analyses were performed and compiled from the study area to access the hydrological and environmental conditions of the period related to changes in flood activity. Some climate modes of low frequency variability such as the El-Niño Southern Oscillation (ENSO) and the Atlantic multidecadal oscillation (AMO) (Knudsen, et al., 2011; Mann et al., 2009; Wei & Lohmann, 2012) will be used to verify the importance of the oceanic variability on the extreme precipitation events in the southeast of Brazil.

2. RESEARCH AIMS

The goals for this research are:

- Reconstruction of the flood frequency based on speleothems from the Southeast of Brazil: (1) Last Millennia flood frequency of Malfazido cave based in a speleothem with a well-resolved chronology (2) Middle to Late Holocene paleoflood frequency of Lage Branca cave based on two speleothems with a coeval growth period.
- Investigate the link between extreme precipitation events with cave floods in the study area and the trace-elements and Carbon and Oxygen stable isotopes in the speleothems
- Reconstruction of hydrological and environmental conditions of the study area by obtaining new stable isotopes and trace elements records combined with speleothem records from previous studies in the region.
- Understand how climate changes in the Southeast of Brazil affect the occurrence of extreme precipitation events and their related climatic forcing.

3. STUDY AREA

The stalagmites samples collected for this study are from two caves (Laje Branca and Malfazido) in two different cave sites in Southeast Brazil (SEB). The Laje Branca Cave (24°54’82.75’’S; 48°72’12.58’’W) is situated on the Parque Estadual Turístico do Alto Ribeira (PETAR) in Iporanga county (southern São Paulo state), about 97 kilometers from the Atlantic Ocean and 523 m above the sea level. Malfazido cave (24°39'40.67"S; 49°32'21.22"W) is situated in Dr. Ulysses county (northeastern Paraná state), about 60 kilometers from PETAR site and 100 km from Curitiba city (Paraná state capital) and at 885 m above sea level.

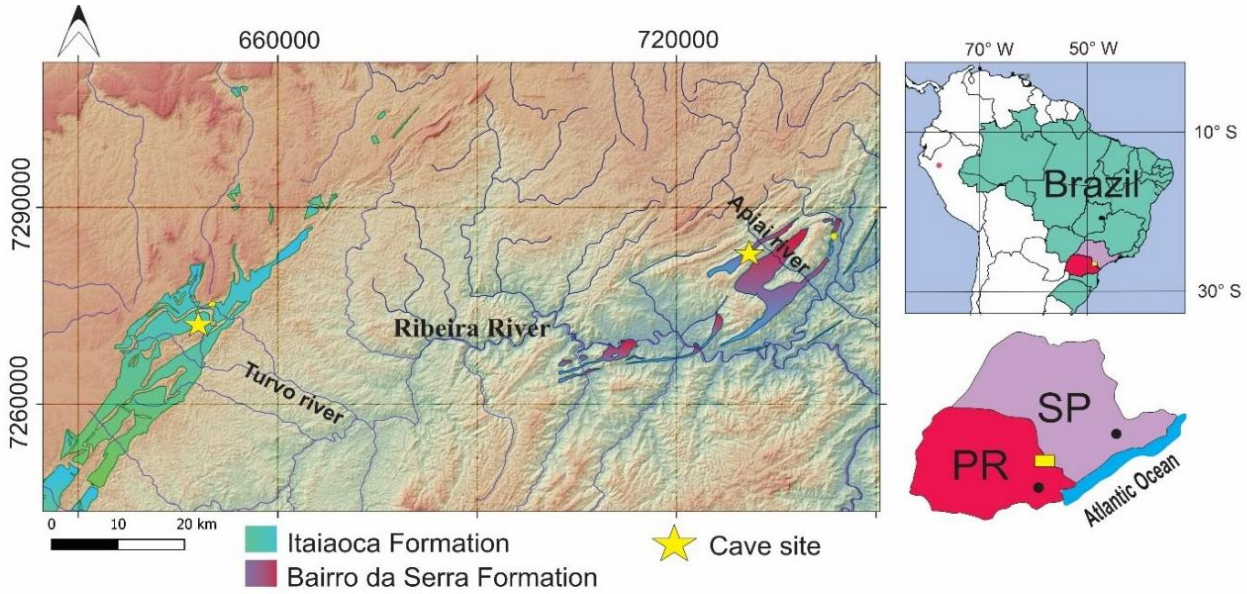

Figure 1 - Study area map showing the cave locations (yellow stars) and the metalimestones in which the cave are inserted

Laje Branca cave (Fig 2) is part of the Pérolas-Santana system, with development of 900 m with large galleries with rectilinear pattern and low sinuosity (Karmann, 1994). The cave is developed in the contact between the metapelites from Betari Formation and metalimestones from Bairro da Serra Formation, with a difference in height of 70 m between the entrance and the sink hole in the lowest gallery (Karmann, 1994). The lower level gallery is characterized by sediments piles reaching approximately 15 m high, composed by clay and silt with ripple marks on surface indicating water flow running to the present drainage during massive flood events. It is possible to observe sediment marks of different water levels along the areas occupied by sediment pile which suggest the presence of intermittent lakes associated with floods. Besides the banks, it is possible to recognize several evidences of those events such as marks of recent mud layers in the walls and ceiling that also covered collapsed blocks and speleothems like stalagmites and aragonite flowers standing in the walls. More importantly, these massive flood events are reported to occur nowadays by local guides in response to extreme precipitation events which makes the clastic sediment layers trapped inside the speleothems during calcium carbonate deposition as a good proxy for ancient floods in the Lage Branca cave.

Malfazido is a rectilinear cave located in the metalimestones from the Itaiacoca Formation and is marked by a sequence of big dry travertines pools subjected to floods during heavy rainfall (Figure 3). The underground stream is a tributary of Turvo river and flows towards the cave entrance until it is captured by a sinkhole inside the cave. Outside the cave is possible to see a

spring flowing a few meters from the cave entrance. The cave floor is covered by fine-grained sediments with recent mud cracks and several stalagmites inside the dry travertine pools. A flood event was observed in the cave during a field work on 06/07/2019, where it was possible to confirm that the speleothems collected in the travertine pools were sequentially submerged in response to a rainfall event of 100mm in three days of rainfall. Another historic flood event reported in Malfazido cave is indicated in the cave map made by the Speleology Study Group of Paraná (GEEP-Açungui) in 02/15/1999, where they draw the flooded travertines as a cave lake (Fig 3).

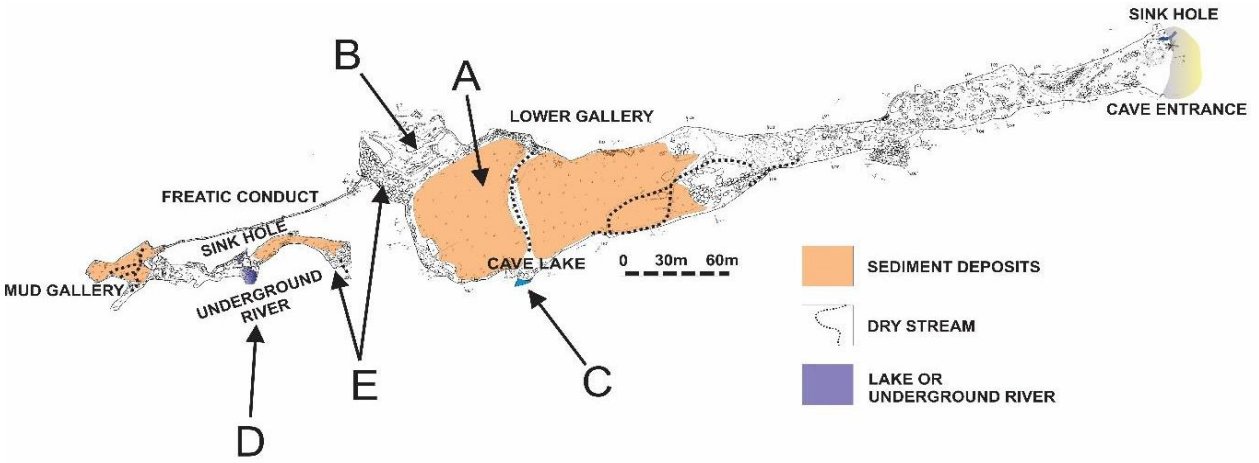

Figure 2 – Laje Branca cave map. A) Fine sediment deposits in the lower gallery; B) higher gallery approximately 20 meters high above the cave lake with aragonite flowers marked by mud marks; C) cave lake with water levels marked in the sediments and in the walls; D) underground river flowing to the mud gallery; E) location of collect of LB-1 and CB-3 samples. Altered from Karmann 1994.

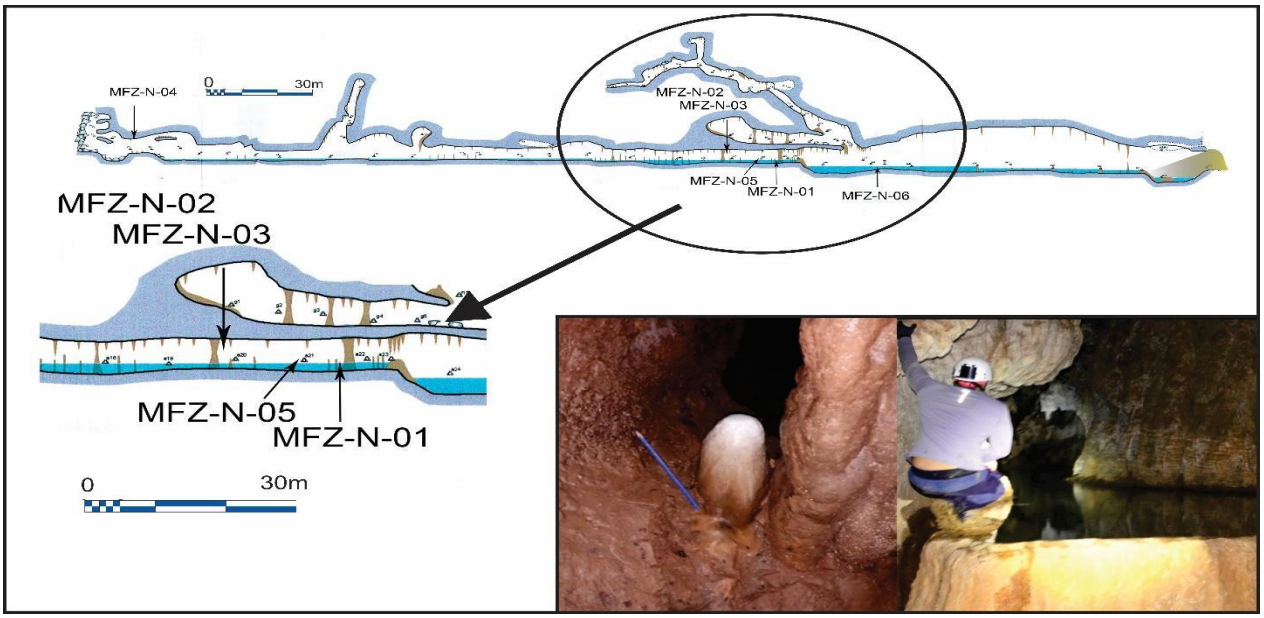

Figure 3 - Topographic profile of Malfazido cave (top), with a zoom for the location of the collected speleothems. The bottom right photo shows the cave flooded and the bottom left the MFZ-N-1 speleothem location.

4. CLIMATOLOGY

4.1 Modern Climatology

The precipitation climatology over southeastern Brazil (SEB) is mostly affected by two main atmospheric features: Cold Fronts (CF), a transient perturbation that affects the region from 1-2 days, present during austral summer and winter and bringing moisture from the Atlantic Ocean into the continent (Cruz et at., 2005b); and the SACZ, a quasi-stationary system that remains over Central-south Brazil for ~3 days or more (Cruz et al, 2005b; Lima et al., 2010). The SACZ is an integral part of the monsoon system and forms by the extension of a convective activity that begins over western Amazon basin, the South America Monsoon System (SAMS) all the way into the Atlantic Ocean, going over SEB thus bringing moisture to the region (Lima et al., 2010). During the monsoon period (November-March), the SACZ presents a strong convective activity responsible for several heavy rainfall events, which makes this system of major importance for the annual rainfall in the region (Carvalho et al., 2002; Lima et al., 2010; Vasconcellos & Cavalcanti, 2010).

In interannual and multidecadal time scales, some climate modes associated to variations in sea surface temperature (SSTs) in Atlantic Ocean affect the South America continent and therefore the SEB. In the Atlantic Ocean, one of these fluctuations is known as Atlantic Multidecadal Oscillation (AMO) (described in detail in section 4.2) where its positive (negative) phase is associated with warm (cold) anomalies in the North Atlantic and thus results in cold (warm) anomalies in the South Atlantic (Alexander et al., 2014; Kayano and Capistrano, 2014; Mann et al., 2009). Therefore, the cold phase of the AMO leads to a warming of the South Atlantic which is then closely related with enhanced SACZ activity, once the Intertropical Convergence Zone (ITCZ) is shifted southward, increasing the moisture transport from the ocean into the Amazon basin and boosting SAMS/SACZ activity (Alexander et al., 2014; Kayano and Capistrano, 2014)

Another major climate module that has high rainfall influence over SEB is the El Niño-Southern Oscillation (ENSO), a cycle of SST variations related to the tropical Pacific Ocean with a timescale of 2-7yr (Grimm et al., 2009) (described in detail in section 4.2). This system consists in anomalies in heat and water vapor generated in the ocean that go into the atmosphere, altering the atmospheric circulation worldwide (Carvalho et al., 2002; Grimm et al., 2009; Kayano and Capistrano, 2014; Liebmann et al., 2001; Wang, 2005). The El Niño phase is broadly known for

enhancing extreme rainfall events over SEB once its mature phase happens concomitant with SAMS, leading to an increase in the number of persistent days (≥ 4) of the SACZ by twice as much as in cold or neutral phases (Carvalho et al., 2002; Liebmann et al., 2001).

Even though the systems mentioned above take place in two different oceans, both play a major role in the interannual rainfall variability over SEB. Also, it is relevant to note that these systems can occur simultaneously affecting one another; the AMO has a significant impact over ENSO phases, which therefore can affect the rainfall over South America. As demonstrated in previous studies (Kayano and Capistrano, 2014; Timmermann et al., 2007), the cold phase of AMO for North Atlantic can intensify El Niño events over SEB mostly from October-January, whereas these events are weaker during warm AMO phases.

As it can be seen, most of the annual rainfall amount over SEB typically comes from the humidity over the Amazon basin in the SACZ, and the remnant amount comes from the winter rains in the form of CF from the Atlantic Ocean. This clear difference in source of moisture changes the oxygen isotopic signature of the rain: the nearby Atlantic source during winter leaves a more enriched rainfall signature in the water (average of -3‰), while monsoon-related rainfall presents more negative values (average of -7‰) due to the amount effect (Cruz et al, 2005b; Taylor, 2014). This source-related oxygen isotopic signature is therefore reflected in the stalagmite δ18O variations such as demonstrated in previous studies with speleothems in SEB (Cruz et al, 2005b; Taylor, 2014), where the increase (decrease) of isotopic values would reflect higher contribution of winter (summer) rainfall. Therefore, some periods may have greater winter (summer) rainfall contributions, which occurs when the SAMS/SACZ is shifted northward (southward) and brings less (more) moisture from the Amazon basin (Cruz et al., 2005b), what will be used as the oxygen isotopic interpretation in this work.

4.2 Modes and Patterns of Climatic Variability in the Pacific

In this section, three modes of variability are associated with climatic conditions over Pacific Ocean that operate in different timescales. The El-Niño Southern Oscillation (ENSO) ranges from 2-7 years, while the Interdecadal Pacific Ocean (IPO) and the Pacific Decadal Oscillation (PDO), vary from 20 to30 years.

ENSO events takes place when the tropical Pacific is anomalous warm in central/eastern Pacific due to a weakening of zonal trade wind and associated reduction of ocean upwelling (Amaya, 2019; Kayano and Andreoli, 2007; Wang and Ren, 2020). The cold phase of ENSO is

named La-Niña (LN), and both warm and cold SST anomalies (SSTA) have been proved to have significant effect on climate in a global scale (Amaya, 2019; Zhang et al., 2019; Kayano and Andreoli, 2007). During El-Niño (EN) phases, the main ocean-atmosphere features are the anomalous high sea level pressure (SLP) over Indonesia and a correspondent anomalous low SLP over central/eastern Pacific due to an eastward Walker cell shift, where the ascending activity occurs due to the warm SST anomaly; during LN, the opposite behavior is observed (Kayano and Andreoli, 2007). As a result, during positive ENSO phases, wetter conditions prevail over subtropical regions in South America, whereas in tropical regions drier conditions are observed (Silva et al., 2011).

Several studies have been pointing out the effects other Pacific variabilities have on ENSO phases, such as the Pacific Decadal Oscillation (PDO) and the Interdecadal Pacific Oscillation (IPO). The PDO is a North Pacific variability mode that was obtained from an EOF (Empirical Orthogonal Function) analysis of its monthly SST during 93 years (1900 - 1993), where it was possible to characterize its positive (negative) phase as warm (cold) SST anomalies in the northeastern Pacific and cold (warm) in western and central North Pacific with a cycle of 20-30 years (Silva et al., 2011; MacDonald and Case, 2005; Kayano and Andreoli, 2006). For instance, it has been observed that SST patterns of PDO over the North Pacific coincides with patterns from ENSO modes, where the intensity of either positive or negative PDO phases presents the same band of ENSO frequencies (2 -7 years) (MacDonald and Case, 2005; Kayano and Andreoli, 2006).

The IPO, in turn, is a sea surface temperature anomaly (SSTA) that occurs throughout the entire Pacific in both hemispheres and its abrupt changes in SSTAs across the Pacific might also last for about 20-30 years, which is then considered to be a wider expression of the PDO variability (Buckley et al. 2019; Silva et al., 2011). Therefore, the PDO and IPO are vastly correlated with each other and ergo both affect ENSO variability and intensity, where in PDO and IPO warm phases an El-Niño-like pattern emerges and western and central North Pacific waters are cold while warmer SSTs prevail over the entire west coast of Americas and over central-eastern tropical Pacific (Buckley et al. 2019; Silva et al., 2011).

Now, looking at how these phenomena impact the climate over South America, some studies have shown that during periods in which ENSO and PDO are in the same (opposite) phase, the teleconnections of ENSO over precipitation in South America become stronger (weaker), which means that during summer in South America (December-February) the ENSO effect on

precipitation is stronger during positive PDO phases when compared to negative PDO phases (Kayano and Andreoli, 2006; Silva et al. 2011). Also, regarding IPO effects over South America, Buckley et al. (2019) reported that during positive IPO phases a drought prevails over northern South America including the Amazon basin, while anomalous wet conditions prevail on more southern regions, which is consistent with the effects that positive phases of ENSO and PDO have over South America. Still according to this study, this would be caused due to a change in the zonal Walker circulation because its ascending branch is now over the anomalous warm SST in the Pacific, leading to a descending branch over northern South America, thus reducing convection; on the other hand, the scenario is inverse during negative IPO phases, where cold SSTs prevail in central eastern tropical Pacific and convection can happen over northern South America.

Finally, according to Silva et al. 2011, a more specific look at South Eastern South America (SESA) reveals the climatic effects that ENSO events during positive PDO phases have: there is a shift of moisture transport over the continent, where the moisture influx is now directed toward southern Brazil (SESA) contributing to positive precipitation anomalies over the region, whereas less convective activity is happening over the Amazon region, weakening the moisture flux in the SACZ region and thus favoring negative precipitation anomalies over northern SESA that is still under SACZ influence.

4.3 Modes and Patterns of Climatic Variability in the Atlantic

The Atlantic Ocean goes through periodic fluctuations in sea surface temperature (SST) that occur in a multidecadal timescale (60 to 80 years) for which has been given the name of Atlantic multidecadal oscillation (AMO) (Alexander et al, 2014; Knight et al, 2006; Keer et al, 2000; Knudsen et al., 2011). This low-frequency variability is based on temperature changes over large areas of the North Atlantic, thus representing its dominant SST pattern, which alternates between cold (positive) and warm (negative) phases (Alexander et al, 2014; Knight et al, 2006). Even though AMO is a North Atlantic SST variation index, previous studies have shown that it is linked to other climatic effects (Wang et al.,2017), such as Sahel drought (Folland et al., 1986), frequency of Atlantic hurricanes (Goldenber et al, 2001) and even changes in Northeast Brazil rainfall patterns (Folland et al.,2001; Knight et al., 2006).

Up to date, the causes for AMO variability and its related multidecadal periodicity are still under debate. Some studies (e.g. Wang et al.,2017; Alexander et al., 2014) have been referring to this phenomenon as Atlantic Multidecadal Variability (AMV) instead of AMO due to some

irregularities on its occurrence and “because it does not imply that it is a mode of variability generated solely by internal climate processes” - Wang et al.,2017. In fact, several processes can lead to decadal variations in North Atlantic SST, such as ocean currents caused by wind, fluctuations in sea ice and changes in surface heat fluxes, but the Atlantic meridional overturning circulation (AMOC) is among the most probable cause of this North Atlantic SST variability named AMO (Wang et al.,2017; Alexander et al., 2014; Knudsen et al., 2011).

For about the last ~150 years, the AMO has been studied through SST anomalies in instrumental data, however records that extend further back in time must be investigated to accurately characterize this oscillation or variability (Knudsen et al., 2011). For that, several paleoclimatic data have been employed to better understand this phenomenon, as it can be seen, for instance, in Mann et al., 2009, Knudsen et al., 2011, Alexander et al., 2014 and Wang et al.,2017. Therefore, to reconstruct a reliable AMO index these studies use statistical methods along with model-base pseudoproxy (climate models) and multiproxy datasets (tree rings, ice cores, sediments, speleothems, etc.), resulting in an AMO index, such as the ones obtained by Mann et al. (2009) and Wang et al. (2017), where AMO variability was reconstructed for the past 1500 and 1200 years, respectively.

In addition, some studies have been pointing out the effects AMO might have over the South American climate. Regarding the Atlantic influence over South America, model data have shown that negative phases of AMO (linked to a low thermohaline circulation thus lower heat transport over to the North Atlantic) cause a southward displacement of ITCZ in the Atlantic, which in turn enhances the moisture income over the continent that eventually reaches southeast Brazil (Zhang and Delworth, 2005). On the other hand, with regard to Pacific climate effects over South America, some studies have found that AMO phases affect ENSO variability, where cold (warm) AMO phases are linked to strong (weak) ENSO variability and reduced (elevated) eastern Pacific SST annual cycle dimension, which in turn leads to an increase in precipitation over southeast Brazil (Timmermann et al.,2007; Kayano et al., 2014; Seager et al., 2010).

Finally, other phenomenon happening over the Atlantic Ocean that affects climate patterns all over the Atlantic, including the AMO, is the North Atlantic Oscillation (NAO). The NAO is an atmospheric circulation pattern that occurs over middle and high latitudes of the Northern Hemisphere, predominantly over the Atlantic (Hurrell et al., 2003). This circulation is responsible for rearranging the atmospheric mass between the Artic and the subtropical Atlantic and thus

altering weather patterns, such as Atlantic wind speed and direction and the distribution of heat and moisture from the Atlantic to the continents (Hurrell et al., 2003). The NAO positive (negative) phase is characterized by a strong (weak) well-defined poleward low-level jetstream over North Atlantic that occurs predominantly during winter season (December-February) due to an anomalous low atmospheric pressure over Arctic and Iceland regions linked to an anomalous high atmospheric pressure over subtropical Atlantic, thus leading to the atmospheric mass circulation (Hurrell et al., 2003; Martineau et al. 2020). Even though this oscillation occurs over the North Atlantic, previous studies have evidenced the consequent influence the NAO has over South Atlantic and ergo over South America climate. It has been reported that extreme NAO positive phases lead to a warming of the tropical South Atlantic that in turn cause the ITCZ to develop in a more southward position (Souza and Cavalcanti, 2009).

5. SPELEOTHEMS AS PALEOCLIMATE RECORDS

Speleothems are cave secondary mineral deposits of CaCO3 (calcite or aragonite) that have already been established as important and reliable continental climate archives due to its potential to record several proxies such as oxygen and carbon stable isotopes and trace elements (Wassenurg et al., 2016; Fairhchild and Treble, 2009). The most used speleothem formations for paleoclimatic studies are the stalagmites, formations that grow vertically on the floor towards the ceiling due to the dripping water and the consequent precipitation of calcite, resulting in formations with an internal structure of concave layers (Fairchild and Treble, 2009). Also, the U/Th dating method for carbonate samples allow an outcome of very precise dates from the present up to 500 ka, which combined with the stalagmite successive deposition and the high-resolution sampling of oxygen and carbon isotopes, it may result in a reliable paleoclimate record (Wassenurg et al., 2016).

5.1 Stable Isotopes

5.1.1 Oxygen stable isotopes in speleothems

The oxygen isotope is currently one of the most employed proxies for paleoclimatic studies based on speleothems once the oxygen incorporated in the speleothem's formation is closely linked to the meteoric water cycle and it's stable over time, thus holding relevant information about amount and source of the rainwater (Lachniet, 2009). During the hydrologic cycle, the water goes through several phase changes and the oxygen present in this water undergoes fractionation

processes in the flux between reservoirs, where one isotope is favored over the other according to their mass, as shown by the equation 1 (Clark and Fritz, 1997):

$$\alpha = {}^{Ra}/_{Rb} \qquad \textbf{Eq. 1}$$

E. g. $$\alpha^{18}O_{(water-vapor)} = {}^{(^{18}O/\,^{16}O)_{water}}\Big/_{(^{18}O/\,^{16}O)_{vapor}}$$

where α is the fractionation factor and R is the isotopic ratio of less/more abundant of the element, such as in the example in Eq.2. The measurements of relative variations of ^{18}O and ^{16}O in a sample is expressed using the δ notation, accordingly with the following equation: n (Lachniet, 2009):

$$\delta^{18}O_{sample} = \frac{\left(\frac{^{18}O}{^{16}O}\right)Sample - \left(\frac{^{18}O}{^{16}O}\right)Standard}{\left(\frac{^{18}O}{^{16}O}\right)Starndad} \qquad \textbf{Eq. 2}$$

The standard values used for calcium carbonate is the Vienna Peed Dee Belemnite (VPDB), while for water samples the most common used reference is the Vienna Standard Mean Ocean Water (VSMOW). Once the outcomes of this equation are rather small, the notation of the relative isotopic variations "δ" is here multiplied by 1000, thus being expressed in ‰ (per mil) to facilitate its understanding. The standard value of both VPDB and VSMOW are defined as 0‰ so the variations in the $^{18}O/^{16}O$ ratio of the samples are always indicated by differences referring to the standard (Lachniet, 2009). Therefore, when obtaining $\delta^{18}O$ values in a sample they are either "enriched" with ^{18}O (higher $^{18}O/^{16}O$ sample ratio), or "depleted" of ^{18}O (lower $^{18}O/^{16}O$ sample ratio).

The fractionation processes that take place during changes of water phase in the hydrological cycle control the $\delta^{18}O$ values in the reservoirs. This is because there are differences in the strength of chemical bonds between the isotopes due to its mass, where the heavier (lighter) the isotope, the greater (smaller) the energy needed to break the bond (Clark and Fritz, 1997), which means heavier (lighter) molecules are less (more) volatile in these processes. In evaporative processes, for instance, the evaporation on the ocean surface (liquid) to the atmosphere (vapor), the lighter isotopologues (H_2O^{16}) tend to be removed in larger quantities from the liquid or solid water reservoir and incorporated into the vapor phase than the heavier ones; the vapor is then more

depleted (lower $\delta^{18}O$ values) than the liquid (ocean). In condensation and precipitation processes, on the other hand, during the water phase change from the cloud (vapor) into rainfall (liquid) the heavier isotopologues (H_2O^{18}) tend to be incorporated into the more condensed phase, in this case the rain, which becomes more enriched (higher $\delta^{18}O$ values) than the remaining cloud vapor (Lachniet, 2009). This equilibrium fractionation is related to the temperature of the phase change and thus to the energy gradient needed to break these bonds, which can be determined by:

$$1000ln\alpha_{(water-vapor)} = 1.137(10^6/{T_k}^2) - 0.4156(10^3/T_k) - 2.0667 \quad \textbf{Eq. 3}$$

where T is for temperature in Kelvin. With this it is possible to observe that the temperature must decrease (increase) for there to be condensation (evaporation). The vapor formed in the ocean is then advected into the continent where a progressive condensation process takes place along the moisture flux pathway, thus lowering $\delta^{18}O$ values of the remaining vapor and, consequently in the precipitation. This process of continues removing of heavier isotopologues from a limited reservoir, i.e. the vapor in the air mass, is called Rayleigh distillation.

The condensation of moisture from a cloud is then directly proportional to the decrease in temperature, which can happen due to cold fronts, orographic lifting, convection, convergence, or advection of the air mass into colder regions and hence alter the isotopic composition of the water during the hydrological cycle, since it is temperature dependent (Lachniet, 2009). This role of temperature is ergo one of the most important factors regulating $\delta^{18}O$ values of precipitation, which is then associated with spatial variations in $\delta^{18}O$ due to changes in latitude, altitude, and moisture source. But this effect is most evident in middle and high latitudes, whereas in the tropics
the amount of the precipitated rather than the temperature, is the major driver of $\delta^{18}O$ variability of the rainfall. The effect that relates the water isotopes variability to the extent of precipitation is called "amount effect", where quantity of precipitation is anti-correlated with $\delta^{18}O$ values (increase in precipitation corresponds to lower $\delta^{18}O$ rainfall values) (Dansgaard, 1964; Lachniet, 2009). Ultimately, the amount effect is a function of the Rayleight distillation process. In this context, for areas far from the coast, the isotope variability of the rainfall water results from the so-called, degree of rainout upstream (Vuille and Werner, 2005). The degree of rainout upstream simply refers to the total isotope effect resulted from the continuous precipitation process along the moisture flux pathway. Thus, over continental regions, the isotope of the rainfall is more related to

the amount of precipitation on regional scale, more specifically, along the moisture trajectories, than the local amount properly (Ampuero et al., 2019).

Another factor that interferes with $\delta^{18}O$ values is the seasonality, once winter and summer rains might have different relative amounts of precipitation and originate from distinct moisture sources, which can result in abrupt changes in $\delta^{18}O$ values (Lachniet, 2009). For southeastern Brazil, for instance, previous studies have shown that seasonal atmospheric circulations changes, such as the prevalence of monsoonal regime during summer and an extratropical regime during winter, lead to an interannual $\delta^{18}O$ variation signal in the rainwater, where more depleted values of $\delta^{18}O$ are characteristic of summer rainfall (monsoonal regime) and more enriched values of winter rainfall (extratropical regime) (Cruz et al., 2005a; Cruz et al., 2005b; Cruz et al., 2007).

5.1.2 Water-rock interactions

In summary, the course of the water from the ocean to the formation of speleothems initiates with its evaporation from the ocean producing water vapor that will be advected over land where it may form clouds and eventually condensate into rainfall; the rainfall water then percolates through the soil and rock until it reaches the cave in form of drip water that will deposit the calcite layers and form a speleothem (Lauzitzen and Lundberg, 1999). The water isotopic fractionation processes that occur from the ocean to the moment of rainfall have been discussed above, but several other chemical and physical processes take place between its interaction with the soil and the speleothem formation, which will vary according to the cave location and the characteristics of the cave system.

The first process that takes place is the interaction between the rainfall water with the soil above the cave. Due to organic matter decomposition, the soil has a higher partial pressure (P_{CO_2}) than the rainfall water (unsaturated in CO_2) so that, when the water infiltrates the soil, the CO_2 is dissolved and reacts with the water resulting in the formation of carbonic acid (H_2CO_3) according to the following chemical reactions (Fairchild and Baker, 2012):

$$H_2O + CO_2 \leftrightarrow H_2CO_3 \qquad \text{- Reaction 1}$$

$$H_2CO_3 \leftrightarrow HCO_3^- + H^+ \qquad \text{- Reaction 2}$$

$$HCO_3^- \leftrightarrow CO_3^{2-} + H^+ \qquad \text{- Reaction 3}$$

These reactions lead to the formation of carbon chemical compounds, also referred to as dissolved inorganic carbon (DIC). The proportion between these DIC species will vary according to the pH value of the solution and the P_{CO_2} of the soil. The HCO_3^- is the most common DIC in solutions at near-neutral pH values (Fairchild and Baker, 2012).

After the water percolates through the soil and becomes more acidic due to its interaction with CO_2, it reaches the epikarst of the cave (the weathered and fissured zone of the limestone where rainwater might be stored and mixed) that lies between the bedrock vadose zone (the aerated zone) and the soil (Ford and Williams, 2007; Lachniet, 2009), and eventually the limestone bedrock. As the water with high P_{CO_2} percolates through the vadose zone occurs the dissolution of carbonate mineral (the higher the CO_2 concentration in the soil, the higher the $CaCO_3$ dissolution), as indicated by the reaction (Fairchild and Baker, 2012; Fairchild, et al., 2006):

$$CaCO_3 + H_3O^+ \leftrightarrow Ca^{2+} + HCO_3^- + H_2O \qquad \text{- Reaction 4}$$

And the entire dissolution can be written in one reaction:

$$H_2O + CO_2 + CaCO_3 \leftrightarrow Ca^{2+} + 2HCO_3^- \qquad \text{- Reaction 5}$$

Following percolation, the solution now saturated in Ca^{2+} reaches the cave environment and is now in contact with its atmosphere, which usually has a lower P_{CO_2} than the solution. This lower P_{CO_2} leads to the most common reaction in speleothem formation: the degassing of CO_2 from the solution to the atmosphere (Eq.X) through molecular diffusion (Dreybrodt, 2008), resulting in the precipitation of $CaCO_3$, as given in the reaction:

$$2HCO_3^- + Ca^{2+} \leftrightarrow CaCO_3 + H_2O + CO_{2(gaseous)}\nearrow \qquad \text{- Reaction 6}$$

This reaction might occur when the water drop resides longer on a stalactite or on the cave ceiling, thus precipitating $CaCO_3$ and forming stalactites, and/or when the water drips onto a stalagmite apex, where it'll lose CO_2 molecules from the solution due to the drop impact and then form a thin layer of water that will degas and precipitate $CaCO_3$ (Dreybrodt, 2008).

The described variations in $\delta^{18}O$ values due to seasonality, amount effect and fractionation processes related to water phase changes clearly take place before the interaction rainwater-soil/rock/cave atmosphere, which leaves the oxygen isotopic composition with a distinct signature that will be later analyzed and interpreted as a paleoclimatic record. However, there are other

factors that must be considered to better interpret the oxygen isotopic record from a stalagmite and the goal is to obtain the most real paleoclimatic signal (McDermott, 2004). One of these other factors that should be considered is the evaporation process of rainwater on the surface prior to infiltration of the rainwater. For instance, it is quite common that in arid/semi-arid regions an enrichment in $\delta^{18}O$ values is observed due to this effect (Lachniet, 2009; McDermott, 2004). Ultimately, the evaporative effects works amplifying the $\delta^{18}O$ variability in response to the amount of precipitation. Another factor that affects $\delta^{18}O$ values occurs prior to the water reaches the cave environment is the mixing of recharge precipitation in the vadose zone. Also called "reservoir effect" the mixing of precipitation in karst reservoir has a large effect in attenuation of the interannual isotope variability (Lachniet, 2009).

When inside the cave environment, one of the first requirements to recover $\delta^{18}O$ as a paleoclimatic data is the speleothem formation under isotopic equilibrium between the cave drip-water and the deposited carbonate, which occurs when there is time for isotopic exchange reactions to happen (Lachniet, 2009; McDermot, 2004). This equilibrium between water and precipitated $CaCO_3$ results in a speleothem that reflects the rainwater isotopic signal (McDermot, 2004). Other cave environment factors that might alter $\delta^{18}O$ signal are poor or highly ventilated caves, an atmosphere with high P_{CO_2} relative humidity and time of residence of the water before it drips (Lachniet, 2009).

The $\delta^{18}O$ variations from speleothems in southeast Brazil have being interpreted in previous works as mainly controlled by source effects driven by shifts in atmospheric circulation of a more monsoonal (extratropical) regime in summer (winter) with more depleted (enriched) values of $\delta^{18}O$, and therefore the $\delta^{18}O$ may reflect relative variations in the contribution of the sources rather than changes in total amount of rainfall. In this sense, the $\delta^{18}O$ of speleothems from Southern Brazil is as suitable proxy for studying tropical-extratropical interactions over the eastern coast of South America (Cruz et al., 2005a; Cruz et al., 2005b; Cruz et al., 2007; Taylor, 2014; Vuille et al., 2012).

5.1.3 Carbon stable isotopes in speleothems

The soil above the cave is the main source of the gas CO_2 that will interact with the rainwater and be a part of the bedrock dissolution process, and further be incorporated in the calcite deposition inside the cave, as given in the equations above. However, due the several processes

that influence the $\delta^{13}C$ variations in a speleothem record, such as vegetation and rainwater, it might be challenging to accurately understand this data (Fohlmeister et al, 2020).

The gas CO_2 in the soil comes mainly from organic matter decomposition and plant respiration, and both processes maintain the plant C isotopic signature when CO_2 transfers into the soil thus holding information about the vegetation. Thus, the carbon incorporated in the speleothems might reflect the characteristic of the vegetation above the cave (Novello et al, 2019; Silva et al, 2008; Fohlmeister et al, 2020; Amundson et al, 1998). Vegetation changes can be detected due to $\delta^{13}C$ variations according to the type and density of vegetation that occupied the area above the cave: whether the dominant plants were of a C4 photosynthetic pathway (typically savanna and grasslands), which have a lower ^{13}C discrimination in photosynthesis resulting in a $\delta^{13}C$ range between -15 to -10‰, or the dominant plants were of a C3 photosynthetic pathway (typical of dense forests) where $\delta^{13}C$ typically ranges from -30 to -24‰ (Silva et al, 2008; Fohlmeister et al, 2020; Pessenda et al, 2010).

After the soil CO_2 is dissolved in the rainwater (as in Reaction 1.), the formed DIC species percolates the soil and eventually reaches the carbonate rock, which will be dissolved until the solution is in Ca^{2+} equilibrium. This dissolution usually occurs in intermediate conditions in nature, where there is gaseous CO_2 present to form DIC species but in limited amounts, instead of enough gaseous CO_2 that allows a total carbon exchange to DIC (open conditions) or not gaseous CO_2 at all to form DIC species (closed conditions) (Fohlmeister et al, 2020; Fairchild and Baker, 2012). Also, another chemical effect controlling $\delta^{13}C$ values is the prior calcite precipitation (PCP), where there is deposition of calcite before the solution reaches the stalagmite, either in the fractures of the bedrock or already in the cave (stalactite). The degree in which PCP occurs will vary accordingly to the P_{CO_2} difference between the percolated water and the air, and to the amount of time this water stays in contact with the cave air before dripping onto the stalagmite (Fohlmeister et al, 2020; Fairchild and Baker, 2012). High PCP tend to increase the $\delta^{13}C$ of the stalagmite, once the losses of light CO_2 isotopologues during the degassing process leads the remaining DIC species depleted in ^{12}C isotopes.

5.2 Trace-Elements in Speleothems

Speleothems trace elements have been used in paleoclimate and environmental reconstructions for several years, but the wide parameters spectrum on which the fluids that form speleothems can vary and the range of geochemical processes to which they can be subjected to in

the epikarst, soil and in the cave environment hamper the definition of a common model that explains the variations in the speleothem trace elements composition (Fairchild et al., 2006; Fairchild and Treble, 2009, Bernal et al., 2016).

The development and availability of modern instrumentation allow a choice of different microbeam techniques with differences between the analysis, such as volume of material analyzed (spatial scale), precision, accuracy, speed, and cost of the analytical process). Laser ablation-ICPMS (LA-ICP-MS), secondary ionization mass-spectrometry and micro-XRF have permitted the reconstruction of high-resolution records which can be used together with $\delta^{18}O$ and $\delta^{13}C$ to complement the speleothems records. For instance, LA-ICP-MS provide a high-resolution (sub-annual resolution) for most of the speleothems and its rapid acquisition of data makes it one of the most promising techniques for retrieving speleothems trace-elements data (Treble et al., 2003; Desmarchelier et al., 2006; Fairchild and Treble, 2009; Bernal et al, 2016)

The most common elements used in speleothems studies are Mg, Sr and Ba, which form divalent cations in solution and are incorporated in the carbonate crystal lattice as a substitute for Ca. Morse and Bender (1990) describe a simple equation of partition coefficient that can be used to relate fluid and mineral composition of the trace elements:

$$\left(\frac{Tr}{Ca_{CaCO_3}}\right) = K_{TR}\left(\frac{Tr}{Ca}\right)_{solution} \qquad \textbf{Eq. 4}$$

where Tr is the trace ion and K_{Tr} is the partition coefficient (or distribution coefficient as used in some works), and it is affected by several parameters as temperature, precipitation rate, crystal morphology or fluid composition and K_{Tr} may differ significantly for aragonite and calcite, so distinguish these phases is crucial (Fairchild and Treble, 2009, Wassenburg et al, 2016; Wassenburg et al, 2019).

The primary source of trace elements and calcium in speleothems is the epikarst (bedrock, overlying regolith) and the soil, with some exceptional cases with different sources like aeolian particles, sea-salt aerosol, or flood water. The transmission of trace elements through the epikarst is dependent on the chemical mobilization in the overlying soil and fractured bedrock and by the hydrological process controlling the surface and soil waters infiltration into the epikarst (Fairchild and Treble, 2009).

Trace Elements shows a range of chemical mobilization behaviors, for instance more rapid mobilizations such as the dissolution of salts, leaching of weakly-sorbed from organic and inorganic substrate, and the virtually instantaneous entrainment of pre-existing solutes, mobilized particles and colloids, and the calcite dissolution, not rapid as the examples above, but sufficiently rapid that equilibrium would be expected within a few hours of infiltration (Fairchild and Treble, 2009).

The dissolution of carbonates to saturation occurs in response to high pCO_2 with the maximum solute loads reached in zones where Pco_2 is at a maxima, and this maxima can be reached either in the soil or the epikarst, depending on the carbonate distribution and of the decomposing organic matter. One of the key process to understand the trace elements variations happens when the infiltrating waters change from a dissolution regime to a precipitation regime, and this can be caused primarily by the encounter with a gas phase with lower Pco_2 resulting in degassing and leading to supersaturation of the solution for $CaCO_3$. This condition happens before the speleothems drip waters are exposed to the cave atmosphere (in the aquifer above the cave dripping), changing the solution composition before it reaches the speleothem, and this process is referred to as prior calcite precipitation (PCP). (Atkinson, 1977; Fairchild et al., 2000, 2007, 2009).

Once Ca is preferentially incorporated into precipitated calcite in respect to the other alkalis, the PCP leads the reaming solution enriched in Mg, Sr and Ba in respect to Ca, therefore Mg/Ca, Sr/Ca and Ba/Ca ratio of the speleothem increase (Huang and Fairchild, 2001). The effect of PCP on trace element composition has been widely used to infer dry climatic periods since the lowering of the water table in the karst aquifer and the decreasing in the stalactite dripping rate favor the PCP. Another relationship between PCP and degassing is the systematic enrichment in $\delta^{13}C$ as mentioned above. (McMillan et al., 2005; Johnson et al., 2006; Fairchild and Treble, 2009). Like PCP, the prior aragonite precipitation (PAP) is observed under certain environmental conditions. PCP and PAP are enhanced during periods of reduced aquifer recharge (drier conditions) when residence time of the solution is higher (more available time for degassing) and more air-filled voids exist in the aquifer. Wassenburg et al. (2019) showed that incorporation mechanisms are similar for calcite and aragonite, and so the application of the concept of a distribution coefficient is valid for both.

Wassenburg et al. (2019) demonstrate, for the first time, that under karst environmental conditions $K_{Mg(aragonite)}$ is considerably smaller than 1, $K_{Sr(aragonite)}$ is above or close to 1 and

$K_{U(aragonite)}$ is larger than 1. Therefore, dry (wetter) climate conditions with enhanced (diminished) prior aragonite precipitation, result in lower (higher) speleothem U and higher (lower) Mg concentrations if PAP is the dominating process. Sr may also lead to lower (higher) concentrations since $K_{Sr(aragonite)}$ is above or close to one (Wassenburg et al., 2019).

Magnesium has been used for paleohydrology reconstructions working as a proxy of effective rainfall at some sites and, despite of the complexities on its use, numerous studies have shown a forceful relationship between dripwater and/or speleothem Mg and rainfall instrumental data (Tooth and Fairchild, 2003; Treble et al., 2003; MacDonald et al., 2004; Karmann et al., 2007). The potential of speleothem Mg as a proxy of rainfall is typically proposed on its covariation with $\delta^{13}C$ and/or $\delta^{18}O$, where Mg and $\delta^{13}C$ may be modulated by the effect of PCP (due to longer residence time). Mg and $\delta^{18}O$ can also be used together to argue the effectiveness of Mg as an indicator of effective water excess, since $\delta^{18}O$ is mainly reflecting changes in rainfall, the covariance between these two variables can strengthen this interpretation. For instance, Cruz et al. (2007) and Bernal et al (2016) showed an impressive covariance between Mg (and Sr) and $\delta^{18}O$ from southern Brazil speleothems, and these trace elements variations were used as a proxy of rainfall amount, where lower of Mg/Ca values coincides with depleted $\delta^{18}O$ (depleted values are related to periods of predominant monsoonal source in the southeast of Brazil as showed in section 8). This relationship is helpful, particularly over sites where sources effects may play a significant role in the control of water rainfall $\delta^{18}O$ variability (Fairchild and Treble, 2009).

Other elements with K_{TR} <1 (Sr, Ba, U) may also be effective palaeohydrological indicators. This co-enrichment can be observed in a vector with a constant slope in a log-log crossplot of Sr/Ca vs. Mg/Ca and Ba/Ca vs. Sr/Ca. The model proposed by Sinclair et al. (2012) demonstrate that if PCP mainly modulate Mg/Ca and Sr/Ca, and in the absence of kinetic control, the molar ratios (mol Mg/mol Ca and mol Sr/mol Ca) should co-vary linearly in a ln-space, with a slope of 0.88 ± 0.13. Sinclair et al. (2011) demonstrate that the same slope is expected for Incongruent calcite dissolution, showing that these co-variations can be interpreted as water-rock interactions, and the covariance between Mg/Ca and Sr/Ca can be used as a test for PCP or incongruent calcite dissolution/ (Fairchild and Treble, 2009; Sinclair et al., 2013; Bernal et al., 2016).

The co-variance described above cannot be used for aragonite speleothems because of the different partition coefficients. In cases of PAP modulating the trace elements to Ca ratios, Mg is expected to show higher concentration during dry periods, and this relationship can be supported

by positive correlations with $\delta^{18}O$ in areas where depleted values are related to higher amounts of rainfall, and by positive correlation with $\delta^{13}C$ since PAP tends to concentrate the heavier isotope in the solution. Sr presents a K_{Sr} above or close to one and so periods of enhanced (diminished) PAP due to drier (wetter) conditions can result in lower (higher) concentrations of Sr/Ca in the speleothem. The same is observed for U, but K_U is considerably higher than 1, following the same behavior as expected for Sr (Wassenburg et al., 2019).

6. MATERIALS AND METHODS

6.1 Speleothem Samples

Laje Branca and Malfazido caves were selected for this study by its potential to record paleofloods in speleothems as detrital layers (clay or silt minerals) among the carbonate layers. Samples with active drops were selected to provide Holocene records, specially covering the last millennia. Although the stalagmites collected in Laje Branca had active drop, U/Th ages showed a hiatus in the speleothem precipitation between the present and 2000 B.P. that preclude its use for the recent period. For this study, LB-1 and CB-3 were selected for reconstructions of the Middle and Late Holocene flood frequency whereas the MFZ-N-1 speleothem was selected for the reconstruction of the past millennium flood frequency.

6.1.2 Lage Branca Samples

The stalagmites were collected in different sectors and depths of the cave in attempt to have records with different sensibility to flood events, resulting in three groups: (i) stalagmites collected in the shallow sectors; (ii) stalagmites collected in the lower gallery (CB-3) (iii) stalagmites collected in the mud gallery (LB-1). The samples from the shallow sector were not used in this study because of problems with the U/Th dating (low uranium concentration associated with low ratio of $^{230}Th/^{232}Th$) or by the absence of detrital layers within the speleothems, precluding its use as paleoflood records.

The samples CB-3 and LB-1 were selected by the presence of detrital layers within the stalagmites and high uranium concentrations associated with high ratio of $^{230}Th/^{232}Th$ of the samples that allow us to obtain ages with errors of less than 1% of 2σ. The samples showed a coeval growth through the Middle and Late Holocene covering the same period between 7400 B.P. and 2000 B.P. The different locations of the collect allow us to verify the replicability of the flood events in different sectors of the cave.

6.1.3 Malfazido Samples

Several samples were collected in the cave flood zones giving priority to active speleothems to obtain flood records of the Last Millennium, but MFZ-N-1 was the only collected sample that covers this period of time. This sample presented a high potential to be used as a high frequency flood record and for high resolution analyses by the presence of detrital layers within the speleothem and by the fastest growth rate of Southeast of Brazil as evidenced by a well-solved chronology based on U/Th ages with errors of 1% of 2σ.

6.2 Instrumental Data

6.2.1 U/Th Ages

For the chronologic analyzes, a Dremel rotatory tool attached to a flexible cable shaft was used to drill the carbonate samples from the speleothem. The dark layers were avoided during sampling as they could be a source of ^{232}Th from the clay minerals. $CaCO_{3(s)}$ samples of approximately 0.1 g were collected and the powder was kept in glass vails. The depth in relation of the speleothem top was measured using a scan image of the speleothem and the software CorelDraw 2019.

The chemistry procedures used for the sample opening and concentration of U and Th consist in 3 steps: (1) weight, spiking and dissolution; (2) Fe precipitation, centrifuge, dissolution; (3) columns.

(1) – First step in the chemistry procedure is to weight the sample. The amount of sample powder that will be weighted is based on the concentration of ^{238}U and ^{234}Th. If the speleothem does not have ages, 0.5 g of sample is utilized. The sample is weighted in a Teflon beaker using a high precision balance. After weighting, a small amount of water is added to cover the powder and avoid loss of mass and contamination in the laboratory. Then the sample is dissolved using between 3 and 6 drops of 7N HNO_3 and its ready for the spike addition. The spike (solution content ^{236}U – ^{233}U – ^{229}U) mass added to the sample depends on the samples mass and the ^{238}U concentration. For MFZ-N-1 all the samples were spiked using an approximately mass of 0.5 g. After spiking the sample, 4 drops of $HClO_4$ (the number can vary between 4 to 15 depending on the content of organics in the sample) are added and the Teflon beaker is closed and set on a hot plate at 150 °C for 30 minutes to reflux. The reflux step is used to improve homogenization of the solution. The last procedure of this step is a completely dry down of the solution in the hot plate at a temperature between 200 C° and 203 C° for 3 to 6 hours until a milky solid be formed.

(2) – After the completely dry down, the milky solid is dissolved with 2N HCl, and the solution is transferred to a centrifuge tube with 2 drops of Fe solution. To precipitate the heavy

elements 4 to 10 drops of NH_4OH (ammonia) are added, and the sample is centrifuged for 7 minutes at 2600 rpm. After the first round of centrifuge, the supernatant is discarded. Two more rounds of centrifuge with SC (super clean) water are made and at the end of the last centrifuge round, the precipitated is dissolved with 7N HNO_3. The solution is transferred again to the Teflon beaker put to dry down completely on the hot plate at 200 °C until a solid with sub-millimetric dimensions is deposit at the bottom of the beaker. The precipitated is dissolved with 2 drops of $HClO_4$ and put to dry down. After drying down, the sample is dissolved again with 1 drop of 14N HNO_3 and the solution is put to dry down again. The procedure with 14N HNO_3 is repeated 2 times and then is added some drops of 7N HNO_3. After this step, the solution is ready for the ion exchange columns.

(3) To collect the Th and U, 8 cm columns with SPECTRA/GEL® ION EXCHANGE 1x8 resin are prepared with 2 steps: (i) SC water is added until fill all the column volume two times, with 1 drop of 14N HNO_3 in the second time; (ii) added 2/3 of the column volume with 7N HNO_3 for two times.

After the resin preparation is done, the sample solution is poured in the columns and the elution of the reagents is made according to the following steps: (a) after the sample is absorbed by the column, the column is filled with 2/3 of volume with 7N HNO_3, then the same procedure with 1/3 of volume. The solution collected in this step is discarded and a clean beaker is used to start the Th collection. (b) To collect the Th the column is filled 2 times with 2/3 of volume of 6N HCl. After the solution is collected, the clean beaker is closed, and the Teflon beaker used on the chemistry previous steps is put under the column to start the U collection. (c) The U collection is made by filling the column with SC water two times.

When the collection is finished, 1 drop of $HClO_4$ is added to the solutions and the beakers are put to dry down on the hot plate in 203 °C. After dry down completely, a sub-millimetric solid is precipitated. After this step, the solid is dissolved and the solution is put to dry down for more 3 times, being the first time dissolved with $HClO_4$ and the last two times with 1 drop of 14N HNO_3. On the last step of the chemistry procedure, ICP-MS standard solution (SC water with 1% of 14N HNO_3 and 60 drops of HF) is added and then the solutions are ready to be analyzed on the ICP-MS mass spectrometer.

The dates were analyzed using an ICP-MS (Inductively Coupled Plasma Mass Spectrometry) mass spectrometer, Finnigan Elements and Finnigan Neptune Type according to the procedures stablished by Shen et al., 2002, and the age calculations were made based on Edwards et al. (1986) and Richards & Dorale (2003) using the isotopic ratios measured and corrections factors to eliminated effects of contamination by detrital Th.

The first set of samples was sent to the Institute of Global Environmental Change at Xi'na Jiaotong University (China) where 13 samples were dated. The second set of samples was sent to the Geochronology Laboratory of the University of Minnesota in the United States where other 35 samples were dated during a three month research internship abroad program (BEPE) funded by FAPESP process number 2019/02791-1.

6.2.2 Detrital Layers and Paleoflood Frequency

To build a flood chronology for the speleothems we considered the detrital layers visually recognized as the result of deposition of fine-grained sediments suspended by floodwaters, interpreted here as individual flood events. To build an accurate stratigraphy for the detrital layers it was used scan images of the speleothems polished face and the software CorelDraw to measure the depth between the top of the speleothem and the interception of each detrital layers with a guide profile defined by the growth axis of the speleothem allowing us to build a flood chronology by the linear interpolation between U/Th ages and the detrital layers depth. The frequency of the cave-floods was calculated by the number of events (or detrital layers) contained in a defined time bin. For the low frequency floods of Middle and Late Holocene, it is used 500-year, 200-year and 100-year bins and for the high frequency floods from the Last Millennium it's used 100-year, 50-year and 10-year bins.

6.2.3 Proton induced X-ray emission (PIXE)

Proton induced X-ray emission (PIXE) analyses were performed in MFZ-N-1 at the Laboratory for Material Analysis with Ion Beams of the University of São Paulo using a 1mm diameter external beam in 1mm steps, resulting in 220 points of analyses of the elements Al, Si, Fe, Ca, Ar, Ti, Mn, Ni, Cu, Zn, Sr and Ba. These analyses were realized to characterize the geochemical properties of the detrital layers from MFZ-N-1 and to investigate whether PIXE analyses can detect these layers in stalagmites sections and so be used as a quick, non-destructive method to detect flood layers within speleothems as it only requires a flat surface that was previously obtained for other analyses.

6.2.4 Stable Isotopes Analyzes

The samples were collected using a micromill with a drill diameter of 0.15 mm following steps of 0.2 mm, collecting approximately 0.2 mg of $CaCO_{3(s)}$ per sample. After drilling the samples

were collected using a pair of Hollenbeck and the powder was kept in a glass vial with a septum cap. The sampling follows the most central point of the speleothem growth axis to avoid the collection of samples potentially subjected to kinetic fractionation.

The samples were analyzed at the Stable Isotope Laboratory (LES) of the Center of Geochronology Researches (CPGEO) in the Institute of Geoscience of the University of São Paulo (IGC-USP), with the use of a gas source mass spectrometer, model Delta Plus Advantage (ThermoFinnigan) coupled to a Finnigan Gas-Bench II automatic sample preparation system. The basic principle of the analytical procedures for obtaining the ratios of the isotopes of O and C consists of the analysis of carbon dioxide ($CO_{2(g)}$) product reaction of $CaCO3_{(s)}$ of calcite and/or aragonite with $H_3PO_{4(l)}$ with a concentration close to 100% in a reactor under controlled temperature at 72 °C, from acid hydrolysis. The released $CO_{2(g)}$ is transported by a neutral carrier gas ($He_{(g)}$) to the Finnigan Gas Bench accessory, where it is separated from the water vapor among other gases by a gas chromatography system, just after the resulting $CO_{2(g)}$ is ionized and accelerated for separation by mass, the whole procedure being automatic.

The determination of the isotopic ratios is made through an ionic source in a triple collector of C and O, where the analytical results are based on the analyzes of nine sequential aliquots of each sample. The analytical precision is approximately 0.08 ‰ for the values of isotopic ratios of $^{13}C/^{12}C$ and ± 0.1 ‰ for the values of $^{18}O/^{16}O$ for samples with a minimum mass of 100 μg of $CaCO_{3(S)}$.

The isotopic ratios are expressed through the notation δ, defined by the difference between the ratio measured in the sample and the reference standard, divided by the reference standard ratio (Eq.2). The international standard VPDB (Vienna Pee Dee Belemnite) utilized for carbonate rocks was utilized for the analyzes. The analyzes were performed in sections of 64 samples, with one standard sample for each six stalagmites powder sample. The $\delta^{18}O$ and $\delta^{13}C$ values are expressed in permil (‰) in relation with the reference standard to facilitate the interpretation of the stable isotope's ratios and the comparison with different records. The equation Eq.5 and Eq.6 shows the expression for the $\delta^{18}O$ and $\delta^{13}C$ values, respectively.

$$\delta^{18}O = \frac{\left(\frac{^{18}O}{^{16}O}\right)Sample - \left(\frac{^{18}O}{^{16}O}\right)Standard}{\left(\frac{^{18}O}{^{16}O}\right)Starndad} \quad \text{or} \quad \delta^{18}O = \frac{\left(\frac{^{18}O}{^{16}O}\right)Sample}{\left(\frac{^{18}O}{^{16}O}\right)Starndad} - 1$$

$$\delta^{18}O\ (‰) = \left[\frac{\left(\frac{^{18}O}{^{16}O}\right)Sample}{\left(\frac{^{18}O}{^{16}O}\right)Starndad} - 1\right] x\ 1000 \quad \textbf{Eq. 5}$$

$$\delta^{13}C\ (‰) = \left[\frac{\left(\frac{^{13}C}{^{12}C}\right)Sample}{\left(\frac{^{13}C}{^{12}C}\right)Starndad} - 1\right] x\ 1000 \quad \textbf{Eq.6}$$

6.2.5 Trace Elements Analyzes

The speleothem MFZ-N-1 was analyzed at the ELA-ICP-MS Laboratory of the Centro de Geociencias of the Universidad Nacional Autonoma de Mexico in collaboration with the Professor Juan Pablo Bernal. For the analyzes was used an Excimer Laser Ablation Inductively Coupled Plasma Mass Spectrometry (ELA-ICP-MS) Thermo X-Series II ICP-MS model fabricated by Resonetics LLC equipped with a two-volume ablation cell.

The laser ablation dispositive use an *excimer laser* Lambda–Physic (LPX) with a length wave of 193 nm and a laser fluence of 5-6 J/cm^2 that run through the blocks with a sampling frequency of 5 Hz and a velocity of 0.8mm/min, using a rectangular 200 x 20 µm laser beam parallel to the stalagmite banding. Before the analyses, the blocks were pre-ablated with the same laser characteristics to avoid any eventual contamination. After ben ablated, the material is loaded by a Helium flux and analyzed as a plasma by the mass spectrometry (ICP-MS).

The ICP-MS was programmed to quantify the following elements/isotopes: ^{7}Li, ^{23}Na, ^{24}Mg, ^{29}Si, ^{30}Si, ^{31}P, ^{44}Ca, ^{46}Ca, ^{47}Ti, ^{48}Ca, ^{51}V, ^{52}Cr,^{53}Cr, ^{57}Fe, ^{66}Zn, ^{88}Sr, ^{89}Y, ^{137}Ba, ^{138}Ba ^{139}La, ^{140}Ce, ^{141}Pr, ^{206}Pb, ^{208}Pb, ^{232}Th e ^{238}U. The Element/Ca molar ratios were obtained by external standardization to NIST SRMs 612 glass by grouping the analysis of which block with a 60 s analysis of the glass standard.

For these analyses the opposite slab of the isotope analyses was cut along the growth axis in 3 blocks named as A, B and C with length of 80.62 cm, 66.70 cm and 63.40 cm respectively, with a width of 23 mm and thickness of 8 mm. Each block was cut diagonally respective to the banding to minimize the amount of material lost during and mainly to the last few millimeters of the ablation track of each block overlapped with the first few millimeters of the next block, allowing to obtain an uninterrupted trace element record. For the 3 blocks, 30278 points of analyzes were

made resulting in a mean of 137 points of analyses per mm and by the interpolation with the U/Th ages a mean of 37 points per year.

6.3 Statistical Analyzes

One of the methods to analyze the isotopic data obtained from the stalagmites will be the use of temporal series processing, which can provide a series of fundamental characteristics of the record and thus lead to better understanding about past features of the system in place. The paleoclimatic records usually present a discrete behavior, which consists in a continuous series considering equal time intervals (Δt), whereas for speleothems this time resolution is the distance from one point to the next. Once speleothems have different growth rates throughout time, an interpolated series is made for each isotopic segment between two U/Th dating, which makes the final record a composite of all these temporal series.

Therefore, the analysis of temporal series based on isotopic records aims to determine several features contained in the record, such as the periodic/random behavior, the frequency in which these periodicities occur and when these occurrences were more intense, and the statistical correlation between two time series or other proxies either referring to similar frequencies or similar behavior throughout time.

To obtain this kind of information from the isotopic data, two main statistical methods were used. First, to obtain the REDFIT analysis, the isotopic record must be interpolated in an evenly spaced time interval, usually the record average resolution. REDFIT is a function that obtains the spectral density of the data, averaging the spectra when splitting the time series into several segments and overlapping by 50%, reducing noise but also spectral resolution. This analysis yields the frequency by time spectra, which can be turned into periodicities when dividing the average time resolution of the record by the correspondent frequency (Hammer, 2019; Schulz & Mudelsee, 2018). The significance tests (from 95% to 99%) are made based on the chi^2 method (Ghil et al., 2002) and when the power of determined frequency goes beyond these significance lines, that data is considered as a relevant periodicity for the record.

The other statistical analysis here used is the wavelet transform, where the main point is to verify the record for occurrence and intensity of small, intermediate, and large scales periodicities (y axis) simultaneously over the given period (x axis). Once the y axis of this plot is a logarithmic size scale of base 2, the plot goes from more detailed view of the record on the top to a more smoothed general view towards the bottom. Also, a color scale is set to address the signal power,

or events intensity, going from more intense (red) to less intense (blue). The plot "cone of influence" is relevant to show where boundary effects are present (Hammer, 2019).

6.3.1 Cross-wavelet analysis

The cross-wavelet analysis is applied when there are two time series that might be somehow connected and it's necessary to verify "whether regions in time frequency space with large common power have a consistent phase relationship and therefore are suggestive of causality between the time series" (Grinsted et al., 2004). This method will then evidence their power and phase similarities in a time-frequency space and the cross-wavelet transform can thus be described as:

$$W^{XY} = W^{X} W^{Y^{*}} \qquad \textbf{Eq. 7}$$

where Wx is the wavelet transform of a time-series Xn, the Wy is the wavelet transform of a time-series Yn, and the "*" stand for the complex conjugation of the transform, and finally Wxy is understood as the common relative phase in time frequency space shared between the two time series (xn and yn). Also, the outcome presents arrows as indicative of whether the time series are in phase (arrows pointing right) or anti-phased (arrows pointing left) in that particular time frequency (Grinsted et al., 2004).

For this study, several combinations were made to understand the common features between the $\delta^{18}O$ of Malfazido cave and climate modes that can affect the area of study. These cross-wavelet analyses were made using the software MATLAB with routines based on the studies of Grinsted et al. (2004) and Torrence and Compo (1998).

6.3.2 PCA analysis

Principal component analysis (PCA) is one of the most popular multivariate statistical technique and is broadly used in almost scientific disciplines. PCA can simplify exploration of larger multivariate datasets by finding hypothetical variables (components) that can represent as much as possible of the variance of the data. The components are linear combinations of the original variables (Hammer et al., 2001; Abdi and Williams, 2010; Jamieson et al., 2015).

The reduction of the data set to components using PCA may be useful for speleothems trace elements (LA-ICP-MS) since these larger multivariate data set can pose difficulties for analysis and interpretation since the element concentrations can be affected by several processes on various timescales and magnitudes. Thus, PCA analysis can identify different modes of trace elements

variation within a time series, allowing the deconvolution of signals of dominant process from the background variation in a multivariate trace element dataset (Jamieson et al., 2015).

In the context of speleothems, Jamieson et al. (2015) used PCA analysis of high resolution trace elements datasets (LA-ICP-MS) to detect the signal of volcanic ash deposition in a Belizean stalagmite, suggesting that PCA can be a valuable tool for identifying dominant controls on trace element chemistry of stalagmites. This approach is used here in MFZ-N-1 and CR-1 trace elements records to identify modes and timing of variations that account to the overall variability of the high-resolution datasets.

The PCA analysis were performed in the software Past 4.0 following the procedure described in Hammer et al. (2001). For the input, the trace elements series were normalized by calculating the z-scores of each dataset by subtracting the record mean of each value and dividing for the deviation standard (y¬anomaly = (y – ymean)/y(sd). The following trace elements ratios with Ca were used in this analysis: Mg/Ca; Sr/Ca; Ba/Ca; U/Ca. In every PCA analysis, the bootstrapping statistical procedure (dataset resampled 9999 times to perform hypothesis testing and a 95% confidence interval) and the broken stick model (to determine which PCA presents statistical significance higher than 95%) were performed.

7 RESULTS

The results from this work will be presented here according to the timescales of the speleothems used in this research, therefore MFZ-N-1 and CR-1 records will be described in section **7.1**, and LB-1, CB-3, TP-6 and CR-1 in section **7.2.**

7.1 Last Millennium

7.1.1 Geochronology result and growth rates

In the total, in this study, 52 U/Th dates was performed for speleothems from Malfazido cave and 16 for speleothems from Varzeão cave. For the Last Millennium reconstructions, we used the stalagmite MFZ-N-1 from Malfazido cave with 19 U/Th ages and compiled the data from CR-1 stalagmite from Cristal cave described in Taylor (2014). Figure 4 shows the age distribution of the speleothems from Malfazido cave, Varzeão cave and CR-1 with a zoom in the Last Millennium.

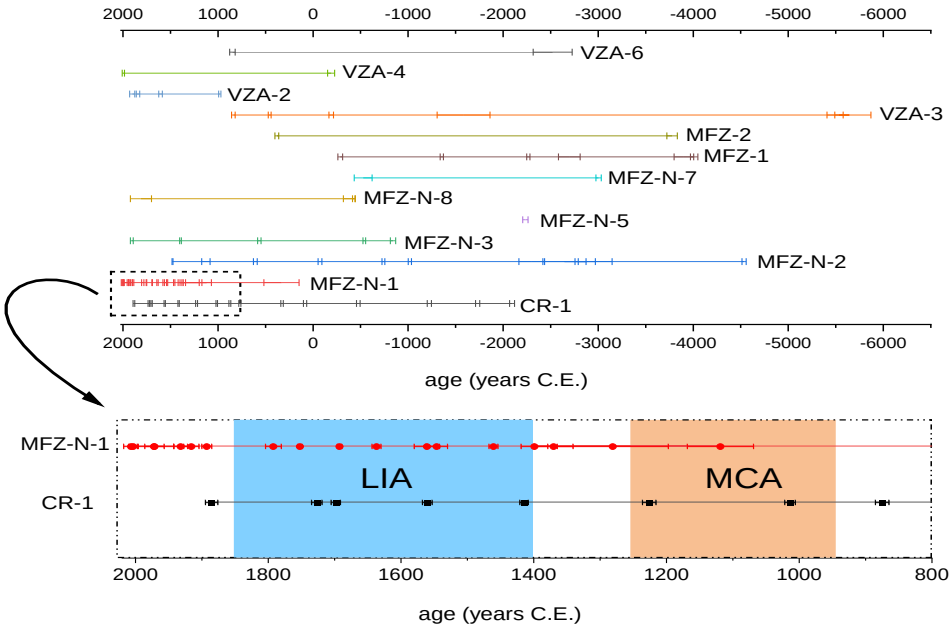

Figure 4 - Age distribution from Malfazido and Varzeão speleothems. Not all the samples showed in the figure were used in this research as described in the text. In the bottom the detail of the Last Millennium with the ages and error bars of MFZ-N-1 and CR-1. MFZ (Malfazido cave sample); VZA (Varzeão cave sample); CR-1 (Cristal cave samples). The blue box indicates the Little Ice Age period (LIA) and the orange box the Medieval Climatic Anomaly (MCA).

MFZ-N-1 is a continuous record covering the last 500 years with a continuous growth rate since the year of 1280 CE to the present (Fig. 5). The base of the speleothem reaches older ages but the high concentration of detrital ^{232}Th from the dark brown layers of clay hamper the U/Th analyses by raising the errors and lowering the accuracy of the ages. The high concentration of clay layers in the base of the speleothem is here described as a hiatus by the significant difference between the growth during the last millennium and this period.

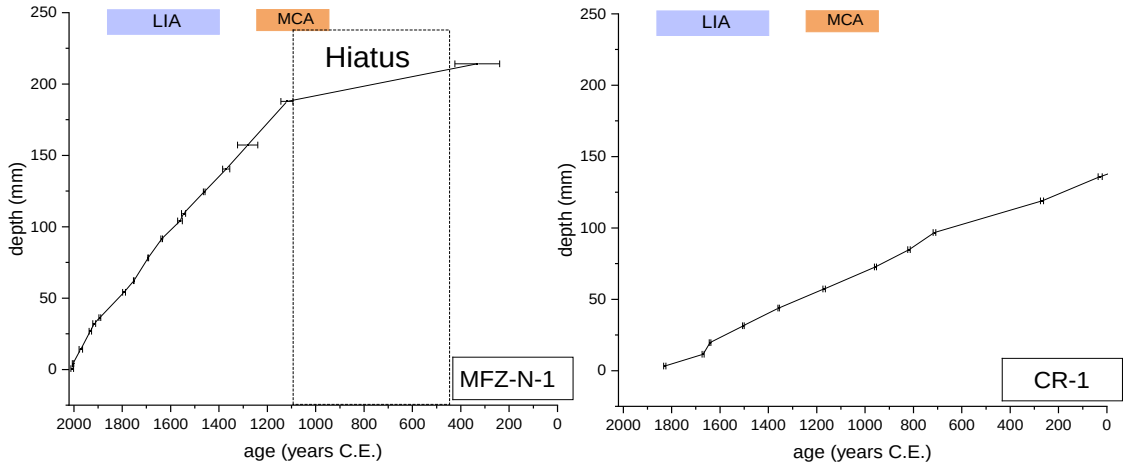

Figure 5 - Age models of MFZ-N-1 (left) and CR-1 (right). Horizontal bars represent the 2σ errors of the U/Th ages.

The last millennia starts with a hiatus in MFZ-N-1, marked by a high sequence of clay layers in the speleothem. It starts to grow effectively at the end of MCA with a median growth rate of 0.18 mm/years between 1119 C.E. and 1547 C.E. (Fig. 6). During LIA it is observed a punctual and abrupt increase in the growth rate to 0.34 mm/year between 1562 C.E. and 1693 C.E and a second increase in the values is observed between 1619 C.E. and 1795 C.E. with the growth rates going up to 0.26 mm/year, matching with a punctual increase in CR-1 growth rates between 1642 C.E. and 1670 C.E. The end of LIA is marked by a decrease in the growth rate to the mean value of the record followed by an abrupt increase to the fastest growth rates of the record reaching up to 0.33 mm/year in the last century to the present.

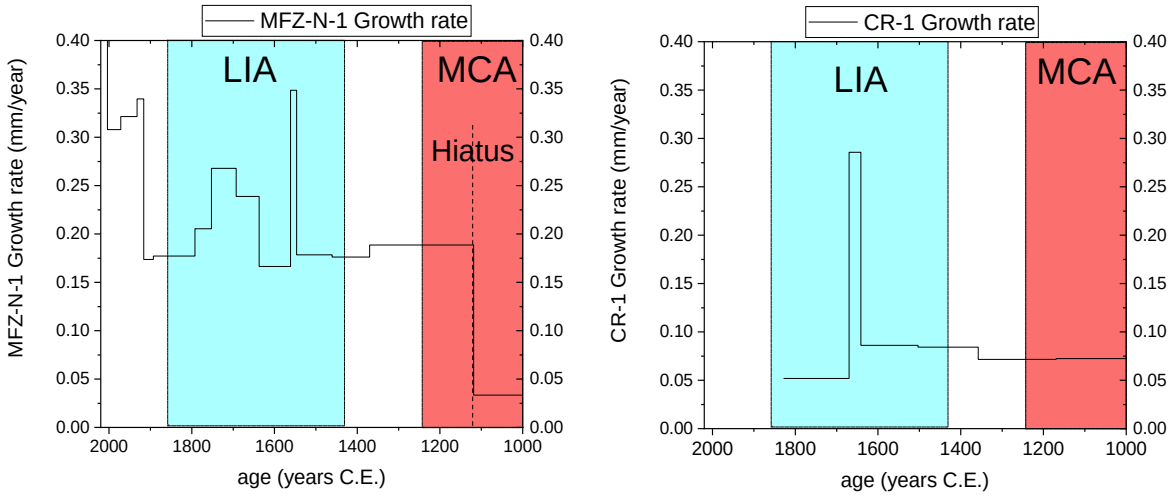

Figure 6 - Growth rates from MFZ-N-1 (left) and CR-1 (right). The colored bars represent the period of Little Ice Age (LIA) a Medieval Climate Anomaly (MCA)

7.1.2 Stable isotopes analyses

The MFZ-N-1 stable isotope record newly obtained allows us to describe the last millennium climate changes during the Little Ice Age (LIA) and the Medieval Climate Anomaly (MCA) in high-resolution with nearly annual resolution, which can resolve interdecadal to multidecadal climate variability. In addition, the CR-1 record from Southern São Paulo State was used for the regional comparison (Taylor, 2014).

Table 1 – Ensemble of the speleothems used for the last millennium.

Cave	Speleothem	Records	N. analyses	Mean Resolution
Cristais	CR-1	$\delta^{18}O$ and $\delta^{13}C$	562	3 yrs
Malfazido	MFZ-N-1	$\delta^{18}O$ and $\delta^{13}C$	1075	1.5 yrs

Malfazido $\delta^{18}O$ record can be divided in four major periods with distinct variability: (1) Medieval Climate Anomaly (MCA) from 950 to 1200 C.E.; (2) Transitional period (between MCA and LIA) from 1200 to 1400 C.E.; (3) Little Ice Age (LIA) between 1400 C.E. to 1850 C.E.; (5) Current Warm Period (CWP) between 1850 to the present (Fig. 7). The terms enriched and depleted are used here to refer to less and more negative values of $\delta^{18}O$, respectively.

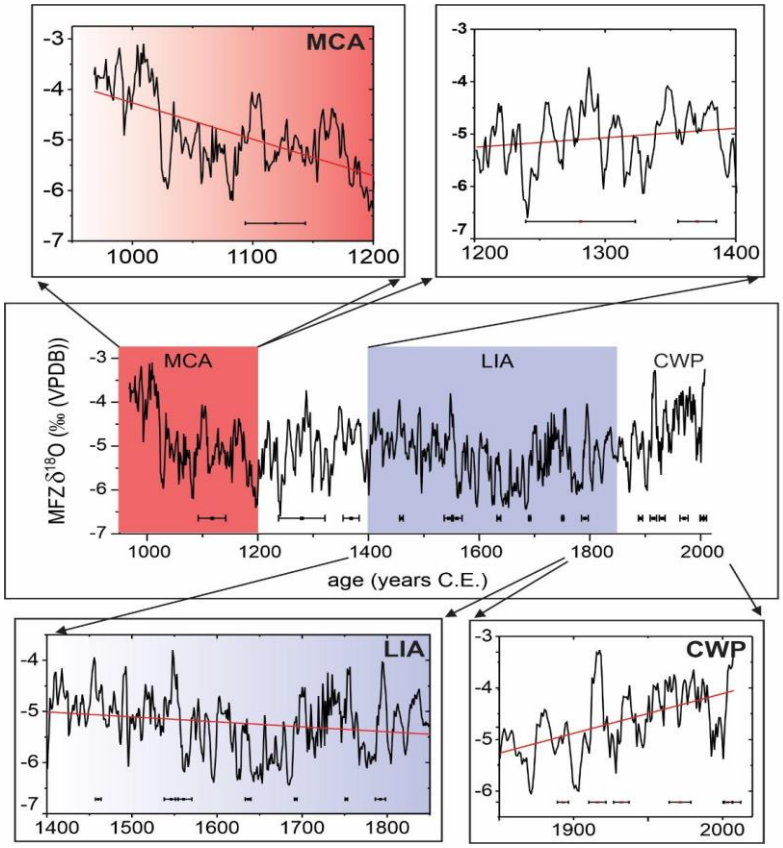

Figure 7 - $\delta^{18}O$ record from MFZ-N-1. The record is divided in four periods (MCA, transition with LIA, LIA and CWP). Each period is showed in a detailed graph. The red lines represent the linear adjustment to the series for those periods.

The record shows a mean value of -5.02‰ with a standard deviation of 0.65‰ varying with great amplitude between -3.0 and -6.6‰. During the MCA the $\delta^{18}O$ record is characterized by a negative trend towards more depleted values and by an abrupt drop in the values, but the period between 950-1020 C.E. has the most enriched values of the entire record (mean of -3.43‰). This period represents the base of the speleothem were the high concentration of detrital layers makes it difficult to obtain precise U/Th ages, thus making the interpretation of the abrupt drop more challenging since this can be caused by a hiatus in the speleothem deposition. After this, the values display a negative trend until it reaches the most depleted values of MCA in 1200 C.E.

The transition period between MCA and LIA, the record has a mean of -5.06‰ and varies between -6.6‰ and -3.72‰ with a slight trend towards more enriched values until almost the middle of LIA (1550 C.E.). Strong decadal excursions up to 2‰ to more depleted and enriched values mark this period, and the most negative value of the record is reached in 1240 C.E. with -6.6‰.

The period between the beginning of LIA until 1550 C.E. has a mean of -4.89‰ and its more enriched than the end of MCA. A drop in the mean value after 1550 C.E. starts the most depleted period of the record between 1550-1690 C.E. with a mean of -5.67 ‰ reaching -6.43 ‰. This depleted period ends with the increase of the $\delta^{18}O$ after 1690 C.E. A second drop in the values of $\delta^{18}O$ is observed between 1755 C.E. and 1827 C.E. were the record reaches a mean of –5.38 ‰. During this period, two decadal excursions (1787-1797C.E.; 1807-1817C.E.) to more enriched values increase the $\delta^{18}O$ up to 2‰. A positive trend towards more enriched values of $\delta^{18}O$ mark the CWP as the period with the most enriched values of the last millennia after the drop in 1020 C.E. observed in the MCA. This period also shows decadal excursions varying between 1-2‰ and reaches the most enriched value in the end of the record in 2007 C.E.

The comparison of $\delta^{18}O$ records from MFZ-N-1 and CR-1 shows a good visual correspondence between the records, with the MFZ-N-1 showing higher variability in the decadal scale (Fig, 8). The most depleted period of CR-1 during the last millennium matches with MFZ-N-1 depleted period between 1550 C.E. and 1700 C.E. The trend towards more positive values is also observed in CR-1 after 1800 C.E. This comparison indicates that MFZ-N-1 record has a regional sensibility to climate variations and can be used to discuss convective atmospheric process.

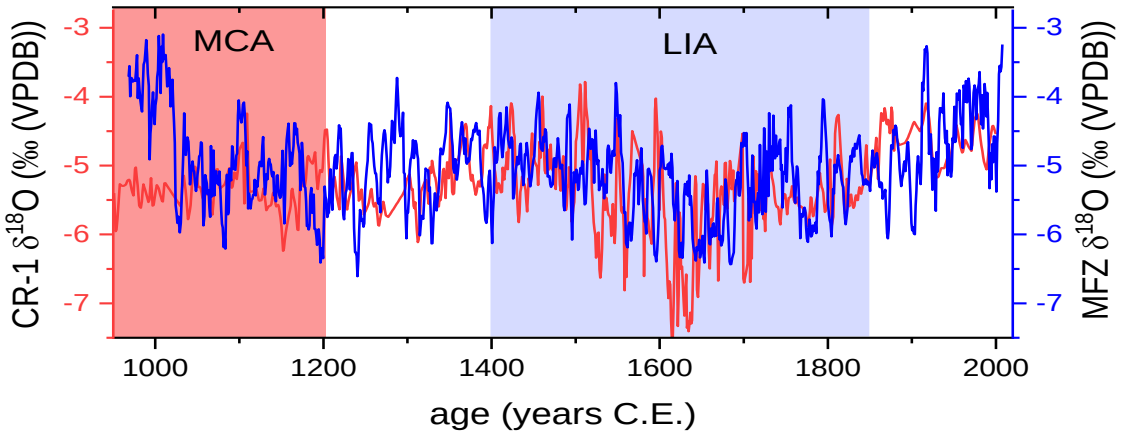

Figure 8 - Comparison between MFZ-N-1 (blue timeseries) and CR-1 (red timeseries) $\delta^{18}O$ records.

The $\delta^{13}C$ record of MFZ-N-1 shows a consistent variation with the $\delta^{18}O$ (Fig. 9). As demonstrated in Figure 9 both $\delta^{18}O$ and $\delta^{13}C$ presents a strike resemblance along speleothem record. The $\delta^{13}C$ values of MFZ-N-1 varies from -8 to -5 ‰, except close to the bottom of the speleothem. In general carbon and oxygen isotopes describes similar variations at decadal to centennial timescale. A major decoupling, however, is recorded at the of the speleothem, after the decade of 1990s.

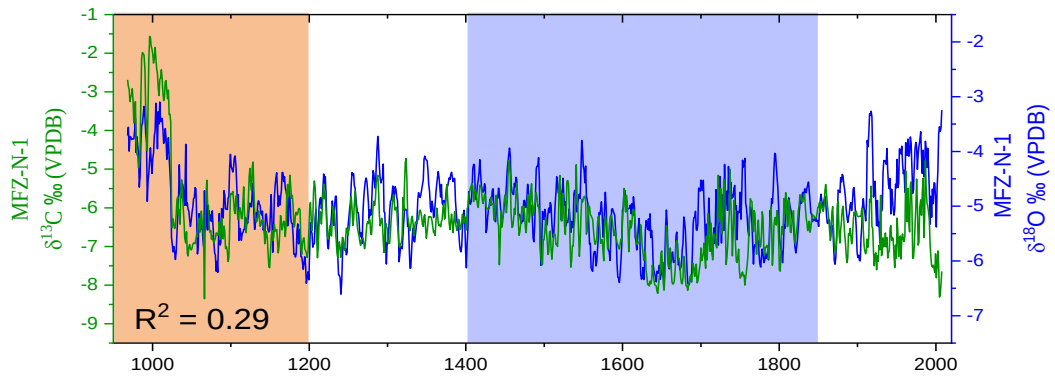

Figure 9 – Comparison between $\delta^{18}O$ and $\delta^{13}C$ of MFZ-N-1 record.

A monthly precipitation series from GPCC is used for comparisons with the $\delta^{18}O$ record for the recent period (Fig. 10). For the comparisons, the annual rainfall accumulation, the summer (ONDJFM) and winter (AMJJAS) accumulations were used to describe the changes in the isotope composition of monsoon and extratropical rainfall, respectively (Cruz et al., 2005b). The annual and winter precipitation series shows a non-significant correlation of with the $\delta^{18}O$ for the period of 1935 and 2007 (R lower than 0,15). In comparison, the summer precipitation shows a negative correlation of with $\delta^{18}O$ (R = -0.32) as it could be seen in the Fig. 10. These results show that depleted (enriched) values of $\delta^{18}O$ are related to more (less) summer contribution on the annual precipitation, which agrees with previously $\delta^{18}O$ published studies for the Southeast of Brazil (Locosselli et al., 2020).

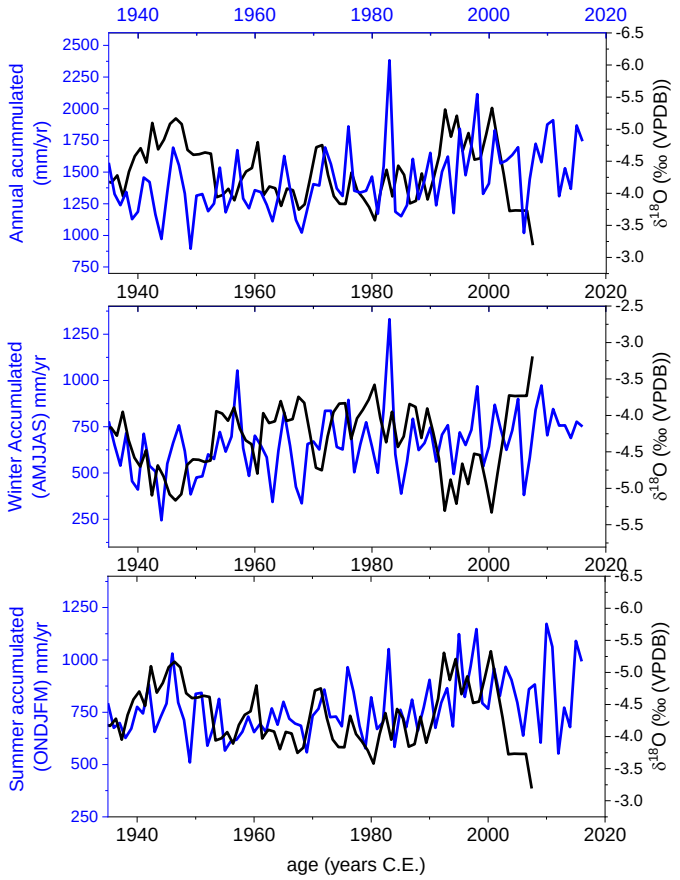

Figure 10 - Comparison between MFZ-N-1 $\delta^{18}O$ record and precipitation series from GPCC.

7.1.3 Redfit and Wavelet analyses

In this section it is presented the results from the statistical analysis (described in section **6.3)** of the MFZ-N-1 $\delta^{18}O$ data. Cross wavelets analysis were used to examine the relations between the $\delta^{18}O$ time series and the climate indexes AMO, NAO, PDO, IPO and Niño modes.

Figure 11 shows the Redfit spectral analysis of the $\delta^{18}O$ data from MFZ-N-1. In a multidecadal scale it was observed periodicities of 29, 19-17 and 11 statistically significant at 95% and periodicities of 31 and 13 significant at 99% confidence levels. Decadal and sub decadal periodicities of 11, 9 and 5 years are also significant at 95%, while interannual periodicities like 7, 3 and 2 years are significant.at 99% levels.

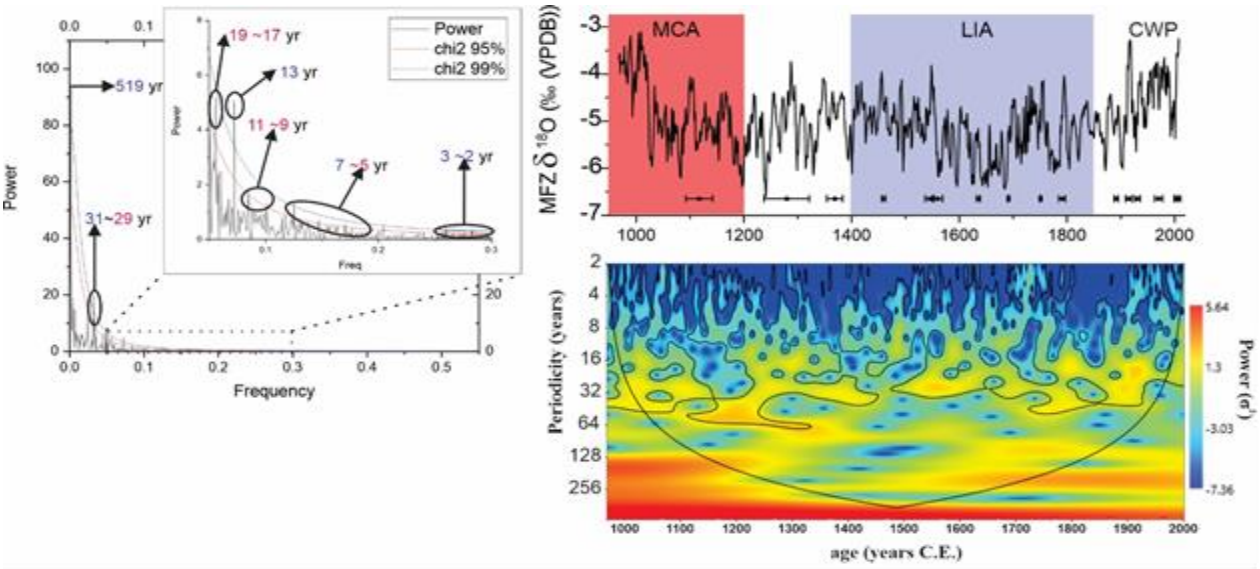

Figure 11 – On the left is the Redfit spectral analysis of MFZ-N-1 $\delta^{18}O$ data equally spaced in 2 years, where the numbers pointed by the arrows represent the most significant record frequencies, where red (blue) numbers represent 95% (99%) statistic reliability. On the top right is the MFZ-N-1 $\delta^{18}O$ record and the position of the U/Th ages with their 2σ error bars. On the bottom right of the Figure is the wavelet analysis for MFZ-N-1 $\delta^{18}O$ record where the y axis represents the periodicities values, the x axis the time interval from the analyzed record, and the color index related to the intensity of the event, being red (blue) for more (less) intense. The outline in black indicates the events that have statistical significance higher than p=0.05. The conic section indicates the data reliance for the areas inside the cone.

Wavelet analysis of climate index reconstructions were performed to recognize the periodicity of those indexes (Fig. 12). All the indexes show some similarity in the periodicities with the ones in MFZ-N-1 $\delta^{18}O$ data. Therefore, the most significant periodicities observed for the indexes that are also in agreement with the ones in MFZ-N-1 are multidecadal-decadal periodicities between 32 to10 years observed in all indexes (AMO, both PDOs, IPO, NAO and Niño 3) and sub-decadal periodicities between 9 to 4 years can be observed in two indexes, the PDO (Biondi et al. 2001) and the Niño 3 index (Conroy et al., 2010).

The results of the cross-wavelet analysis of $\delta^{18}O$ and the reconstruction index time series are presented below with a comparison between the time series. The warmer colors (closest to yellow) indicate a higher relationship between the records in a temporal interval for a periodicity, and the areas marked by a black line include the events with statistical significance higher than 95%. The black arrows indicate the if the records are in phase (antiphase) when it is pointed right (left).

The cross-wavelet of $\delta^{18}O$ and PDO index from Mann et al (2009) shows an interval between 1300 and 1800 C.E. limited by the influence cone with the periodicity of 256 years well marked by a continuous band and the arrows indicate that the records are in phase (Fig.13). This periodicity does not show correspondence in the Redfit and wavelet analysis and it's probably

caused by a secular trend common to both records with the visual fit in a multidecadal scale of the series from 1500 C.E. to the present. The cross-wavelet also shows some specific periodicities from 16 to 5 years between 1300-1450 C.E. and a small interval closest to 1950 C.E.

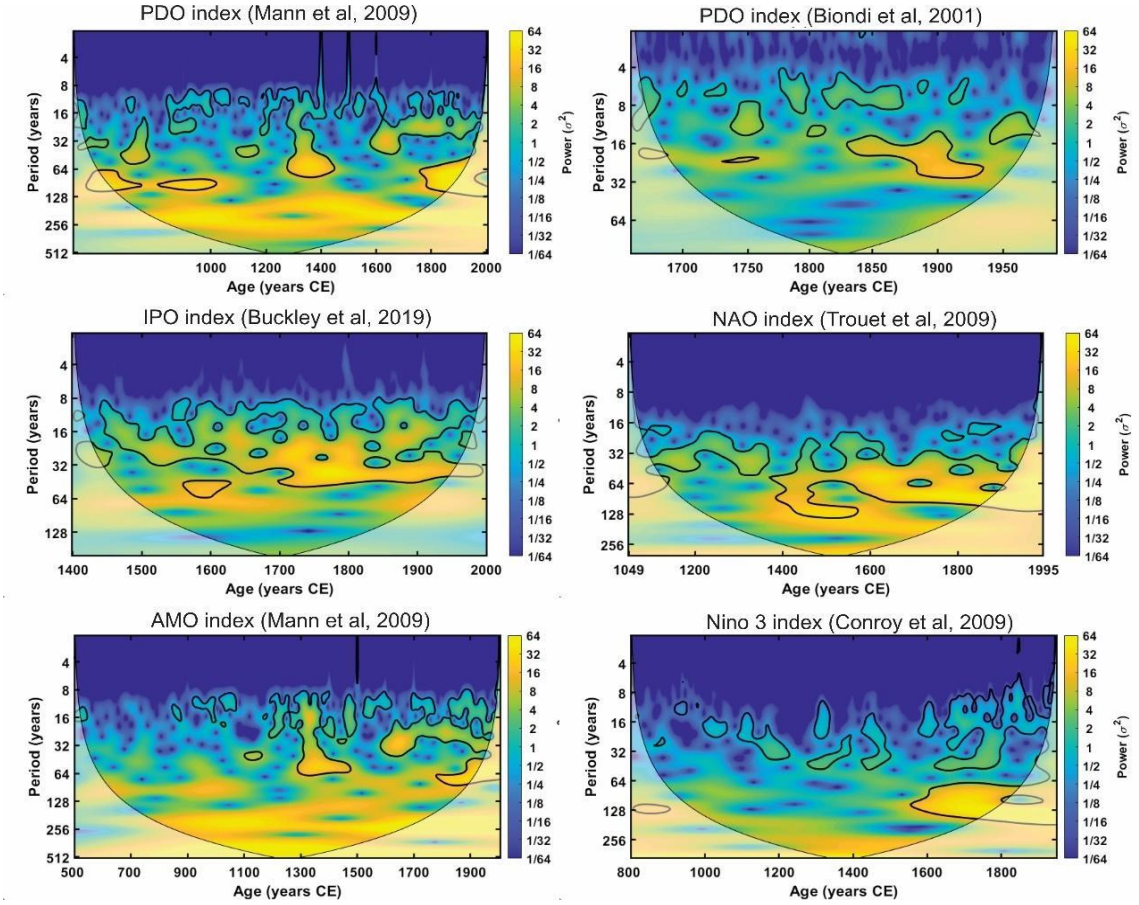

Figure 12 - Wavelet analysis for the indexes (PDO, IPO, NAO, AMO, Niño 3) where the y axis represents the periodicities values, the x axis the time interval from the analyzed record, and the color index is related to the intensity of the event, with yellow (blue) for more (less) intense. The outline in black indicates the events that have statistical significance higher than p=0.05. The conic section indicates the data reliance for the areas inside the cone.

For the PDO from Biondi et al (2001) and $\delta^{18}O$, the cross-wavelet analysis does not show an expressive interval with high coherence (Fig. 14). The periodicity of 30 years is marked between 1890 and 1935 C.E. with the arrows showing the series in phase. Two intervals with the periodicities between 16 and 10 years were observed between 1735-1765 C.E. (antiphase) and between 1940-1960 C.E. Periodicities between 8 and 4 are observed punctually in 1700 C.E., between 1750-1800 C.E. and 1890 C.E. With exception to some specific and short intervals, the series do not show a good coherence.

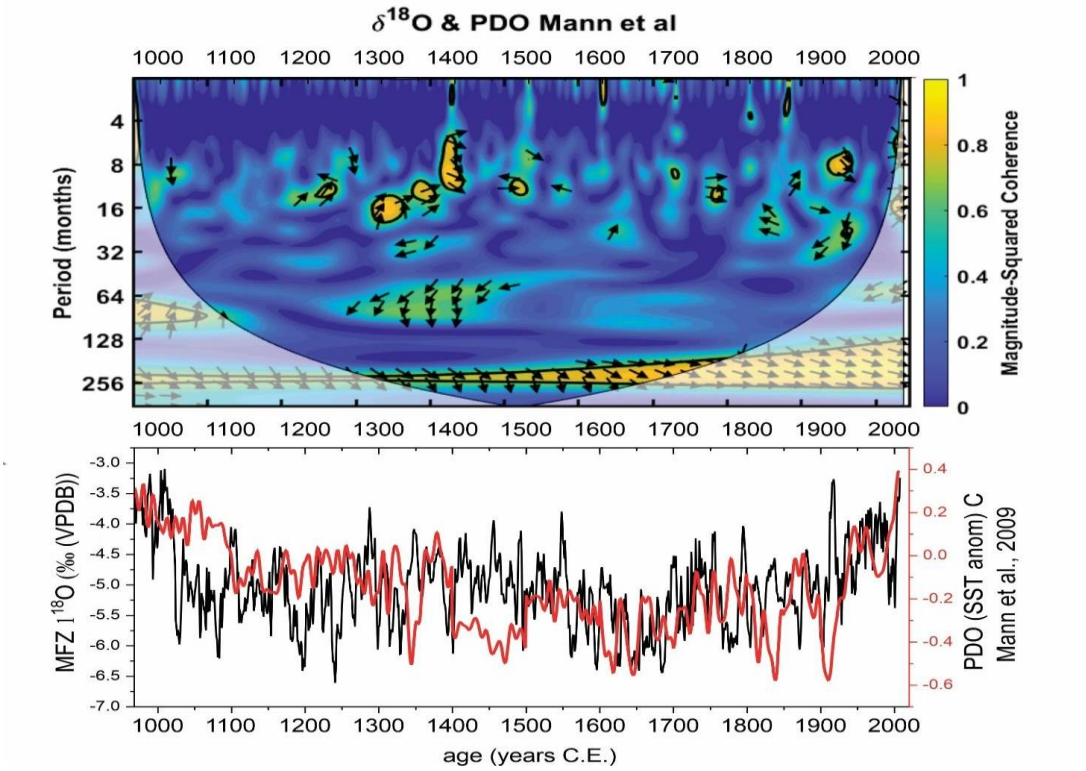

Figure 13 – On the top is the cross-wavelet analysis between MFZ-N-1 $\delta^{18}O$ data with PDO (Mann et al., 2009). On the graph below is presented the timeseries of MFZ-N-1 $\delta^{18}O$ record and PDO index.

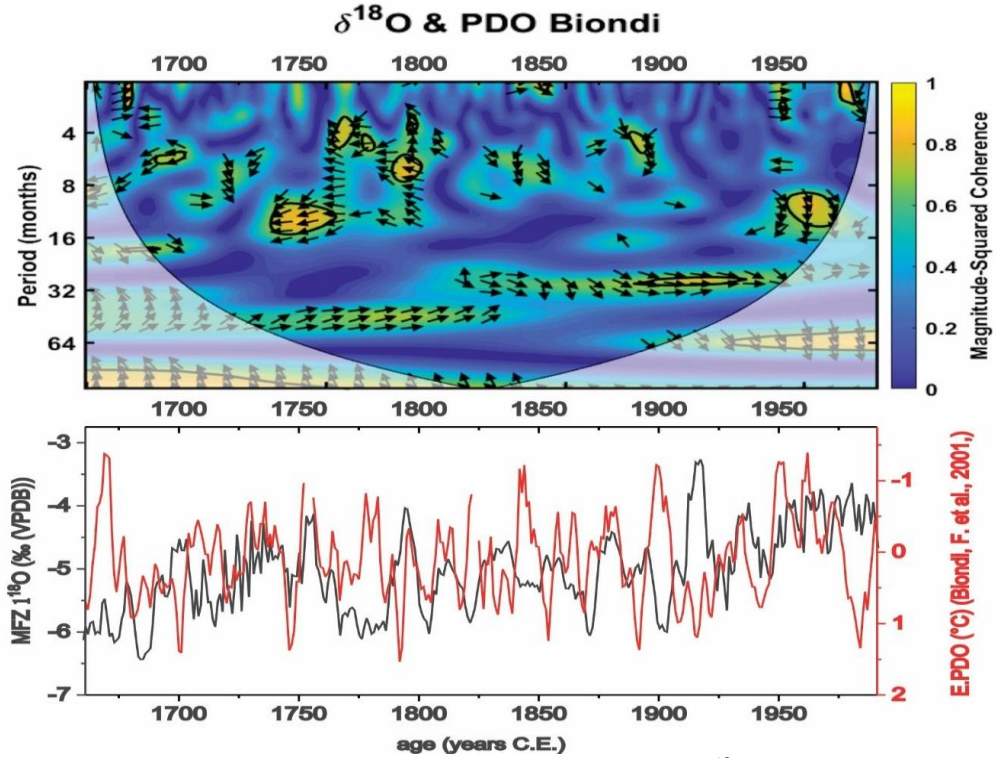

Figure 14 - On the top is the cross-wavelet analysis between MFZ-N-1 $\delta^{18}O$ data with PDO (Biondi et al., 2009). On the graph below is presented the timeseries of MFZ-N-1 $\delta^{18}O$ record and PDO index.

During the interval between 1500 and 1680 C.E. it is observed a periodicity of 64 years with high coherence between the records of $\delta^{18}O$ and IPO index from Buckley et al (2019) (Fig. 15). Interdecadal periodicities between 16 and 8 years are observed discontinuously from 1350 to 1970 C.E. where the demarked area cross the influence cone. Some specific intervals of sub-decadal periodicities from 6 to 2 are also marked in the cross-wavelet analysis.

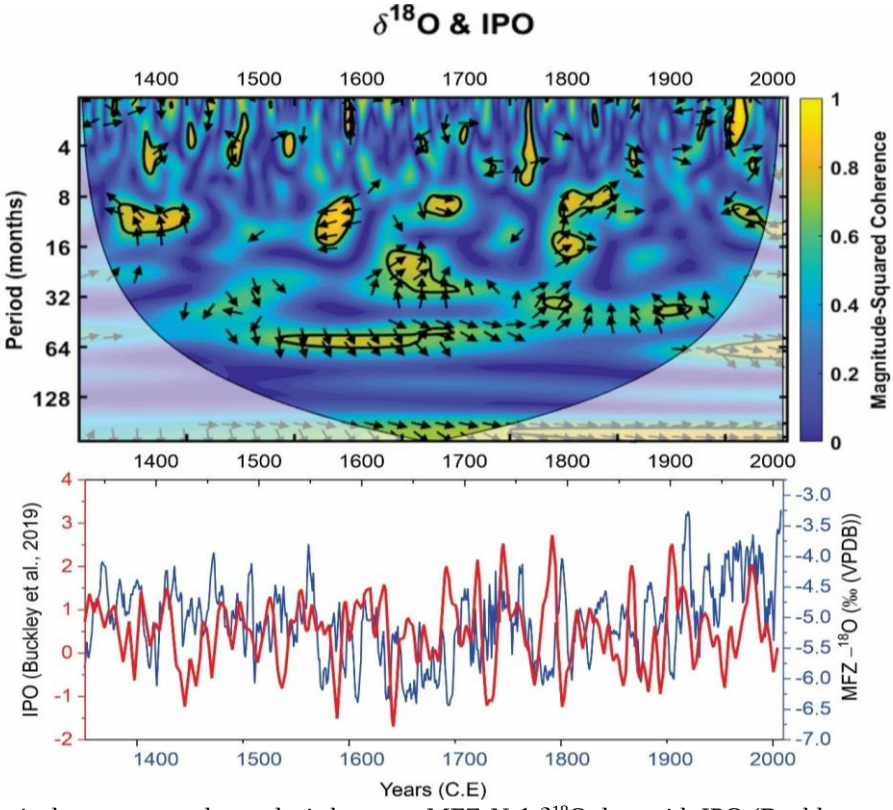

Figure 15 - On the top is the cross-wavelet analysis between MFZ-N-1 $\delta^{18}O$ data with IPO (Buckley et al., 2019). On the graph below is presented the timeseries of MFZ-N-1 $\delta^{18}O$ record and IPO.

The cross-wavelet analysis between NAO index from Trouet et al. (2009) does not show intervals of high coherence between the series, with short breaks marking the periodicities of 32, 16 and 8-4 years, but the spot of high coherence for those periodicities are so short that they were not considered (Fig. 16).

The cross-wavelet analysis between $\delta^{18}O$ and AMO from Mann et al (2009) shows an interval from 1300 to 1800 C.E. limited by the influence cone with a periodicity of 256 years and the arrows showing that the series are in phase for this periodicity (Fig. 17). This periodicity can also be observed in the comparison between the time series where they share a secular trend. For almost the same interval it is observed a periodicity of near 64 years with high coherence and the arrows showing an antiphase behavior of the series in this periodicity. Some short intervals present

periodicities from 16 to 8 years with high coherence. The comparison between the time series shows a remarkable fit between them in a secular scale with negative anomalies of AMO accompanied by more depleted values of $\delta^{18}O$.

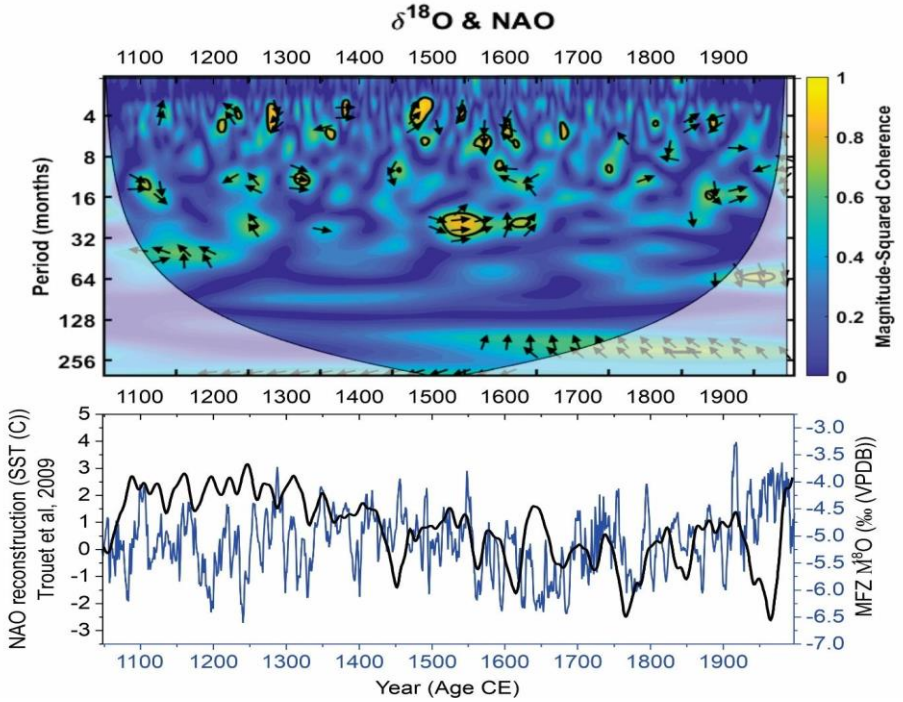

Figure 16 - On the top is the cross-wavelet analysis between MFZ-N-1 $\delta^{18}O$ data with NAO (Trouet et al., 2009). On the graph below is presented the timeseries of MFZ-N-1 $\delta^{18}O$ record and NAO index.

Nino 3.0 index from Conroy et al (2010) does not show significant intervals of high coherence with the $\delta^{18}O$ time series as showed by the cross-wavelet analysis (Fig. 18). Short intervals of high coherence are observed for the periodicities of 128, 32, 20-10 and 8-2 years, but it is limited to short ranges.

Nino 3.4 index shows only short intervals of high coherence with the periodicities of 32, 16-8, 5-2 years and the intervals observed are like those recognized in the cross-wavelet analysis between the of $\delta^{18}O$ and the IPO index. Despite the lack of coherence between the time series in the cross-wavelet analysis, the series shows a similar trend in a decadal scale with a visual fit between the series during the interval of 1300 and 1620 C.E. and from 1700 to 1900 C.E.

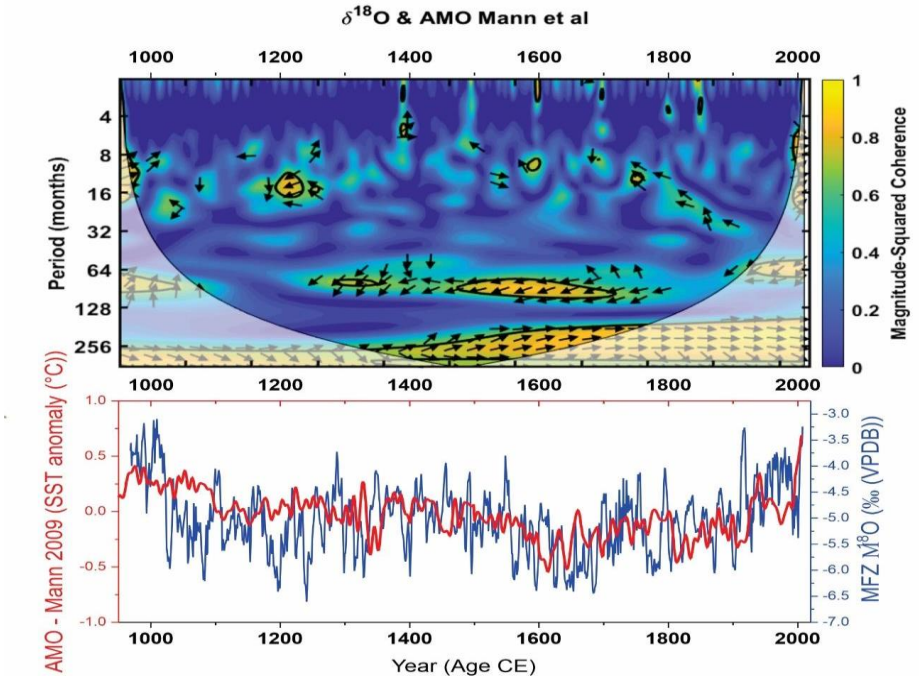

Figure 17 - On the top is the cross-wavelet analysis between MFZ-N-1 $\delta^{18}O$ data with AMO (Mann et al., 2009). On the graph below is presented the timeseries of MFZ-N-1 $\delta^{18}O$ record and AMO index.

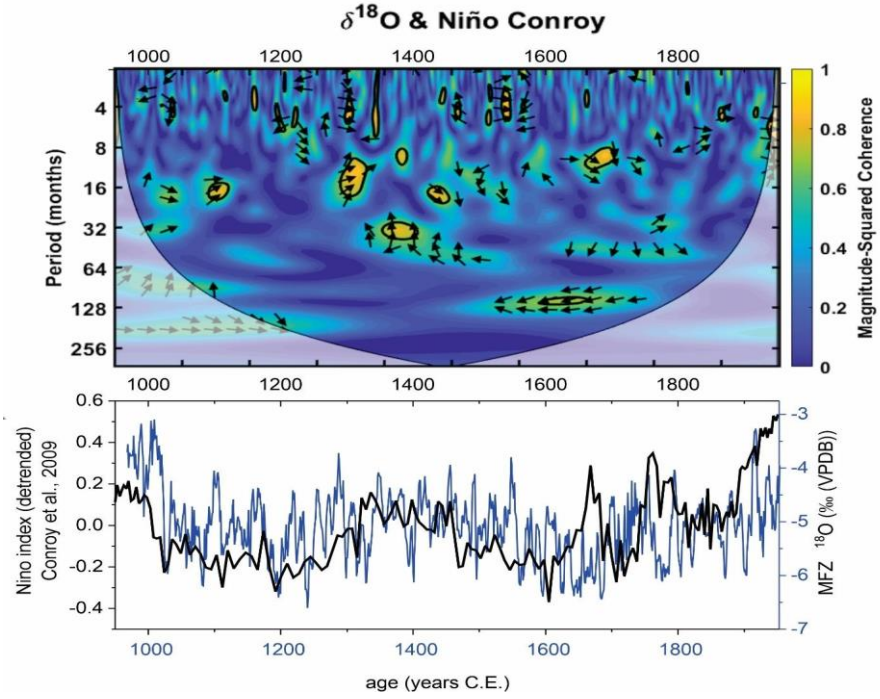

Figure 18 - On the top is the cross-wavelet analysis between MFZ-N-1 $\delta^{18}O$ data with Niño 3 index (Conroy et al., 2010). On the graph below is presented the timeseries of MFZ-N-1 $\delta^{18}O$ record and Niño 3 index.

7.1.4 Paleoflood record and cave flood frequency

The detrital layers from MFZ-N-1 are visually recognized by its dark brownish color with lateral continuity and with a weak central axis washing, and it also has unconsolidated clay in the most distal part of the layers. An effort to characterize the chemical pattern and to investigate a proxy for the detrital layers, PIXE analyses were performed in the speleothem and compared with the flood record as is described in section **6.2.3.** The total amount of layers visually identified in MFZ-N-1 were 130, with the higher concentration in two periods during the LIA and one after the end of MCA. The base of the speleothem is marked by brownish homogenous calcite with a high concentration of detrital layers that cannot be visually distinguished, and the high concentration of detritus preclude us to obtain U/Th ages, so this part of the speleothem was not considered (Fig. 19). As the detrital layers recognized in the speleothems are interpreted as formed by the deposition of fine-grained sediments suspended by floodwaters, a paleoflood frequency is calculated by grouping flood layer data into a variety of multi-decadal bins as 10, 50 and 100 years for the Last Millennium to reconstruct a paleoflood frequency time series for the speleothem (Fig. 20).

MFZ-N-1 recorded 130 cave-floods in the Last Millenia with an average frequency of 13 floods per century. MCA (950-1200 C.E.) shows a low frequency of events with 0.76 flood per decade and a total of 20 floods. The transition between MCA and LIA shows a small increase in the average frequency to 0.91 flood per decade with the floods concentrated in the end of the MCA (1200-1300 C.E.). The beginning of LIA is marked by a low frequency of floods with an average of 0.46 floods per decade and only 7 floods recorded between 1400-1545 C.E. An increase of four times in the flood frequency is observed after 1545 C.E. corresponding to 1.84 floods per decade from 1545-1665 C.E. The period 1665-1745 C.E. shows a decrease flood frequency, being 4 of the 6 floods in the decade of 1730. The higher frequency is reached in the end of LIA (1765-1875 C.E.) with an average flood-frequency of 3.58 floods per decade getting up to 4.8 from 1800-1850 C.E., and the highest value in the decade of 1800 C.E. with 7 floods per decade. CWP shows a frequency of 1.11 floods per decade (Fig 19). The frequency of mud layers allows to identify the first half of the XIX century as the most extreme in terms of precipitation during the last 1000 years in the eastern of Paraná State.

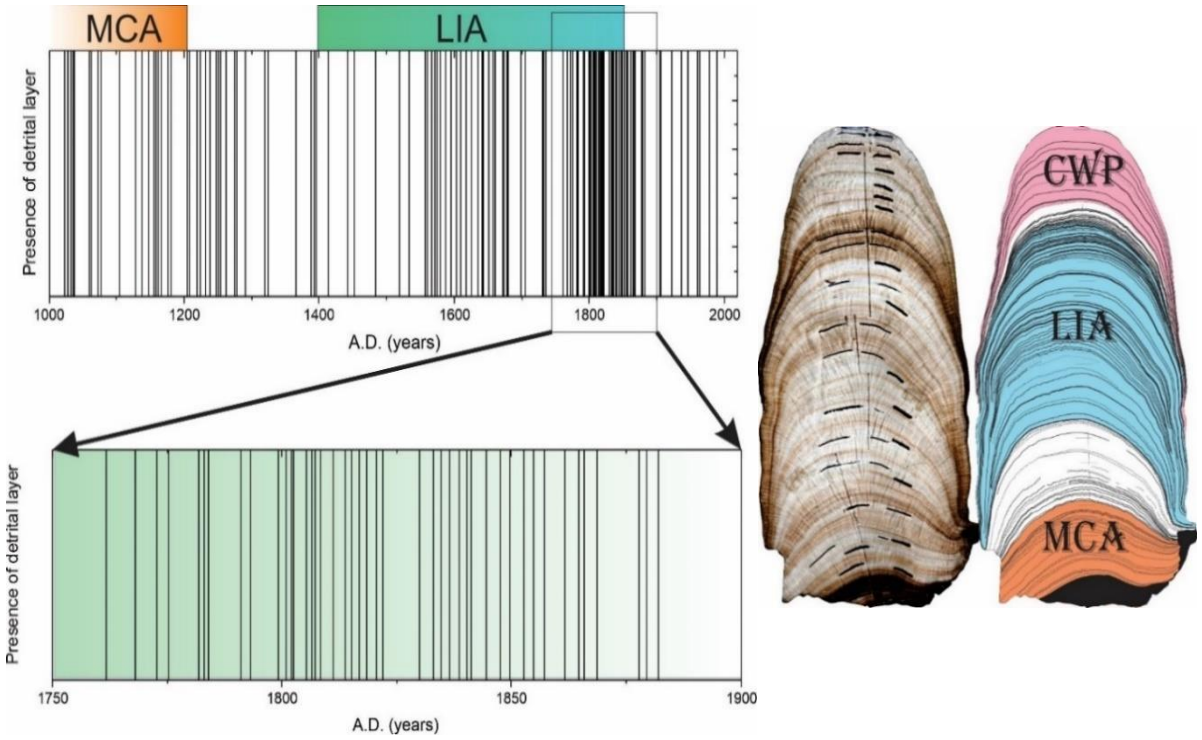

Figure 19 - On the left is represented the paleoflood record from MFZ-N-1 for the Last Millennium. Each bar represents a detrital layer visually recognized in the speleothem. A zoom of the period of high occurrence of flood layer is showed in the bottom. On the right is showed a scan from MFZ-N-1 where it can be seeing the brownish dark layers (flood layers) and the ages analyses drills (horizontal drills) and the stable isotope profile (vertical drills). The illustration shows the detrital layers marked individually in the software CorelDraw and the colors are used to illustrate the climate events of the Last Millennium (LIA, MCA). Current Warm Period (CWP) is used here as the period between 1850 and the present.

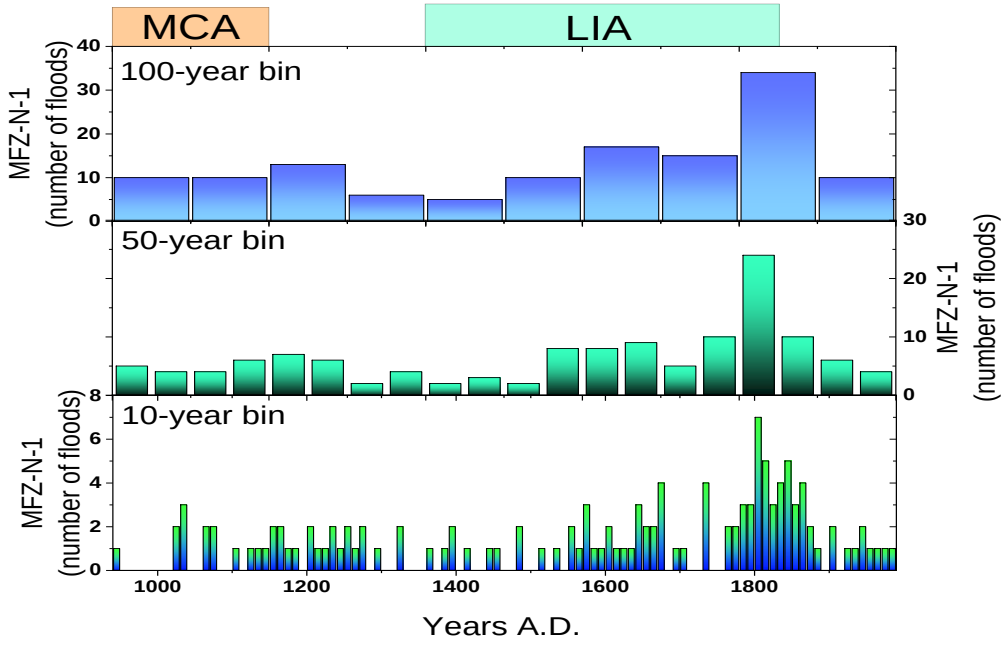

Figure 20 - Paleoflood frequency from MFZ-N-1 using different bins (10, 50 and 100 years).

For further comparisons with other proxies, it was calculated a cave-flood index from the Malfazido frequency of mud layers by subtracting the mean number of events per decade (calculated for the last millennium) from the observed number of events in a given decade and then dividing that value by the standard deviation. The cave flood index represents the number of standard deviations above (positive) or below (negative) the decadal mean flood frequency (Fig. 21). The positive values of this index indicate decades with most extreme events while negative values represent below average to non-occurrence of extreme rainfall.

Figure 21 shows the cave flood index of MFZ-N-1 with periods of values above the average of the decadal frequency marked by grey intervals (A1, A2, A3 and A4) and the periods with the predominance of decadal frequency values below the average are marked by the beige intervals (B1, B2, B3 and B4).

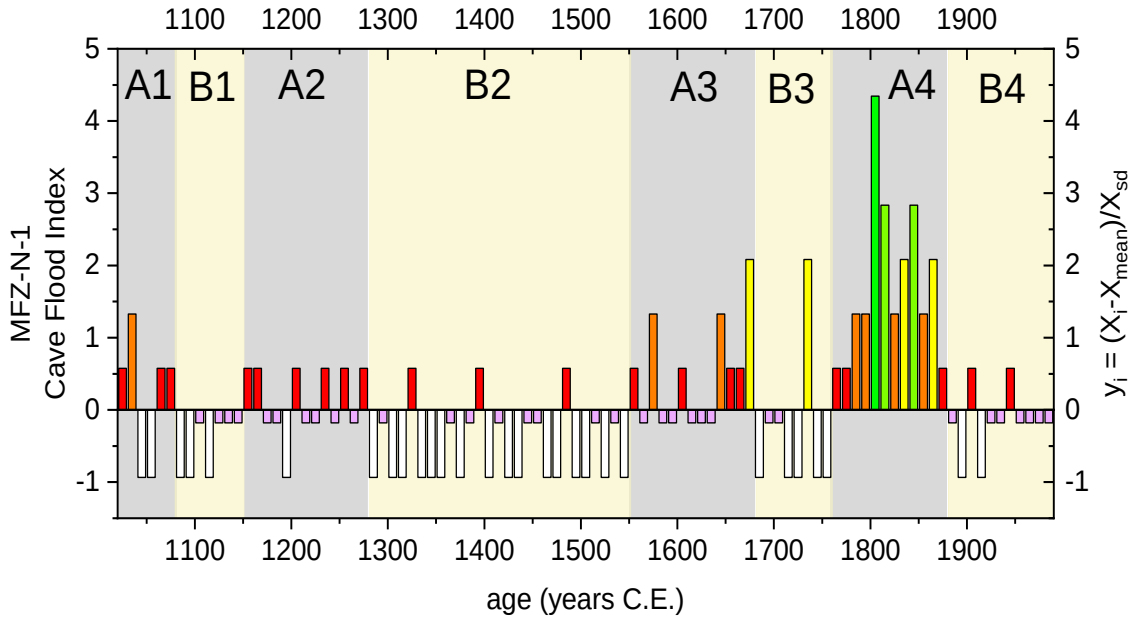

Figure 21 - Cave flood index of Malfazido cave for the last millennium. Colored bars indicate the number of standard deviations above or below the mean for each decade. White bars indicate the absence of events.

7.1.5 PIXE analyses (Proton Induced X-ray Emission)

In this study we explore the use of PIXE analysis to investigate the recurrence of mud layers associated with variations in the concentration of trace elements such as Al, Si, Fe, Ti, Mn, Ni, Cu, Zn (Fig. 22). The use of PIXE analysis offsets the advantage of a non-destructive and short time-consuming method that may, potentially, provides independent confirmation of detrital material deposition. The analysis resolution of 1mm step does not allow us to identify individual layers, with thickness approximately of 0.2 mm for this speleothem. Ti and Al records shows

correspondence with the detrital layers, but they weren't detected in most part of the speleothem. The elements Ca, Sr, Ba, Si, Mn, Ni, Cu and Zn, however, do not show a clear correspondence with the detrital layers.

On the other hand, Fe counts show a good correspondence with the detrital layers, showing a potential for recognizing the periods with more detrital layers occurrences. Indeed, the peaks in Fe counts shows a good match with periods of higher number of flood events (Fig. 23). The comparison with the cave flood index indicates that periods with the predominance of decadal frequency above the average shows correspondence with the Fe counts of the PIXE analysis. Figure 24 shows the comparison between the anomaly timeseries of Fe counts and the cave flood index. Here, the periods with decadal frequency above the average matches with the positive anomalies of Fe counts. The last century also shows positive anomalies of Fe, but it is not observed a counterpart with the mud layers occurrence within the speleothem. Periods with decadal frequency below the average are marked by negative anomalies of Fe counts.

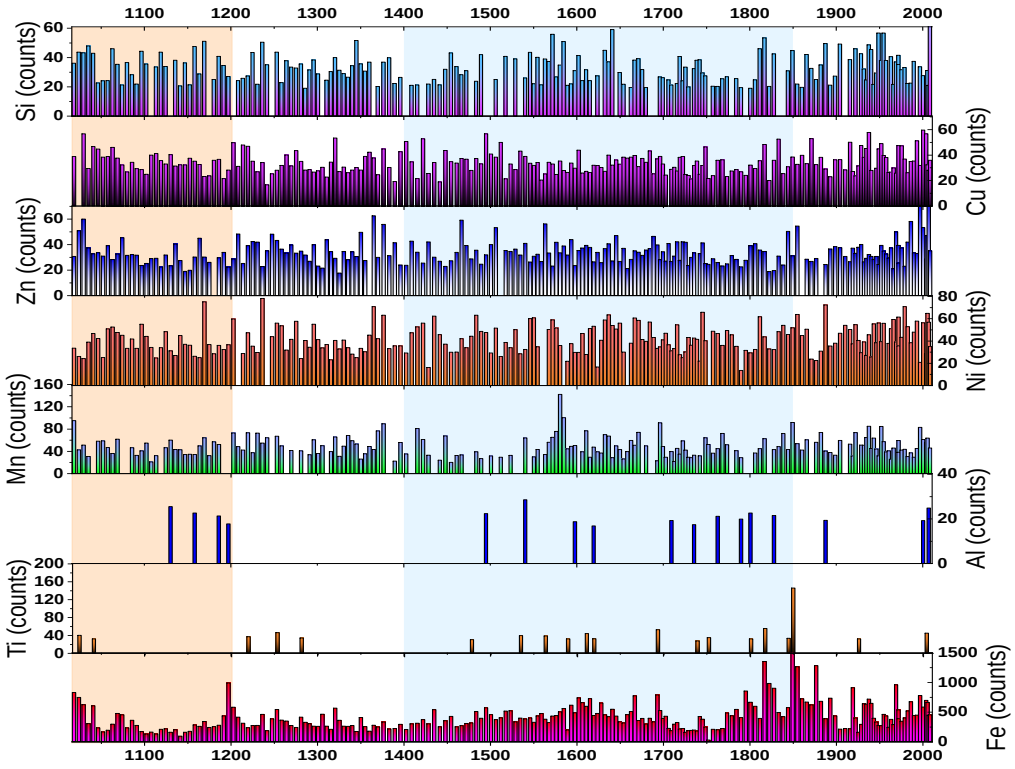

Figure 22 - PIXE analyses of trace elements related to soil erosion.

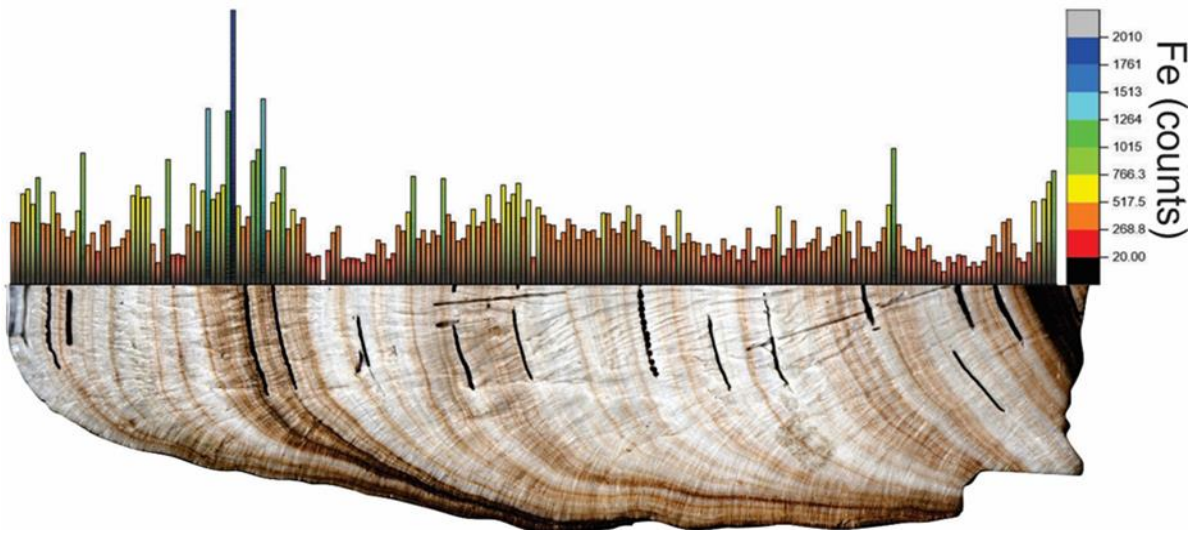

Figure 23 - Scan image from MFZ-N-1 with the comparison between the dark brownish layers (flood layers) and the Fe (counts) from the PIXE analyses. It is observed a good correspondence between periods of high concentration of flood layers and higher peaks of Fe.

The PIXE analysis is then a good technique to identify periods of high recurrence of detrital layers within the speleothem, thus it can be used as a rapid and non-destructive method to recognize flood events together with mud layers in Malfazido.

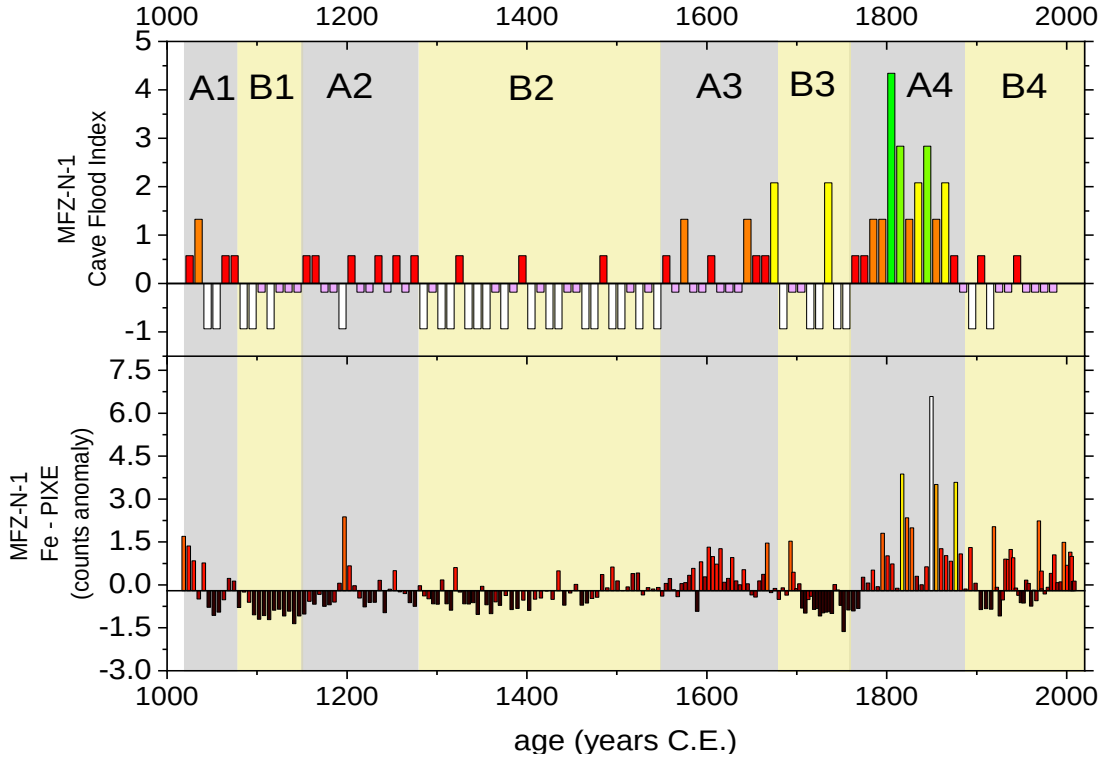

Figure 24 – Comparison between the cave flood index of MFZ-N-1 with the anomaly timeseries of Fe counts (PIXE).

7.1.6 Trace elements (LA-ICP-MS)

In this section we present the novel trace element record from CR-1 covering the last 4000 years, obtained in previous analyses, and the new high-resolution record from MFZ-N-1 covering the last 500 years. Here it is described the trace elements ratios of Mg, Sr, Ba and U with Ca to verify whether these ratios can be used as hydroclimate proxies. The CR-1 records are composed of 17750 independent points, resulting in a time series of sub-annual resolution with an average of 16 points per year between 850 C.E. and 1944 C.E. The MFZ-N-1 record is composed of 26028 independent points, resulting in a time series of sub-annual resolution with an average of 26 points per year. To reduce the larger variability of the record a 200-point running mean and Ln (Napierian logarithm) series were calculated by extracting the Ln for each independent point.

In order to check if the element ratio shows a potential to be used as a proxy for PCP or incongruent calcite dissolution (ICD) the crossplots of Ln(Sr/Ca) vs Ln(Mg/Ca) and Ln(Ba/Ca) vs Ln(Sr/Ca) were made. These correlations in CR-1 indicate that the same process must modulate the concentrations, and the slope calculated of 0.93 for Ln(Sr/Ca) vs Ln(Mg/Ca) show that Mg/Ca and Sr/Ca co-vary linearly in a ln-space, as modeled by Sinclair et al. (2011) and Sinclair et al. (2012) for PCP/ICD as the main factors modulating these ratios. MFZ-N-1 record doesn't show a high covariation between Ln (Sr/Ca) vs Ln(Mg/Ca) with slope of 0.027 and correlation of 0.18 and for Ln (Sr/Ca) with Ln(Ba/Ca) with a slope of 0.58 and a correlation of 0.3 (Fig. 25).

The trace elements records from CR-1 are highly correlated among themselves with the correlations between Mg/Ca with Sr/Ca and Ba/Ca of 0.7 and 0.91 respectively, and the correlation between Sr/Ca and Ba/Ca of 0.57. Figure 26 shows a plot of the anomaly series of trace elements ratios with Ca of CR-1. It is observed in the overlap plot a distinction of two periods, with the period from 1000 and 1500 C.E showing predominantly positive anomalies and the period between 1500 and 1950 C.E. with the predominance of negative anomalies. The anomalous positive period is marked in all the records by an enhancement of the anomaly values after 1200 until 1400 C.E. with a negative anomaly between 1320-1375 C.E. Mg/Ca and Ba/Ca shows a first drop in the anomaly values in 1400 C.E. and a second drop recorded by all the records in 1500 C.E. The period between 1500 and 1950 C.E. documented the most negative anomaly of all record between 1800 and 1880 C.E. followed by an enhancement in the anomaly values until 1920 C.E. and a subsequently drop until 1950 C.E. to negative values close to the observed in 1800 C.E.

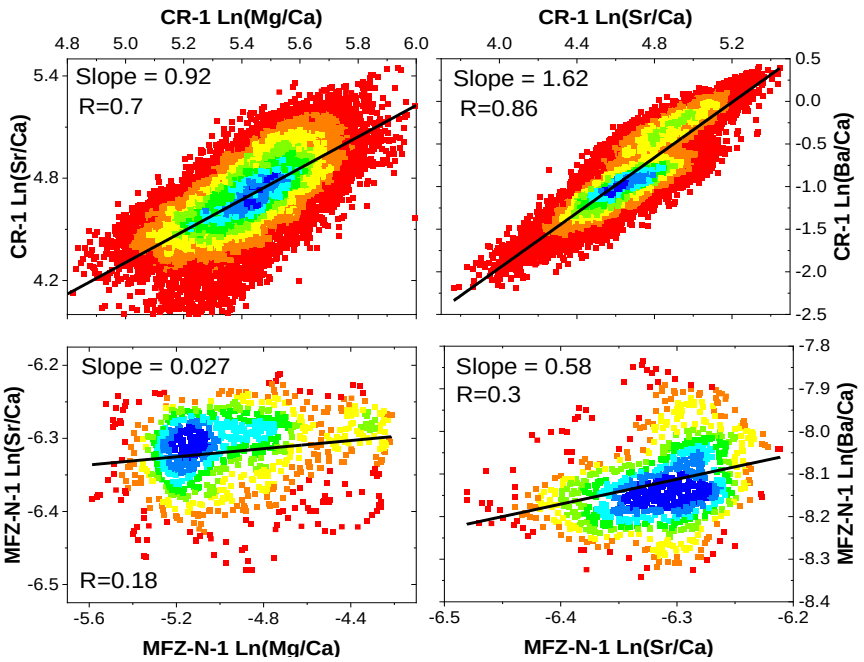

Figure 25 - Covariation of trace elements ratios with Ca (Ln(tr/Ca) vs Ln(tr/Ca)) of MFZ-N-1 and CR-1. The black lines correspond to linear regressions. The colors of the points are related to the density of points with the blue color indicating the higher concentration of points and the red color indicating the lower density.

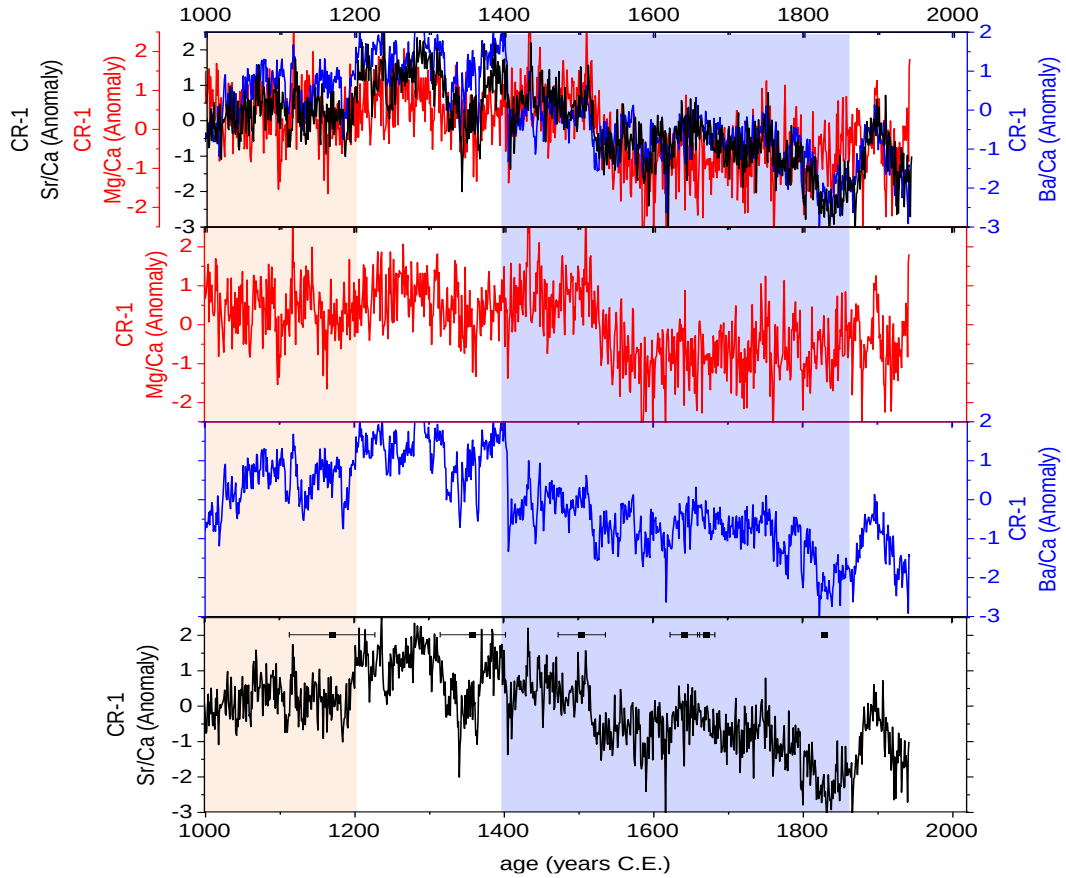

Figure 26 – Graph showing Cr-1 trace-elements anomalies.

The trace element records present a good visual similarity with $\delta^{13}C$, even though they show only a week positive correlation with Sr/Ca (R=0.25), and Mg/Ca and Ba/Ca (R=0.15) (Fig. 27). Positive and negative excursions in the trace element series are also shows correspondence with the $\delta^{13}C$ periods of more enriched or depleted values. The Sr/Ca series shows a modulation like the $\delta^{18}O$ and the series are positive correlated (R=0.16) (Fig. 28). Mg/Ca and Ba/Ca shows periods of similar modulations as between 1500 and 1800 C.E. The positive correlation and the modulation of Sr/Ca and $\delta^{18}O$ indicate that the same modulation process may be affecting both records.

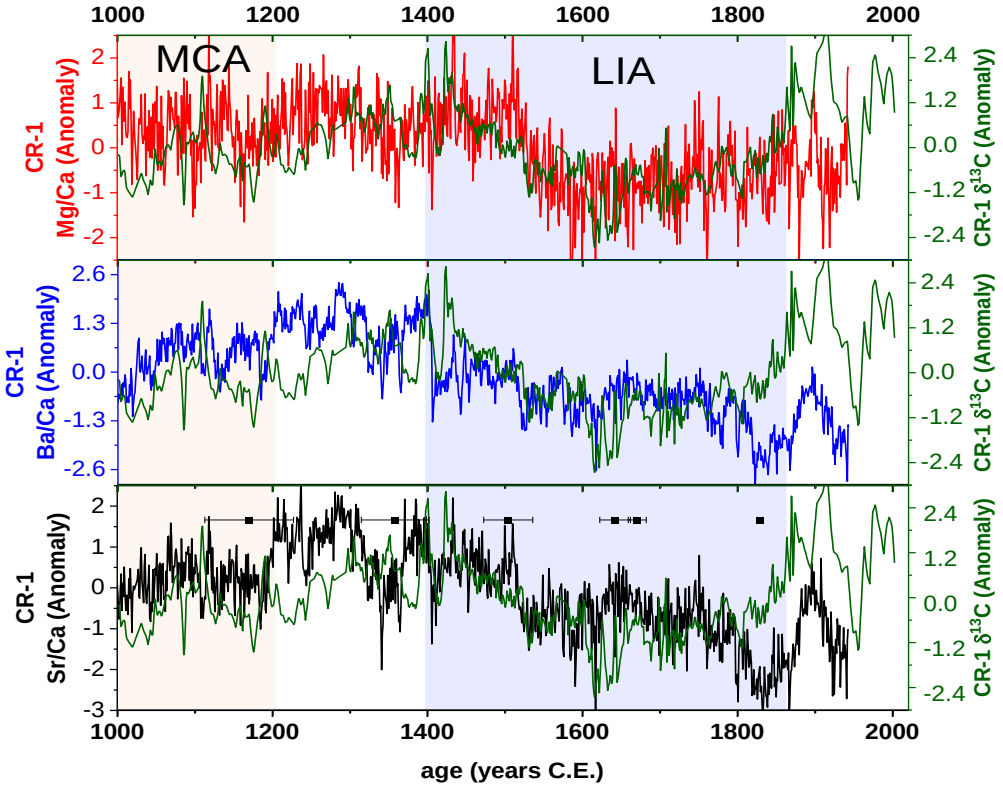

Figure 27 – Comparisons between trace elements anomaly timeseries with $\delta^{13}C$ from CR-1. Horizontals black spots and the bars represent the U/Th ages and the 2σ errors.

MFZ-N-1 trace elements (Mg/Ca, Sr/Ca and Ba/Ca) do not show a linear covariance in a ln-space as expected in case of PCP/ICD mainly modulating the trace element ratios with Ca as modeled by Sinclair et al. (2011) and Sinclair et al. (2012). When compared, the Ln(Sr/Ca) and Ln(U/Ca) from MFZ-N-1 speleothem show consistent variations at decadal and centennial time-scale (Fig. 29). During the LIA, large excursion towards lower values are observed in both proxies, between 1400 to 1600 and 1750 to 1850 CE. Also, during the XX century both proxies show a steep lowering trend.

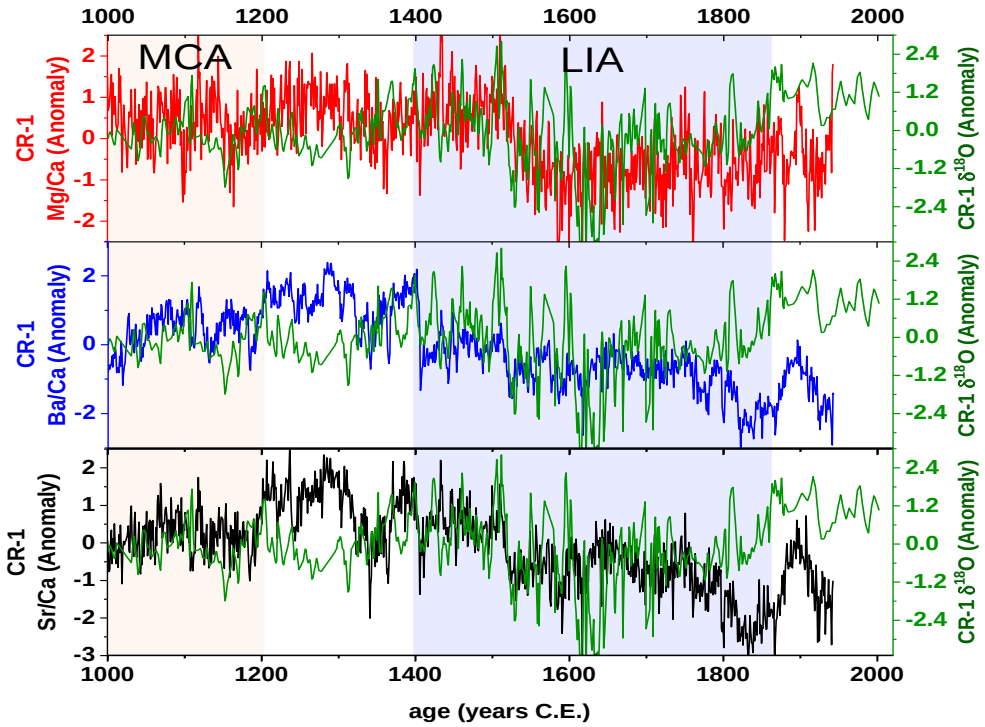

Figure 28 - Comparisons between trace elements anomaly timeseries with $\delta^{18}O$ from CR-1.

The Ln series of Mg/Ca and Ba/Ca seems to have the same modulation with an exception for the first century of the series with a correlation of 0.42 for the entire record, reaching 0.6 during some intervals (Fig. 29). Both records show a drop to more negative values after the end of the MCA, and the transition between the MCA and LIA is marked by a trend towards higher values until 1400 C.E. The LIA begins with the highest values of both records and the period between 1400-1540 C.E. is marked by abrupt variations in both series caused by peaks of higher concentration of the trace element ratios. Between 1550-1700 C.E. the values concentrate above the mean of the record. To better assess the consistence among the proxies, the $\delta^{18}O$ time series is compared to the element/Ca ratios in Figures 30 and 31. As it can be observed in Figure 30, in general, Mg/Ca ratios shows a better coupling with the stable isotope proxies in comparison with Ba/Ca. A more consistent peak is observed between 1700-1740 C.E. and coincides with an enriched period of the $\delta^{18}O$ record from MFZ-N-1. An excursion towards the most negative values of the record is observed between 1760-1810 C.E. and matches the excursion to the most depleted values of $\delta^{18}O$. The last century is marked by a trend towards higher values until the present. These series show a remarkable coherence with the $\delta^{18}O$ series, with the periods of depleted (enriched) $\delta^{18}O$ matching with more negative (positive) values of the elementary ratios.

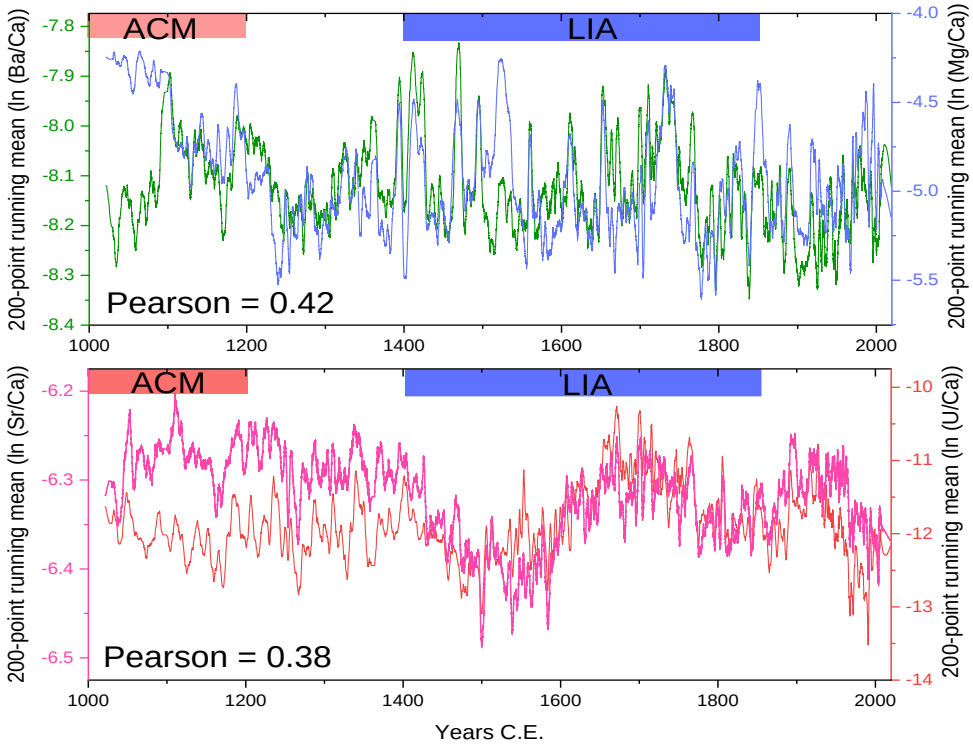

Figure 29 - Comparison between the MFZ-N-1 trace element records. In the top of the figure is represented the 200-point running mean series of the ln (Mg/Ca) (green) and ln (Ba/Ca) (blue). In the bottom the 200-point running mean series of the ln (Sr/Ca) (pink) and (U/Ca) (red). Mg/Ca and Ba/Ca showed the high correlation between the series with 0.42, followed by Sr/Ca and U/Ca with 0.38.

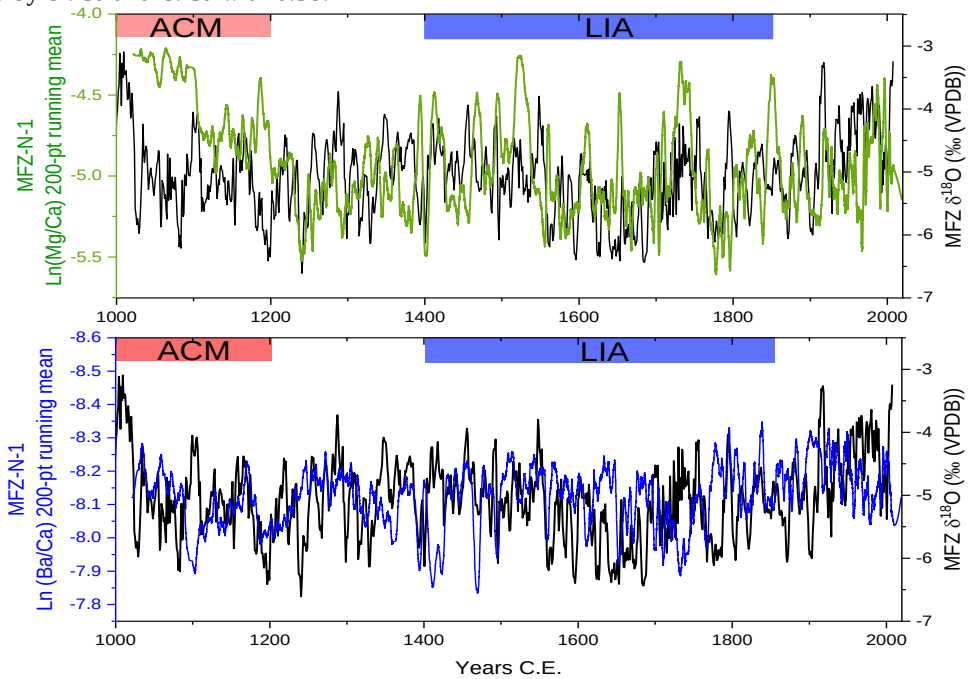

Figure 30 - Comparison between the 200-point running mean timeseries of ln(Mg/Ca) and ln(Ba/Ca) with the δ18O series of MFZ-N-1. It is observed a positive correlation between the records with periods of δ18O more depleted (enriched) values related to lower (higher) elementary ratios (trace-element/Ca).

Comparison between the 200-point running mean timeseries of ln(Mg/Ca) and ln(Ba/Ca) with the $\delta^{18}O$ series of MFZ-N-1. It is observed a positive correlation between the records with periods of $\delta^{18}O$ more depleted (enriched) values related to lower (higher) elementary ratios (trace-element/Ca).

The Ln (Sr/Ca) and Ln(U/Ca) shows the same modulations (Fig. 29) with just a decoupling between the series from 1000-1400 C.E, with a correlation of 0.38 reaching more than 0.5 during some intervals. In this period, the series vary in a plateau defined by the period mean. After 1420 C.E., the values of both series decrease and here on the series are coupled. The period between 1420 C.E. and 1590 C.E. is marked by the lower values of both series and is followed by an increase in values until 1670 C.E., where the values remain high until 1760 C.E. The series shows a drop in values between 1760-1880 C.E. After 1920 the records show a strong trend towards negative values, with the Ln(U/Ca) reaching the lowest value of the entire record (~1980 C.E.). A comparison with the $\delta^{18}O$ record is presented in Figure 31 and it is possible to observe that periods of more depleted (enriched) $\delta^{18}O$ visually matches with periods of higher (lower) elementary ratios of Ln (Sr/Ca) and Ln(U/Ca).

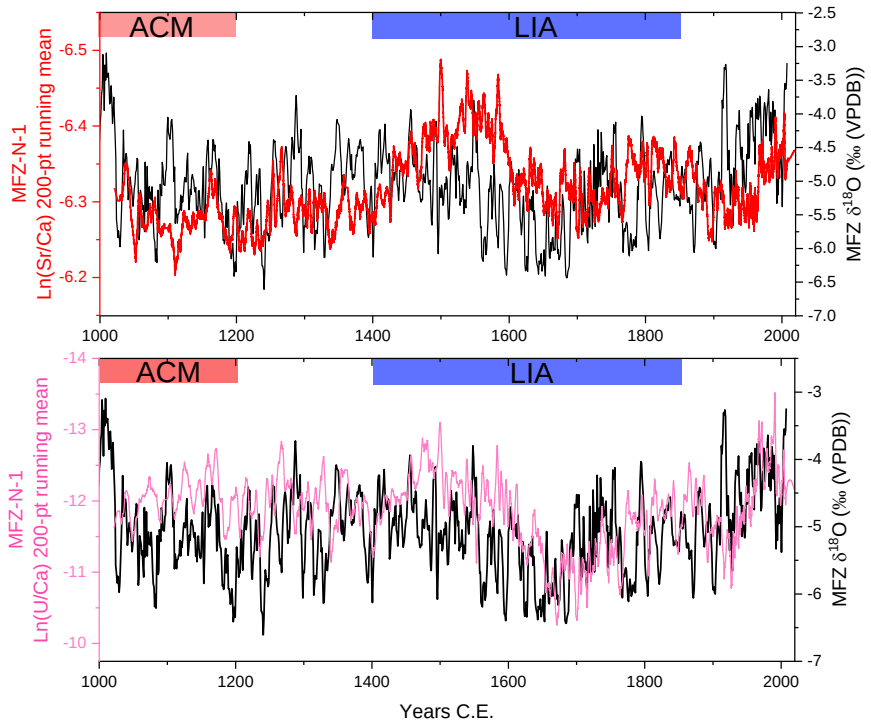

Figure 31- Comparison between the 200-point running mean series of ln(U/Ca) and ln(Sr/Ca) with the $\delta^{18}O$ series of MFZ-N-1. It is observed a negative correlation between the records with periods of $\delta^{18}O$ more depleted (enriched) values related to higher (lower) elementary ratios (trace-element/Ca).

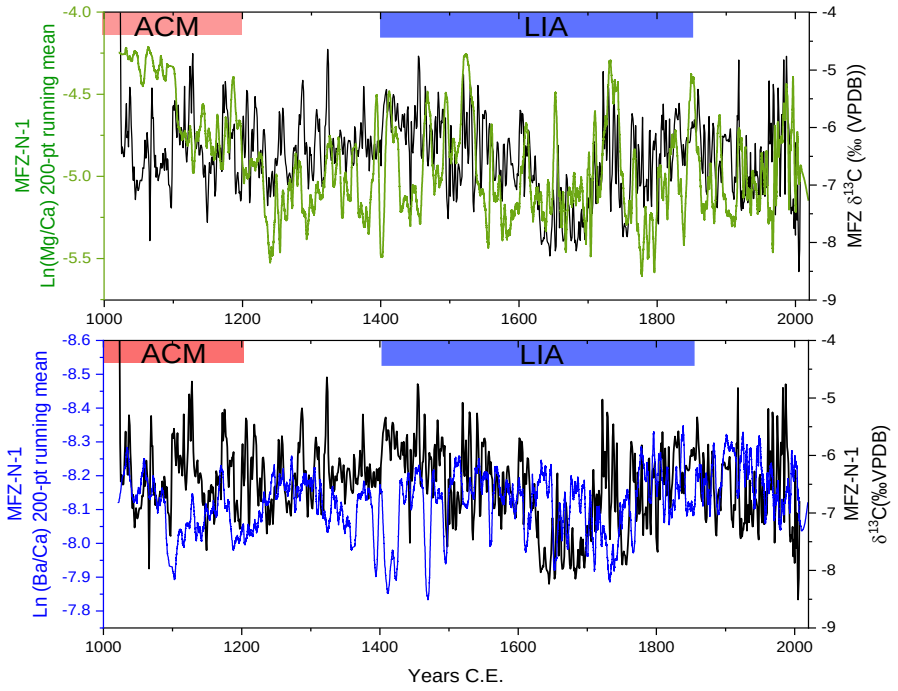

Figure 32 - Comparison between the 200-point running mean series of ln(Mg/Ca) and ln(Ba/Ca) with the $\delta^{13}C$ series of MFZ-N-1. It is observed a positive correlation between the records with periods of $\delta^{13}C$ more depleted (enriched) values related to lower (higher) elementary ratios (trace-element/Ca).

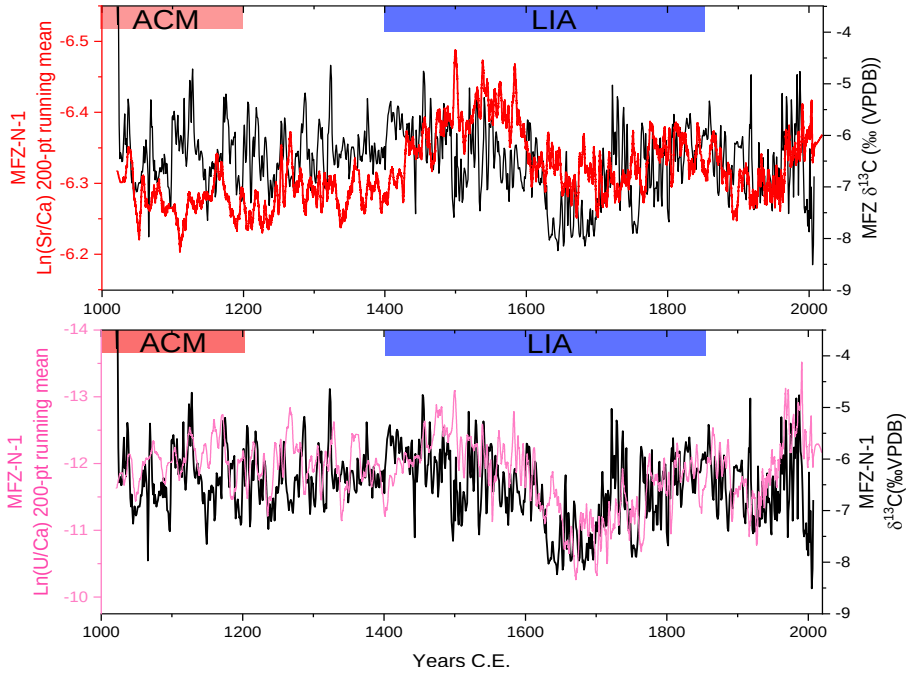

Figure 33 - Comparison between the 200-point running mean series of Ln(Sr/Ca) and Ln(U/Ca) with the $\delta^{13}C$ series of MFZ-N-1. It is observed a strong negative correlation between the records with periods of $\delta^{13}C$ more enriched(depleted) values related to lower (higher) elementary ratios (trace-element/Ca).

Comparisons between the trace elements and $\delta^{13}C$ shows a remarkable fit between the Ln(Mg/Ca) series and the $\delta^{13}C$ and a positive correlation between the records. The Ln(Ba/Ca) series

shows a similar relation with $\delta^{13}C$, but it is not so clear in the entire record (Fig. 32). The series of Ln(Sr/Ca) and Ln(U/Ca) have a good match with the $\delta^{13}C$ series with a negative correlation between the records (Fig. 33).

7.1.7 Principal components analysis of trace elements dataset

Principal Component Analysis (PCA) were performed to reduce the large multivariate trace element records produced by LA-ICP-MS from CR-1 and MFZ-N-1 speleothems. This technique is used to identify the modes and timings of components that can best explain the overall variability of the records. All the series utilized in the analysis were normalized by calculating the z-scores, and the series were interpolated for annual resolution.

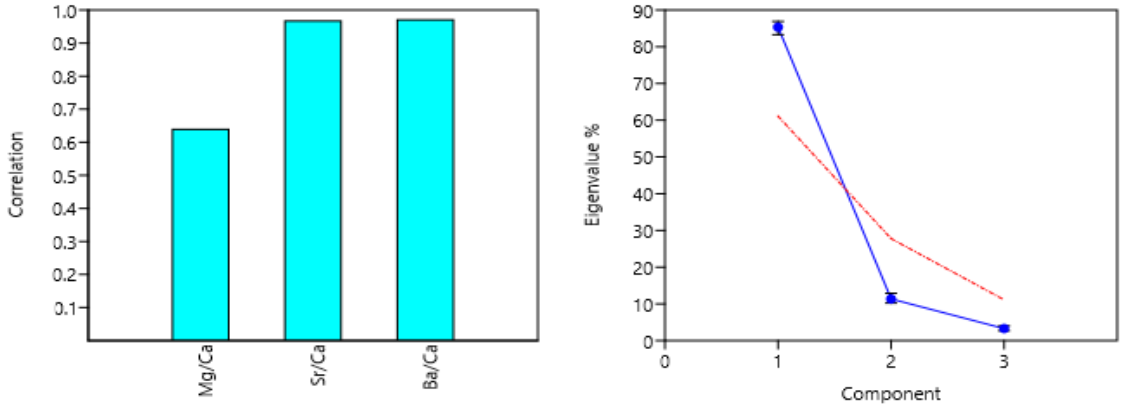

Figure 34 - Left graph shows the correlation between $PC1_{CR-1}$ with the normalized trace elements datasets and the right graph shows the eigenvalues of PCs with the blue points representing the PCs, the black bars representing the eigenvalues calculated by bootstrapping with n of 9999 and the red line showing the 95% of statistical significant calculated by the broken-stick model. The PCs with eigenvalues above the red line shows statistical significance higher than 95% and the PCs under the red line represent non-significant components.

As described in section 7.1.5, the trace elements ratios of CR-1 show a strong positive correlation between Mg/Ca, Sr/Ca and Ba/Ca, and the crossplot showed that they co-vary linearly in a ln-space. Since this trace elements seem to be mainly modulated by the same process it was calculated a PCA with the normalized series of Mg/Ca, Sr/Ca and Ba/Ca (Fig. 34). Principal Component 1 ($PC1_{CR-1}$) is defined by a strong correlation between the multiple elements, with positive correlation with Mg/Ca (0.63), Sr/Ca (0.96) and Ba/Ca (0.97) (Fig. 35). The eigenvalue calculated was 3.04 and the $PC1_{CR-1}$ account for 86.8% of the variance of the datasets with more than 95% of statistical significance as showed by broken-stick model and by confidence limits based on bootstrap re-sampling. $PC2_{CR-1}$ and $PC3_{CR-1}$ shows eigenvalues below the brokenstick curve and may represent non-significant components.

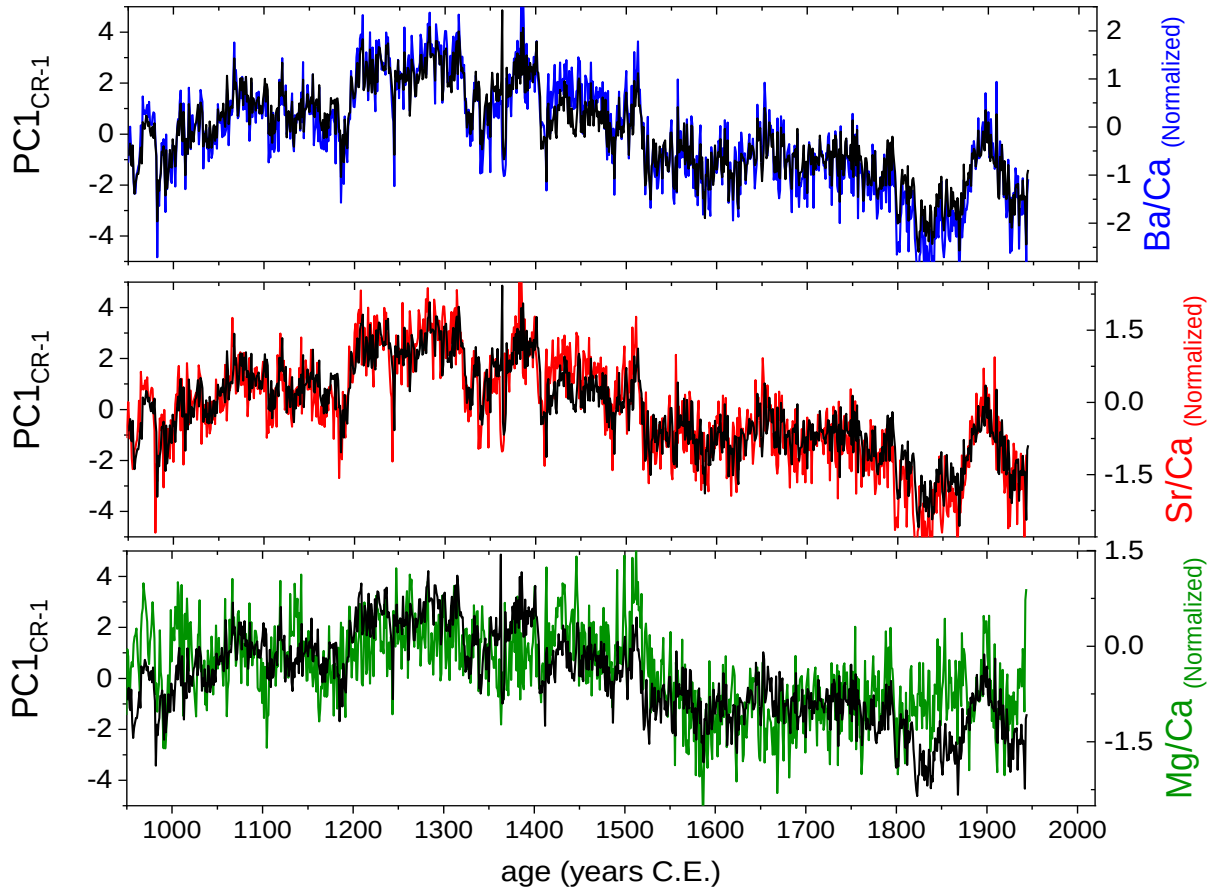

Figure 35 - Comparison between $PC1_{CR-1}$ with trace elements time series normalized. It is observed a remarkable match between the $PC1_{CR-1}$.

The trace elements ratios with Ca of MFZ-N-1 shows positive correlations between U/Ca with Sr/Ca and between Mg/Ca with Ba/Ca (Fig. 36). The crossplot is used as an indicator of PCP/ICD, once concentration controls of the trace elements indicates that the their expected covariances don't agree with the PCP/ICD hypothesis. The PCAs were calculated from the normalized dataset of Mg/Ca, Sr/Ca, Ba/Ca and U/Ca. The $PC2_{MFZ}$ is defined by positive correlations with U/Ca (0.78) and Sr/Ca (0.36) and negative correlations with Mg/Ca (0.64) and Ba/Ca (0.27) (Fig. 36 and 37). The eigenvalue calculated is 1.24 and the $PC2_{MFZ}$ accounts for 31% of the variance of the datasets with more than 95% of statistical significance as showed by the broken-stick model and by confidence limits based on bootstrap re-sampling. $PC1_{MFZ}$ and $PC3_{MFZ}$ shows eigenvalues below the brokenstick curve and may represent non-significant components (Fig. 36).

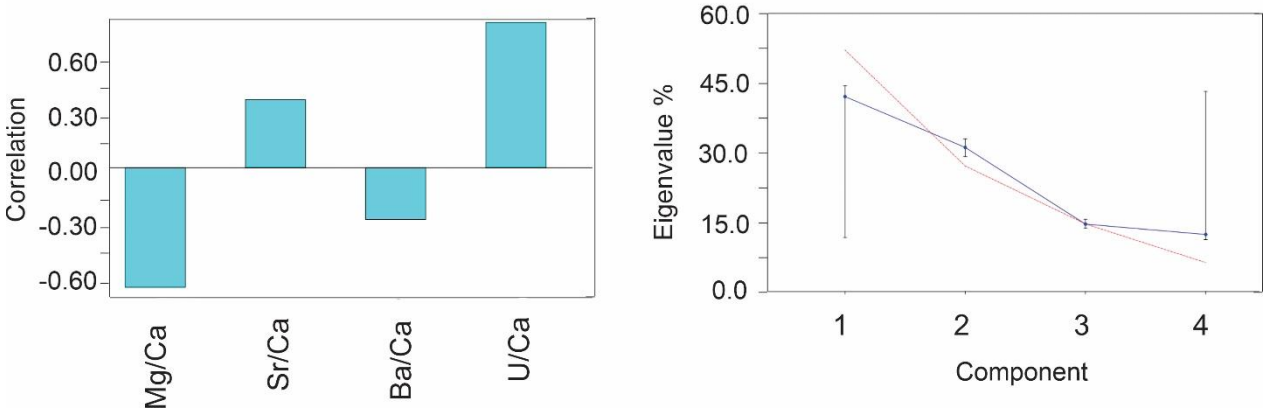

Figure 36 - Left graph shows the correlation between $PC1_{MFZ\text{-}N\text{-}1}$ with the normalized trace elements datasets; right graph shows the eigenvalues of PCs with the blue points representing the PCs, the black bars representing the eigenvalues calculated by bootstrapping with n of 9999 and the red line showing the 95% of statistical significant calculated by the broken-stick model. The PCs with eigenvalues above the red line shows statistical significance higher than 95% and the PCs under the red line represent non-significant components.

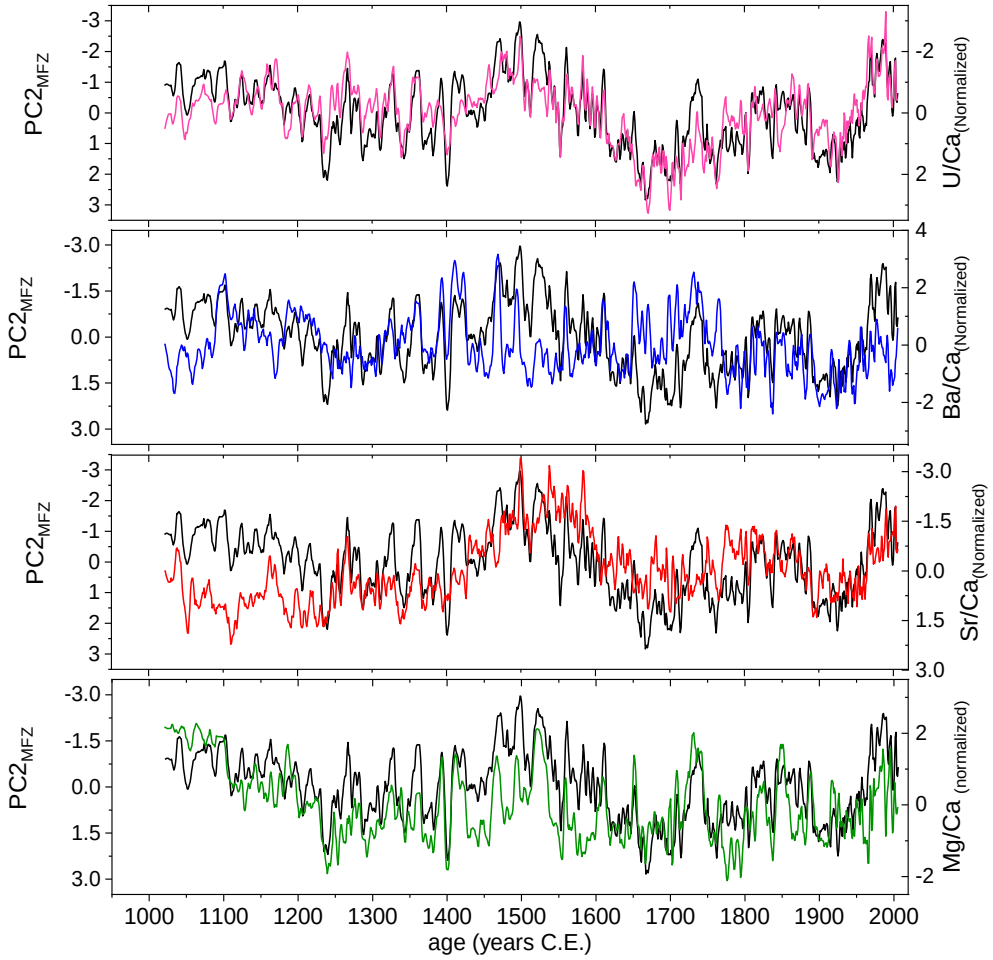

Figure 37 - Comparison between $PC2_{MFZ}$ and the normalized trace elements time series of MFZ-N-1.

7.2 Middle and Late Holocene

7.2.1 Geochronology result and growth rates

During the project, 37 U/Th dates were obtained for Lage Branca samples, 33 U/Th dates from CR-1 Cristal cave speleothem (Taylor, 2014) and TP-6 Tapagem cave speleothem (unprecedent data) were integrated. For Middle and Late Holocene, the stalagmites LB-1 and CB-3 were used with 14 U/Th dates, each one covering the period between 2000-7400 B.P., and the data from TP-6 and CR-1 were used for comparisons with Laje Branca speleothems. Other samples were analyzed for Laje Branca but not used because of the time period covered or by the absence of detrital layers within the speleothem, and in some case due to high concentrations of detrital ^{232}Th that increases errors and reduces accuracy of the ages. Figure 38 shows the age distribution of the speleothems dated and compiled during this project.

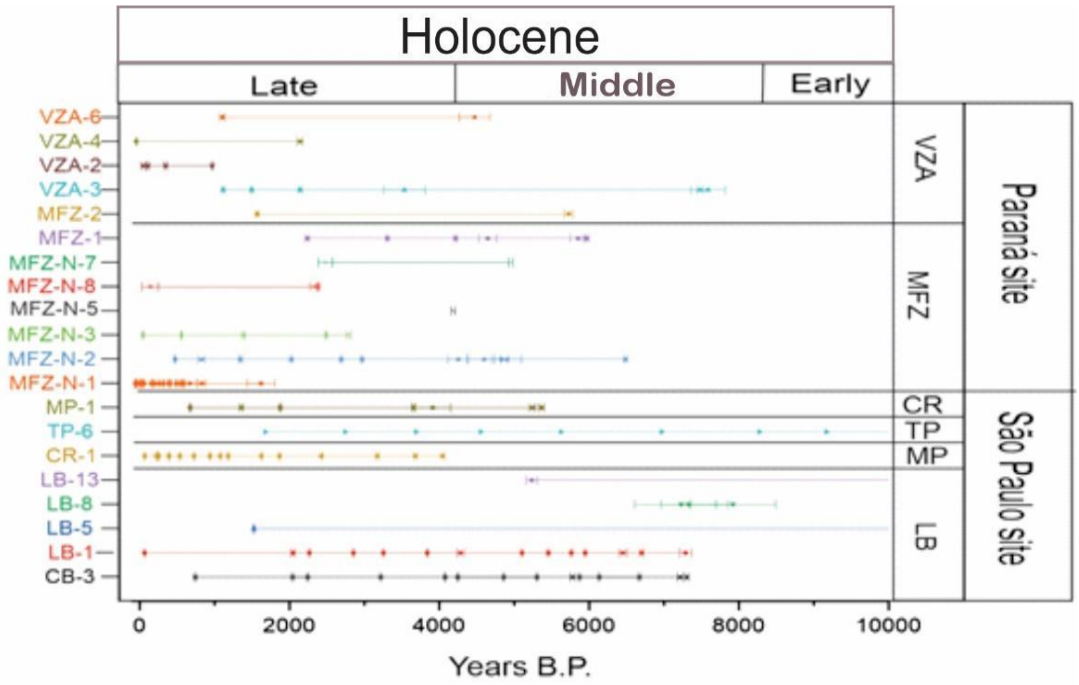

Figure 38 – Ensemble of all the speleothems collected and their age distribution.

The samples from Laje Branca cave with the samples from Cristal cave and Tapagem cave were selected due to their high potential for reconstruction of Middle and Late Holocene. The data from LB-1 and CB-3 showed a continuous growth from the Middle Holocene to the Late Holocene (2000 B.P.), with a hiatus recognized in both speleothems, from 740-2200 B.P. in CB-3 and from 64-2000 B.P. in LB-1 (Fig. 39).

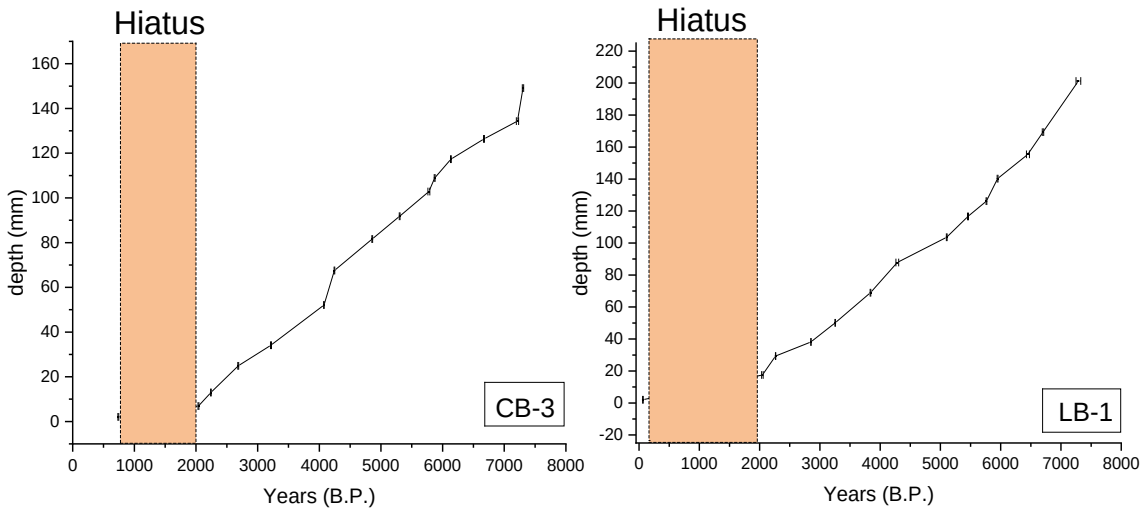

Figure 39 - Age models of CB-3 and LB-1. The orange bar represents the period with a significant hiatus in the growth of the speleothem.

The hiatus is also visually marked in the speleothem as a sequence of detrital layers composed by clay, and in CB-3 is associated with a strong change in the growth axis of the speleothem, and this hiatus is not recognized in CR-1 and TP-6. The 2σ error of the ages are less than 1% for both CB-3 and LB-1 samples, allowing the reconstruction of a continuous record between 2000-7200 B.P.

The age model from CR-1 shows a continuous growth throughout the Late Holocene with no sign of hiatus, being used in this study as a high-resolution record of the Late Holocene. TP-6 shows a continuous growth throughout all the Holocene (Fig. 40).

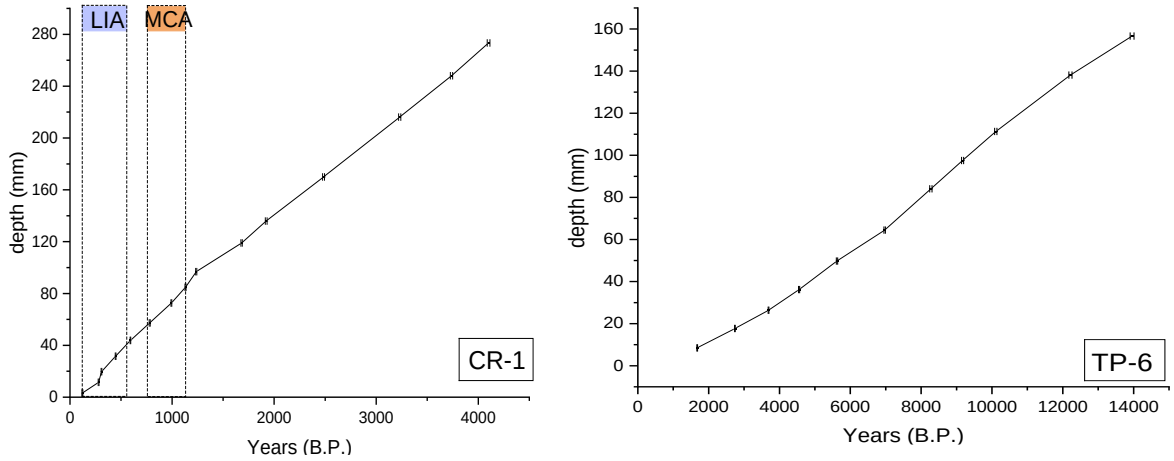

Figure 40 - Age models of CR-1 and TP-6. The blue box (LIA) represents the period of the Little Ice Age and the orange box (MCA) represents the Medieval Climate Anomaly

The growth rates values for the speleothems of Lage Branca show a mean of 0.025 mm/year for CB-3 and 0.037 mm/year for LB-1(Fig. 41). The higher growth rate for CB-3 (0.16mm/year) is

from 7200-7300 B.P., and for LB-1 (0.076 mm/year) is from 5700-5900 B.P. CB-3 growth rates start with the highest growth rate of the record (0.16 mm) followed by an abrupt fall to mean values of 0.025 mm/year between 7200-2000 B.P. The growth rate of LB-1 shows a downward trend to slower rates from Middle Holocene to the transition to Late Holocene, with values of 0.054 mm/year before 6700 B.P. (highest growth rates) to values of 0.019 mm/year until 4280 B.P. A second growth rate downward trend follows until 2000 B.P., where it reaches the lowest value of the record with 0.015 mm/year between 2200 B.P. and 2800 B.P. Before the hiatus in 2000 B.P. an abrupt increase in the values occurs between 2000-2200 B.P., reaching again 0.054 mm/year. Both samples show an increase in the growth rate between ~5700-6000 B.P. and the transition from Middle Holocene to Late Holocene is also marked by a local abrupt increase in the growth rates around the year 4000 B.P.

TP-6 has the lowest growth rate among the speleothems used in this study. The highest rates occur during the end of Early Holocene and at the beginning of Middle Holocene reaching up to 0.015 mm/year, followed by an abrupt decrease between 5600-6900 B.P. The values increase again close to the transition to Late Holocene, but with a downward trend as observed in LB-1 between 1600-2700 B.P. where the values decrease to the lowest values.

CR-1 has the fastest growth rates among the PETAR speleothems for the Late Holocene and, although there are differences between the rates, CR-1 and LB-1 show the same trend towards slower growth rates from 4000-2000 B.P. followed by an increase in 1900 B.P. and by the slowest rates of the record after 1680 B.P.

The ensemble of speleothem growth rates (Fig. 42) shows a trend toward slower growth rates from the Middle Holocene to the Late Holocene and from the Late Holocene to approximately 2000 B.P. This trend is interrupted between 5900 B.P. and 5700 B.P. by an abrupt increase in the growth rates of CB-3 and LB-1. These speleothems also show the transition between the Middle and Late Holocene with an abrupt increase in their growth rates. The Late Holocene (after 4000 B.P) is then marked by the slowest growth rates in all the speleothems, with exception of CR-1 that from 1250 B.P. until the present has its highest growth rate.

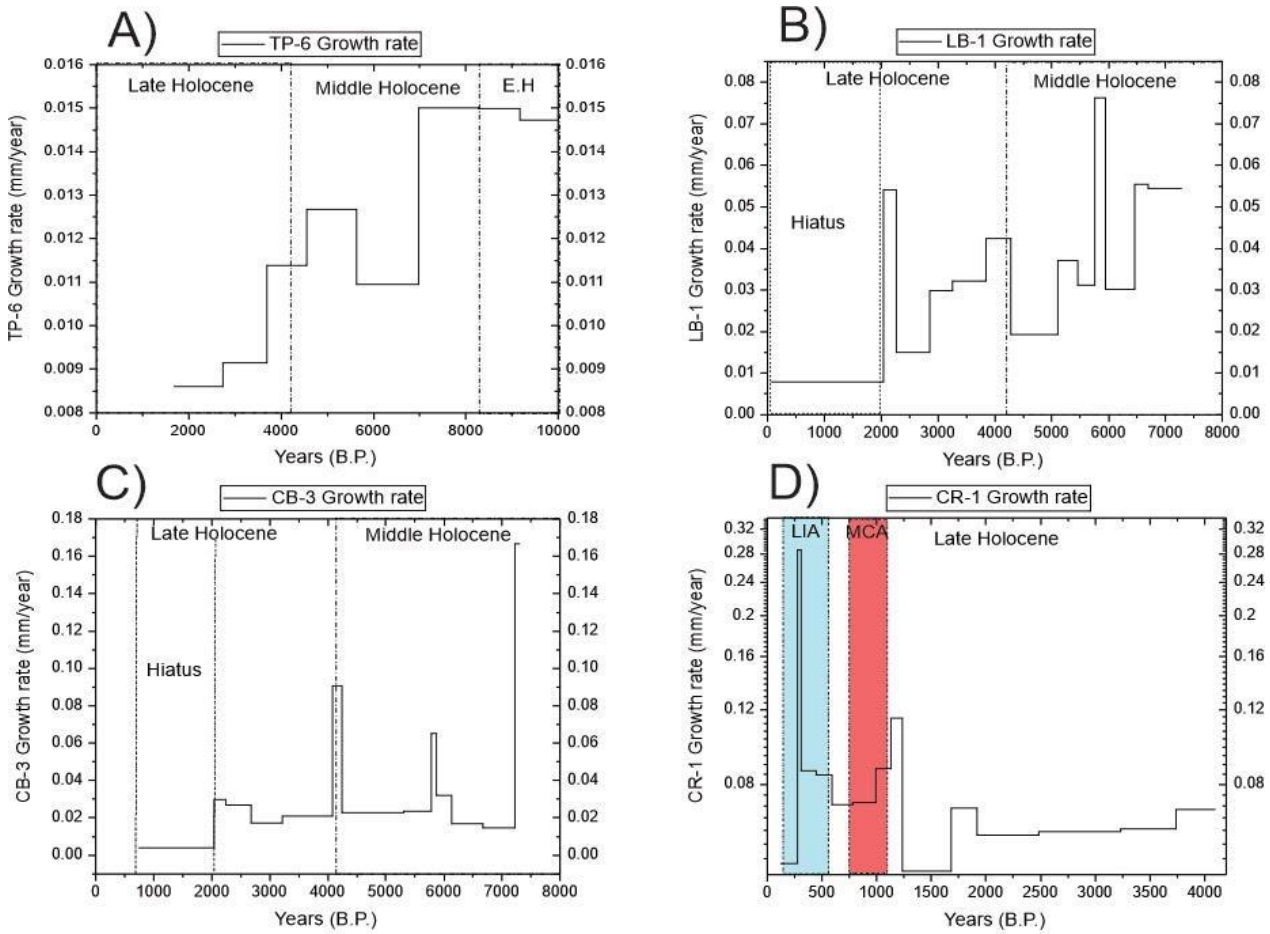

Figure 41 - Growth rates of the speleothems used in this study. A) TP-6; B) LB-1; C) CB-3; D) CR1; LIA (Little Ice Age) and MCA (Medieval Climate Anomaly).

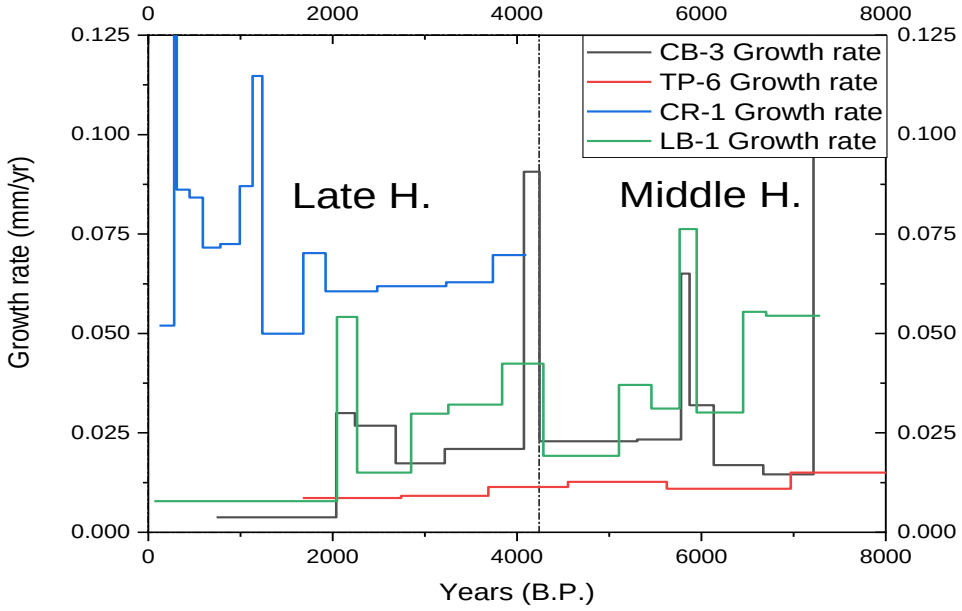

Figure 42 - Combination of all the speleothem growth rates with a delimitation between Middle and Late Holocene.

7.2.2 Middle and Late Holocene paleoflood record and its flood frequency

For the samples from Laje Branca cave, the thickness of the detrital layers and the presence of unconsolidated clay in some of these layers facilitate the use of visual method for their recognition. For LB-1 speleothem, two types of detrital layers were identified: (L1) thin detrital layers with central axis washing and detritus concentrated in the side of the speleothem; and (L2) thick detrital layers without central axis washing and with lateral continuity, in some cases with cavities with clay. For CB-3 three types of detrital layers were described: (C1) thin layers with central axis washing, mainly recognized in the side of the speleothem; (C2) thick layers with lateral continuity and no central axis washing; (C3) thick layers associated with abrupt changes in the growth axis of the speleothem.

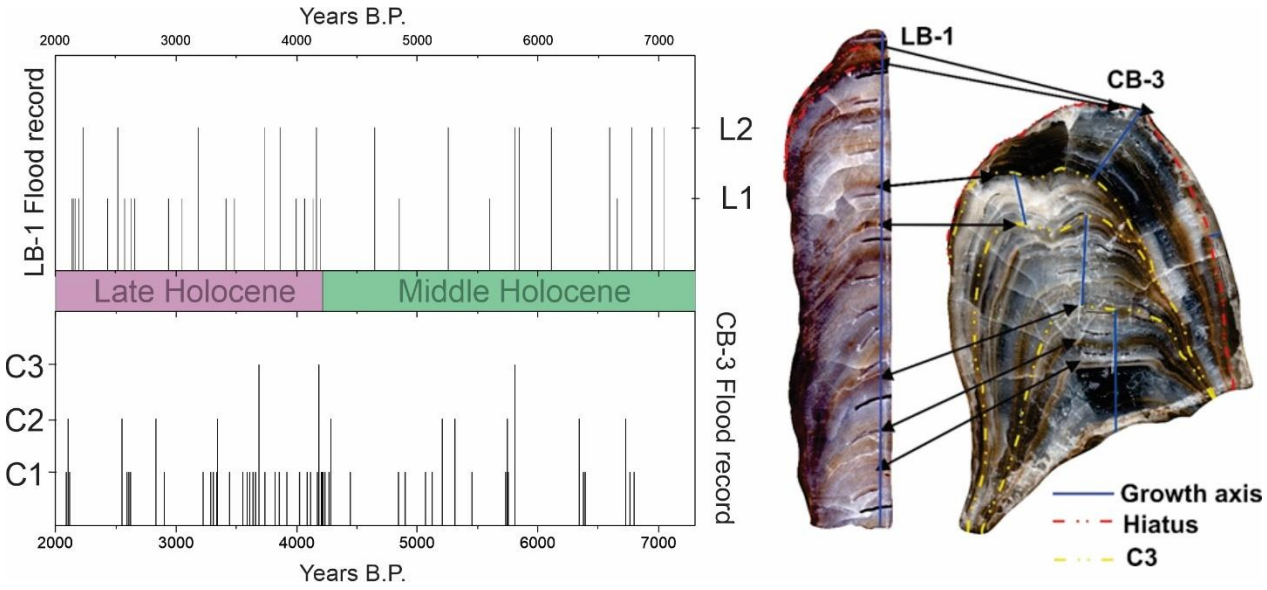

Figure 43 – On the left a graph of the flood record from Laje Branca cave-flood based on detrital layers within the speleothems (CB-3 and LB-1), with a delimitation of Late Holocene (4.2k to present) and Middle Holocene (8.2k to 4.2k). On the right there are CB-3 and LB-1 scan images of the speleothems polished face. The detrital layers (C3) of CB-3 are marked by yellow dash lines and the Hiatus identified in the speleothems are marked by the red dashed line. The black arrows indicate the correspondence between the thick detrital layers in LB-1 and the detrital layers of C3 type in CB-3. Blue line represents the central growth axis of the speleothems.

In total, 35 layers were recognized in LB-1 with 19 described as L1, 15 as L2, and in CB-3 were recognized 55 detrital layers, with 42 described as C1, 9 as C2 and 4 as C3. Both speleothems show a tick detrital layer correspondent with the hiatus observed in the U/Th ages with an abrupt change in the growth axis of the CB-3. The differences in the number of layers between speleothems can be caused by their different susceptibility to flood events once these samples are in different elevations in the cave and therefore are more or less exposed to the variations of water

levels in response to floods. Still, the tickers detrital layers (L1, C2 and C3) shows a good correspondence in time, potentially representing big flood events that affect both galleries (Fig 43).

To reconstruct a paleoflood frequency time series of the Middle and Late Holocene it was used bins of 100, 250 and 500 years as Lage Branca speleothems record low frequency events (Fig. 44). For the 5000-yr period of Laje Branca record, the average frequency of flood per century is 1.1 for CB-3 and 0.72 for LB-1. The Middle Holocene is characterized by lower numbers of events, with 18 floods recorded in CB-3 with a flood frequency per century of 0.64 and 12 floods in LB-1 with a mean of 0.41 flood per century. The transition from the Middle to the Late Holocene is marked by a significant increase in the flood frequency, with 5 floods per century in both speleothems. The frequency values calculated for 500 years bin shows a trend to higher flood frequency during the Late Holocene of LB-1, while CB-3 shows an opposite result, with a decrease trend in the flood frequency.

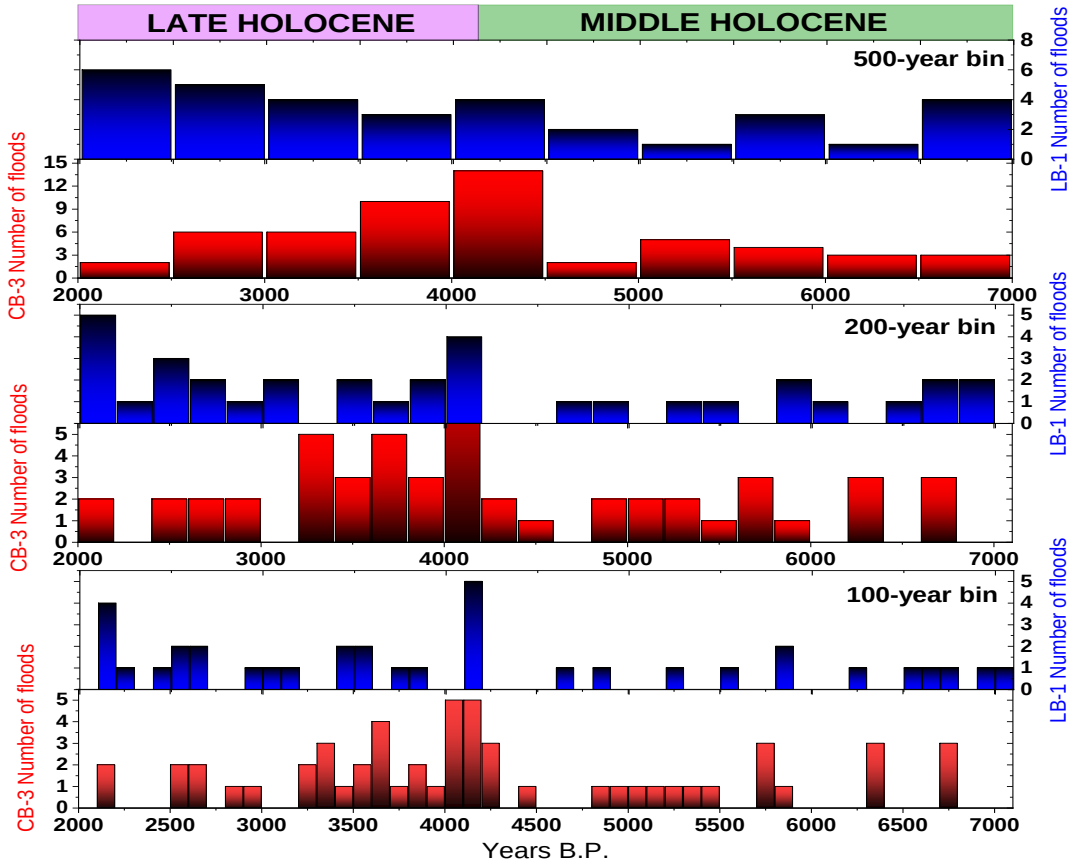

Figure 44 - Laje Branca cave flood frequency. The red (blue) bars represent the flood frequency in 100, 200 and 500-year bin of CB-3 (LB-1).

During the Late Holocene, CB-3 shows an average of 2.63 floods per century with 37 floods between 4200-2000 B.P., with 78% of the floods occurring between 4200-3250 B.P., including two

thick detrital layers with abrupt change in the growth axis. Between 3250-2000 B.P. is marked by a decrease in the flood frequency for 0.72 floods per century and for the abrupt change in the growth axis approximately in 2000 B.P., marking a hiatus in the deposition of the speleothem. LB-1 shows an average of 1.14 floods per century with 24 floods between 4200-2000 B.P. The Late Holocene is also characterized by a higher number of centuries with floods recorded in both speleothems.

7.2.3 Stable isotope records of $\delta^{18}O$ and $\delta^{13}C$

During this project two speleothems were analyzed from Laje Branca cave (LB-1 and CB-3). They were compared with the isotopes records of Cristal cave speleothem (CR-1) from Taylor (2014) and the unpublished $\delta^{18}O$ record from Tapagem cave (TP-6), also knowns as Caverna do Diabo. The records from LB-1, CB-3 and TP-6 were used to reconstruct the climate based on the isotopic variations through the Middle Holocene (8200 B.P. to 4200 B.P.) and the transition with the Late Holocene. To describe the climate during Late Holocene all these samples were used.

Table 2 – Ensanble of speleothems used for the Middle and Late Holocene.

Cave	Speleothem	Records	N. analyses	Mean Resolution
Laje Branca	LB-1	$\delta^{18}O$ and $\delta^{13}C$	493	11 yrs
	CB-3	$\delta^{18}O$ and $\delta^{13}C$	336	15 yrs
Tapagem	TP-6	$\delta^{18}O$	289	35 yrs
Cristais	CR-1	$\delta^{18}O$ and $\delta^{13}C$	1602	3 yrs

The samples CB-3 and LB-1 shows a correlation between their own $\delta^{18}O$ and $\delta^{13}C$ of 0.63 and 0.48, respectively (Fig. 45). The $\delta^{18}O$ values of Lage Branca speleothems vary between -2.82‰ and -4.91‰ with mean values of CB-3 and LB-1 of -3.69‰ and -3.91‰ respectively (Fig. 46). The $\delta^{13}C$ from LB-1 varies between -0.81 and 3.05‰ with a mean of 0.74‰ while CB-3 shows more negative values varying between -3.89 and -0.14‰ with a mean of -2.34‰. CR-1 shows a correlation between $\delta^{18}O$ and $\delta^{13}C$ of 0.51, similar to Lage Branca speleothems with $\delta^{18}O$ varying in a larger range between -7 and -3.8‰ with mean value of -5 ‰ and with the $\delta^{13}C$ varying between -4.4 and -9.7‰ with mean of -7‰. TP-6 $\delta^{18}O$ varies between -2 and -4.9‰ with mean of 2.8‰. The $\delta^{18}O$ and $\delta^{13}C$ of MFZ-N-1 have values similar to CR-1 between -7 and -3‰ and mean of -4.95‰ for $\delta^{18}O$ between -1.8 and -8.5‰ with mean of -6.4‰ for $\delta^{13}C$. Distinct from the other

samples, MFZ-N-1 shows a correlation of $\delta^{18}O$ and $\delta^{13}C$ of 0.16, and the values are plotted in the same field as CR-1 (Fig. 45).

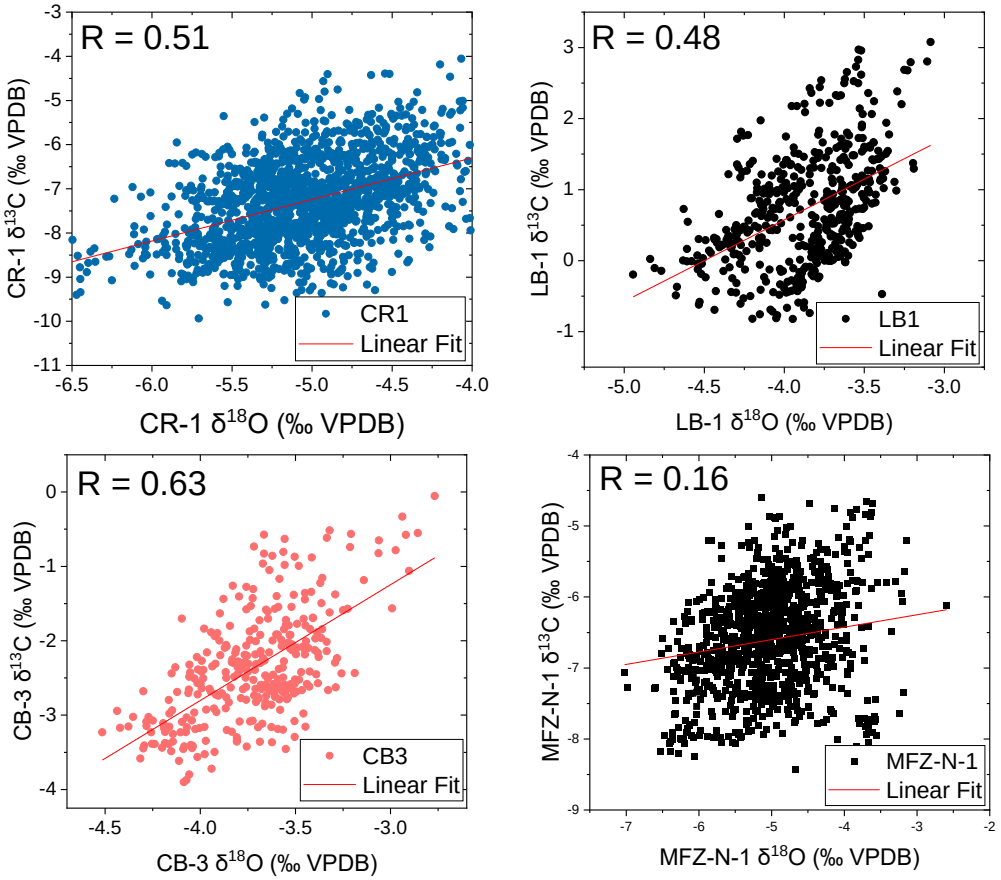

Figure 45 - $\delta^{18}O$ and $\delta^{13}C$ fields of SEB speleothems. MFZ-N-1 and CR-1 are plotted in the same field and shows depleted values of $\delta^{18}O$ and $\delta^{13}C$ in comparison with Laje Branca speleothems.

The speleothems from Laje Branca show more enriched values of $\delta^{18}O$ in the Middle Holocene with an average of -3.6‰ for LB-1 and -3.56‰ for CB-3 and more depleted values for the Late Holocene with average of -4.19‰ for LB-1 and -3.91‰ for CB-3. In the Middle Holocene, the $\delta^{18}O$ values vary in a plateau defined by the average, with negative excursions in 6400 B.P. - 6800 B.P., 5600.BP. - 5900B.P. and 4500 B.P. - 4600 B.P., being the last one characterized in CB-3 by an abrupt increase in $\delta^{18}O$ after 4500 B.P. and in LB-1 by a downward trend to more negative values until the transition with the Late Holocene. The transition is marked in LB-1 by the lowest value of $\delta^{18}O$ from the Middle Holocene record, reaching -4.2‰ in 4.200 B.P., while CB-3 shows a shift of 1‰ to more depleted values between 4300-4100 B.P. In the beginning of the Late Holocene there is a small increase in $\delta^{18}O$ in both records, between 4200-3700 B.P. in LB-1 and 4200-3500 B.P. in CB-3. The $\delta^{18}O$ of LB-1 varies in a plateau until it reaches the lowest values of

the entire record in 2100 B.P. of -4.9‰. CB-3 varies in a plateau between 3500-2600 B.P. After 2600 B.P. the record shows a negative excursion going from -3.7 to 4.4‰ in 2200 B.P.

TP-6 shows the same pattern of more enriched values of $\delta^{18}O$ in the Middle Holocene and depleted values in the Late Holocene with an average of 2.77‰ and -4.3‰ respectively (Fig. 47). The Middle Holocene is characterized by a downward trend in the $\delta^{18}O$ values with a drop in the values between 6800-6400 B.P. and between 5800-5400 B.P. as observed in Lage Branca speleothems. An abrupt drop of 2‰ for more depleted values is observed between 3500-3700 B.P. as observed in CB-3. The direct comparison of the isotope shifts is more difficult between 3600-4500 B.P. due to lack of U/Th ages, which can change the timing of the shift. The shift in TP-6 is also observed as a change of the speleothem color from a translucent dark grey to an opaque white.

CR-1 isotope record covers only the Late Holocene and show a downward trend from 4.4 to 5.3‰ between 4000-2000 B.P like CB-3, with a bigger drop after 2800 B.P where the record shows more depleted values (average of -5.24‰) between 2800-1000 B.P (Figure 47).

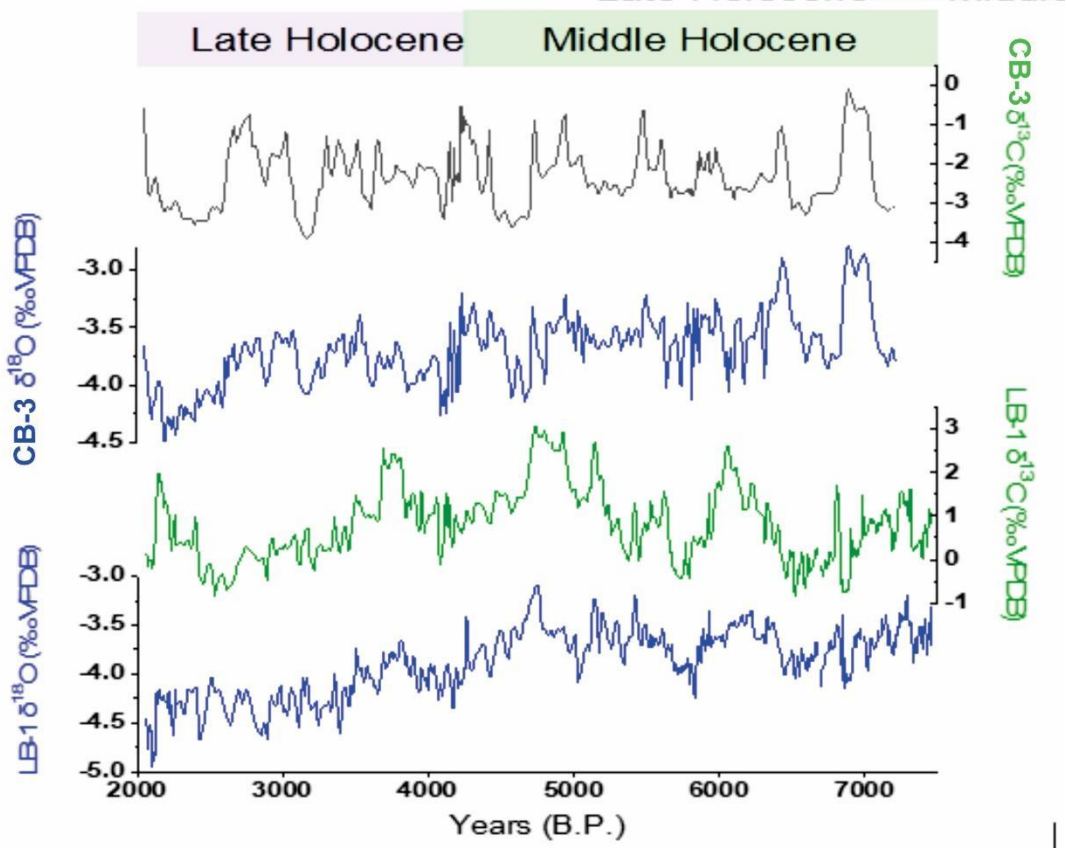

Figure 46 - $\delta^{18}O$ and $\delta^{13}C$ stable isotopes records of Laje Branca speleothems.

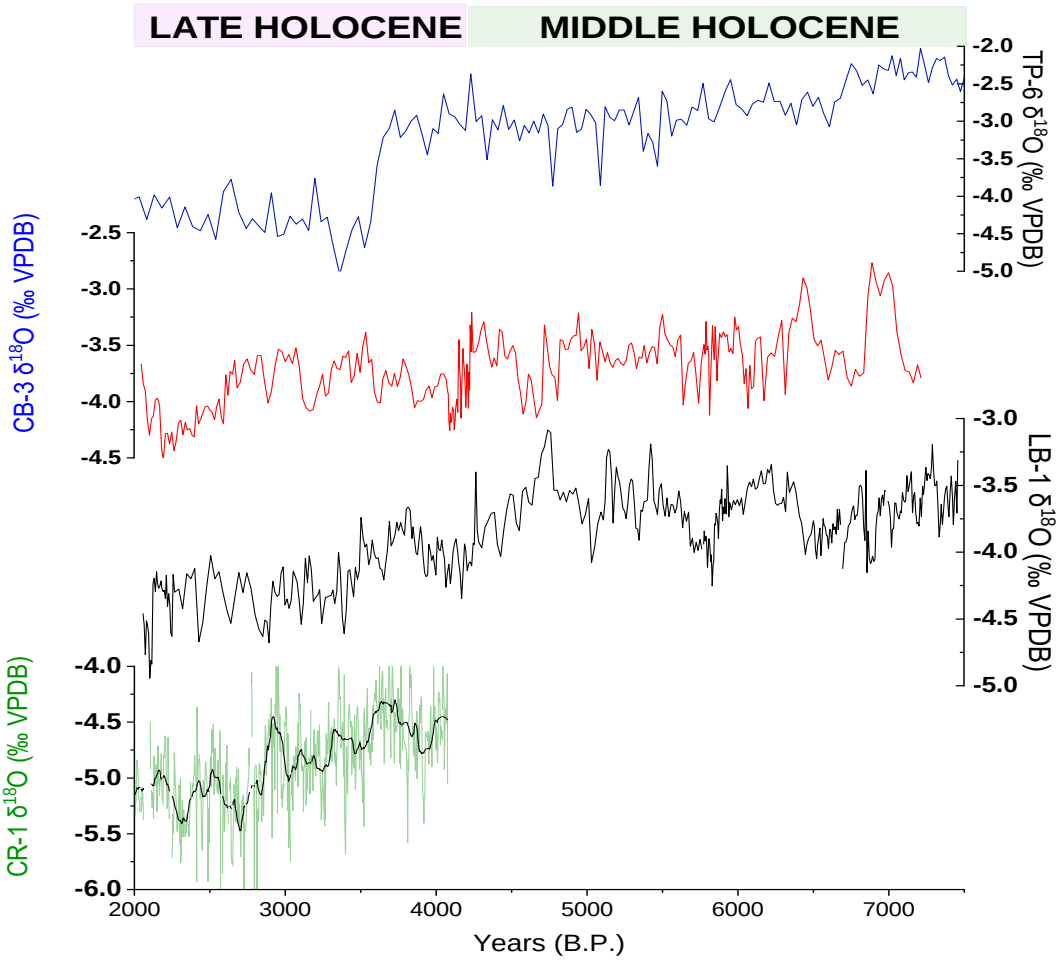

Figure 47 - $\delta^{18}O$ time series of SEB speleothems covering the Middle and Late Holocene.

7.2.4 Trace elements

In this section it is presented the high-resolution CR-1 trace element record covering the Late Holocene (from 4100 to 6000 B.P.) with 58833 points of analysis resulting in a mean resolution of 14 points per year. As showed in section 7.1.5, the ln series of trace elements ratios with Ca shows a high correlation between them and are co-vary linearly in a ln-space, agreeing with the model presented by Sinclair et al. (2011) and Sinclair et al. (2012) for cases where PCP/ICD are mainly modulating the trace elements ratios with Ca concentrations. Next is presented the comparisons between the trace elements records and with the stable isotopes of CR-1 and with Lage Branca speleothems records.

For better comparison between the series, it was calculated the anomaly series of the trace element ratios with Ca. The records shows common periods of predominant negative anomalies in 70-420 B.P., 930-1300 B.P., 1570-1630 B.P., 2060-2350 B.P., 2550-2660, 2780-3000 and 3130-

3230 B.P. The correlation between Sr/Ca-Mg/Ca and between Sr/Ca-Ba/Ca are of 0.75 and 0.73 respectively, with the lowest correlation between Mg/Ca and Ba/Ca of 0.48. It is possible to observe the match between the trace elements records in Figure 46.

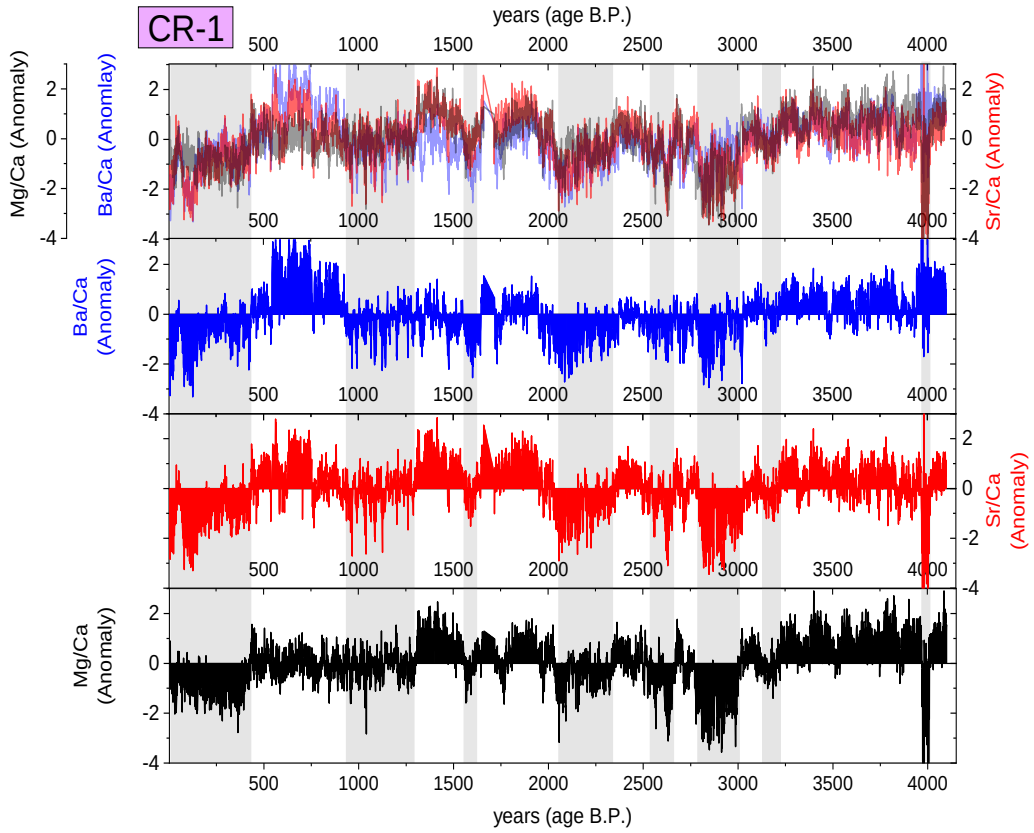

Figure 48 – Trace elements time-series from CR-1 record (Cristal cave).

To better understand the variations of the trace elements observed in the CR-1 records, the anomaly series of the trace elements with $\delta^{13}C$ from CR-1 are compared in Figure 46. The $\delta^{13}C$ series shows the higher correlation with Mg/Ca (R=0.22), and relative low correlations with Sr/Ca and Ba/Ca (R=0.14 for Sr/Ca; R=0.09 for Ba/Ca). The trace elements series show matches with $\delta^{13}C$ periods of negative anomaly as in 150-460 B.P., 930-1300 B.P., 2100-2300 B.P. and 2540-2680 B.P., and a match between the period of positive values between 3200-4100 B.P., and $\delta^{13}C$ shows a likely modulation with the trace elements records. The $\delta^{18}O$ series does not show correlation with the Sr/Ca series, while with Mg/Ca and Ba/Ca the $\delta^{18}O$ record shows a correlation of 0.22 and 0.11 respectively. Periods of negative anomaly predominating do not necessarily show correspondence between the $\delta^{18}O$ series and the trace elements series.

8 DISCUSSION

8.1 Paleoclimatic interpretations of the stable isotopes and trace-elements records from the last millennium from Southeast Brazil

Previous studies from Southeast Brazil showed that the variability of $\delta^{18}O$ in speleothems is mainly related to variations in the contribution from two different sources of moisture with more depleted (enriched) values related to monsoonal (extratropical) sources (Cruz et al., 2005), thus leading the $\delta^{18}O$ record to be used as a suitable proxy for changes in precipitation regimes from tropical-extratropical interactions over South America moisture source. The comparison with instrumental records of the study area (rainfall series) showed that MFZ-N-1 $\delta^{18}O$ variations is mainly controlled by the difference contribution between the winter and summer rainfall in the annual amount (Fig. 10). Therefore, it is interpreted here as a proxy for moisture contribution between the summer monsoon (SAMS) with major contribution from distal moisture sources from Amazon region and the extratropical regimes that use sources mainly from nearby Atlantic Ocean, allowing the observation of shifts in atmospheric circulation during the last millennium over the study region. This consistence of the speleothem isotope records with regional climate is reinforced by the good match between the archives from different caves such as Malfazido and Cristal cave when the smooth series (decadal resolution) of CR-1 and MFZ-N-1 are used (Fig. 8). Thus, the variations in the $\delta^{18}O$ values of the speleothems are mainly controlled by regional atmospheric features rather than local process.

The records show predominant negative anomalies during the MCA with short intervals of positive anomalies that characterizes this period as dominated by SACZ (Fig. 49). The strong positive anomaly observed in MFZ-N-1 record between 950-1020 C.E. does not have correspondence in CR-1 record and the uncertainty that is possibly caused by the lack of ages during this interval hampering the interpretation of this anomaly. An enhancement of SACZ contribution is observed in the end of MCA with strong negative anomalies in MFZ-N-1 record from 1170-1250 C.E. The CR-1 record shows similar anomalies between 1130-1170 C.E. and from 1240-1300 C.E. Positive anomalies predominates between 1250 and 1560 C.E in MFZ-N-1 and between 1320-1520 C.E. in CR-1. This positive anomaly indicates a decrease in moisture from SACZ between the end of MCA until the first part of LIA. The strongest negatives anomalies in $d^{18}O$ happen during the second part of LIA until the beginning of the last century and are recorded in MFZ-N-1 between 1550-1900 C.E. and in CR-1 from 1520-1850 C.E. These negative anomalies

represent the most intense activity of SAMS in the study area of the last millennium, with the interval from 1600-1700 C.E. concentrating the negative anomalies. The last century is marked by the strongest positive anomalies of both records (not considering the positive anomaly at the beginning of MFZ-N-1) indicating a tendency of less contribution of monsoonal moisture, thus the recent period shows the weaker contribution of SAMS in the study area, although this feature could be also related with higher contribution from heavier isotope winter rainfall events.

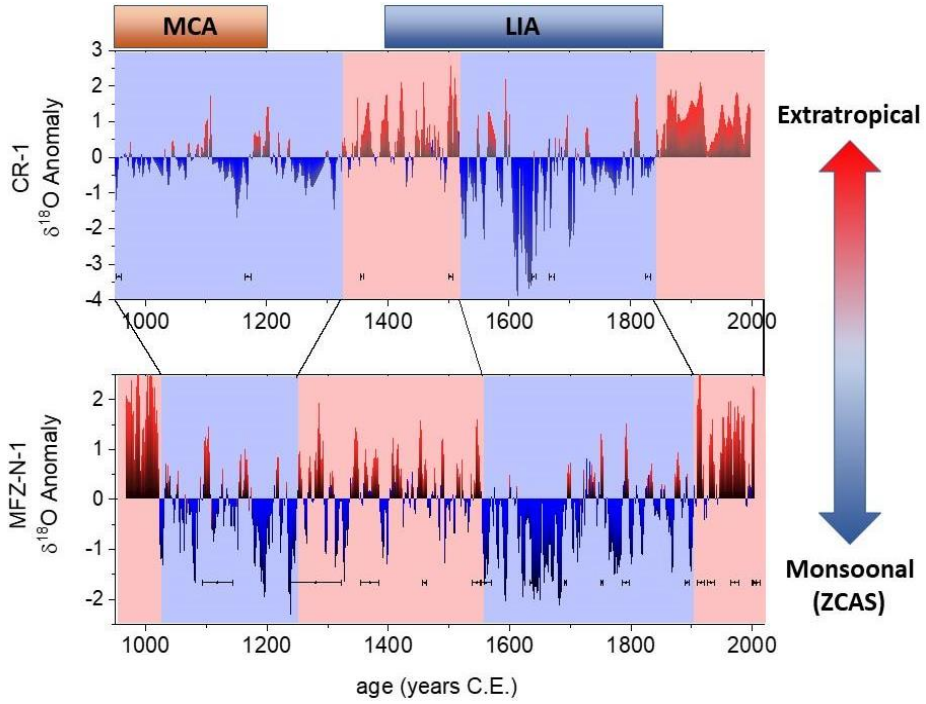

Figure 49 - Anomaly $\delta^{18}O$ timeseries of CR-1 and MFZ-N-1. The blue(red) box represents the periods with predominance of negative(positive) anomaly values. The positive anomaly periods are interpreted as result of an enhancement of extratropical contribution or a weakening of SAMS activity, while the negative anomaly periods are interpreted as the opposite. The horizontal dots with bars represent the U/Th ages of the speleothems with the 2σ errors.

Novello et al. (2018) presents a data set of isotopic proxies ($\delta^{18}O$) recording SAMS variability that indicates a moist/dry dipole modulated by the positioning of the SACZ during the last two millennia, where shifts in SACZ position leads to drier and wetter conditions on either side of this system. The southwest records of SACZ were here used to compare whether negative (positive) anomalies from MFZ-N-1 and CR-1 could be directly related to an enhancement (reduction) of the SAMS/SACZ activity in the study area by southwards (northwards) shifts in SACZ position. The periods of predominant negative anomalies of $\delta^{18}O$ in the study area (1000-1250 C.E. and 1550-1900 C.E.) are represented in figure 49 by light blue boxes and the periods where positive anomalies predominate are signaled by light red boxes.

In general, along the last millennial, the precipitation variability recorded in the oxygen isotope records from Southeastern and central western Brazil shows a consistent variability at centennial timescale. For instance, the anomalous negative period present in MFZ-N-1 and CR-1 between 1550 and 1900 C.E. is consistent with the wet conditions documented for the records located southwest of SACZ axis mean position as Pau d'Alho and Curupira Cave (Novello et al., 2016), Jaraguá Cave (Novello et al., 2018) (Figure 50). These climate features are also confirmed statistically in the principal component analyses performed in Campos et al., (2019). The strongest negative anomalies are concentrated between 1560 and 1700 C.E in MFZ-N-1 and CR-1 while Jaraguá cave speleothems concentrate the negative anomalous values between 1712 and 1800 C.E. and Pau d'Alho between 1770 and 1850 C.E (MFZ-N-1 also shows strong negative anomalies in this period). Novello et al. (2018) posit that a southward shift in SACZ axis during LIA has enhanced rainfall along the sites located in the southwestern side of the SACZ. This southward shift could cause a strengthening of SACZ influence over the study area, providing more monsoonal moisture (depleted in $\delta^{18}O$). Despite LIA represent an anomalous negative period for all the $\delta^{18}O$ records, the timing of the strongest anomalies during this period are different among the areas (MFZ-N-1 and CR-1) and for Jaraguá cave record and Pau d'Alho cave record.

The last century is characterized by anomalous positive values of $\delta^{18}O$ in all records. In both central-western and southeastern region in Brazil the XX century is marked by strong positive anomaly values in the record. These results suggest that the last century is characterized by a weakening in SAMS/SACZ activity in the southeastern/southern Brazil by a change in the atmospheric circulation with less contribution of monsoonal moisture, and the high positive values of CR-1 and MFZ-N-1. This feature may also be explained by an enhancement of extratropical moisture (enriched in $\delta^{18}O$).

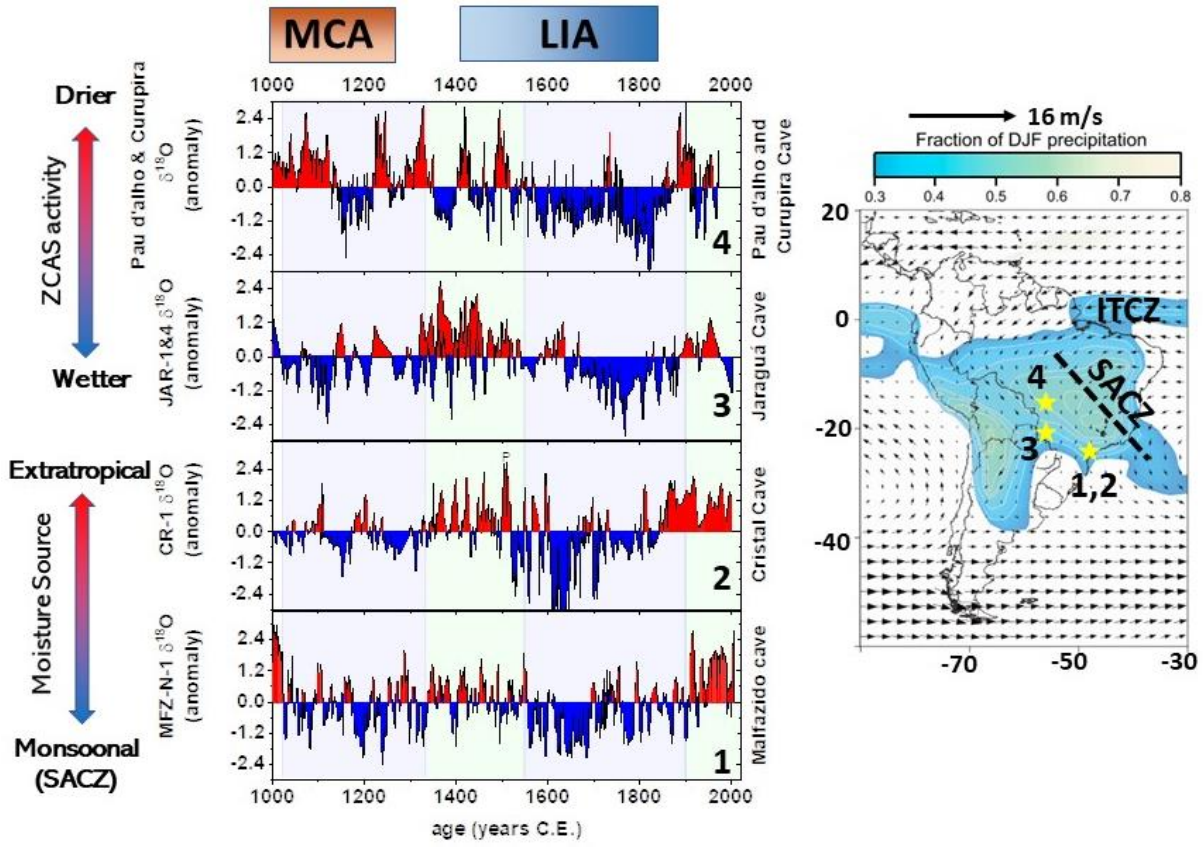

Figure 50 – $\delta^{18}O$ anomaly timeseries of speleothems of Southeastern and central western Brazil. (1) MFZ-N-1 from Malfazido Cave in eastern Paraná. (2) CR-1 from Cristal Cave in southwest of Sâo Paulo. (3) JAR1 and JAR4 of Jaraguá Cave from Mato Grosso do Sul. (4) Pau d'Alho and Curupira samples from Pau d'alho and Curupira Cave in Mato Grosso. $\delta^{18}O$ variations from JAR1, JAR4, Curupira and Pau d'Alho are interpreted as more (less) SACZ activity and consequently as wetter or drier conditions in central western Brazil. Novello et al. (2018) interpreted the enhancement of SAMS/SCAZ activity in the central western Brazil as a southward displacement of the SACZ axis. The map in the left represent the samples locations and the modern SACZ axis (modified from Novello et al. (2018)).

MFZ-N-1 records of Mg/Ca and Ba/Ca show a positive correlation of R=0.42 with some intervals reaching 0.6 and are positive correlated with $\delta^{18}O$ and $\delta^{13}C$ with the Mg/Ca showing a remarkable fit with both series. In comparison, the Sr/Ca and U/Ca ratios present a positive correlation of R=0.32 reaching 0.5 between 1400 to 2007 C.E, and are negative correlated with the stable isotopes, both records show a reasonable match with the stable isotope's records (Fig. 30 and 31). The relationships between trace elements and stable isotopes reinforces the hypothesis of prior-aragonite-precipitation (PAP) as the main process modulating the concentration of the trace elements (Wassenburg et al., 2019). This is possibly the main process controlling trace element variation in the MFZ-N1 speleothem because it is totally composed by aragonite. As showed by Wassenburg et al. (2019), the partition coefficient of the trace elements for aragonite ($K_{Mg}<1$; $K_{sr}>1$;$K_U>>1$) tends to concentrate (reduce) the Mg (Sr and U) in the fluid during drier (wetter)

periods due to the higher (lower) residence time, degassing and to more (less) air-filled spaces in the epikarst. The positive correlation between the Mg concentrations and the $\delta^{13}C$ and the negative correlation between U and Sr with $\delta^{13}C$ strengthens the arguments in favor of PAP since the prior precipitation of aragonite is driven by degassing that tend to enrich the $\delta^{13}C$ of the solution. The same relationship is observed for $\delta^{18}O$ with a remarkable fit with the ln(Mg/Ca), ln(Sr/Ca) and ln(U/Ca) and indicates that the process modulating the trace element concentration is related to an hydrological feature since the speleothem $\delta^{18}O$ is assumed to largely reflect changes in rainfall.

CR-1 trace elements records are highly correlated among themselves and they show a strong linear covariation in an Ln space. Sinclair et al. (2011) and Sinclair et al. (2012) demonstrated that if PCP/ICD modulates Mg/Ca and Sr/Ca variability in the absence of kinetic control, the molar ratios should co-vary linearly in a ln-space with a slope of 0.88 ± 0.13. The slope calculated for Ln(Sr/Ca) with Ln(Mg/Ca) from CR-1 is in agreement with the calculated values presented in these studies, reinforcing the hypothesis of PCP and ICD as the main controls of the trace elements variability in Cristal Cave speleothem. The positive correlation with $\delta^{13}C$ with similar modulation between the stable isotope and trace elements timeseries, corroborate with PCP since degassing of CO_2 from solution tend to increase $\delta^{13}C$ by preferential loss of lighter isotopes. The same positive correlation is observed $\delta^{18}O$ and since it is assumed to reflect changes in rainfall it corroborates with a hydrological feature modulating the trace element concentrations (Fig. 30 and 31).

A change in the chemistry of the water forming the speleothems is often considered to be a dominant factor for speleothem records that show Mg and/or Sr variations (Verheyden et al., 2000; Baldini et al., 2002; McMillan et al., 2005; Li et al., 2005; Johnson et al., 2006; Cruz et al., 2007). Drip water composition is closely linked to hydrological conditions in the cave system because processes controlling carbonate dissolution and precipitation are highly dependent on the rate at which meteoric water infiltrates down in the soil-bedrock profile (Fairchild et al., 2000; Musgrove and Banner, 2004; Tooth and Fairchild, 2003). These features were confirmed in a monitoring program performed in Santana Cave (Karmann et al., 2005), located very close to Cristais cave. In this context, the trace element incorporation in the CR1 speleothem probably reflect the decreased water levels in the vadose aquifer above the cave can enhance air ventilation through the fractures or proto-conduit networks and trigger CO_2 degassing, while promoting prior calcite precipitation (PCP) during dry periods. Ca is favorably incorporated into calcite precipitated in the vadose zone right above the cave (D_{Sr} and $D_{Mg}<<1$), resulting in higher Sr/Ca and Mg/Ca in drip waters (Huang

and Fairchild, 2001). This process is likely to produce coherent variations in these trace element ratios in speleothems.

A four-year long hydrochemistry monitoring program performed in nearby Santana cave (Fig. 1), reveals that prior calcite precipitation is most likely the dominant process affecting the drip water composition (Karmann et al., 2007). Because the Santana cave system is located about 20 km apart from Crystal Cave and shows very similar climatic, hydrogeological and environmental (e.g. soil and vegetation cover) characteristics, it provides an excellent analogue for understanding the dissolution-precipitation processes taking place during deposition of CR1 speleothem.

In CR1 calcite speleothem, lower Mg/Ca and Sr/Ca ratios are interpreted as found following rainfall associated with the South American monsoon in Southern Brazil, similarly to previous studies in calcite speleothem from Botuvera cave in Southern Brazil (Cruz et al., 2007; Bernal et al., 2016). Thus, the PCP is possibly the dominant process affecting trace-element variations in speleothems also in Cristais cave.

Because the trace element ratios also show a coherent positive covariation pattern with stable oxygen and carbon isotope ratios in CR1 record, we interpret that PCP is the main process controlling the incorporation of Sr and Mg in the calcite. Therefore, it is possible to relate the trace element variations to the level of the unsaturated aquifer above the cave, a factor that is directly dependent on local rainfall conditions (Cruz et al., 2007). These authors argue that the PCP is dependent on the degree of ventilation in the vadose zone, which makes the process less effective when the rainfall recharge events are more intense and more evenly distributed throughout the year. In this case, the residence time of water in the karst aquifer is, on average, lowest, and the least degree of PCP is achieved.

To simplify the interpretation of the trace elements variations the multivariate dataset of CR-1 and MFZ-N-1 were reduced using PCA, and the obtained PCs are used to identify modes and timing of variations that account to the overall variability of the datasets. The $PC1_{CR-1}$ account for 86.8% of the variance with statistical significance above 95% (tested by brokenstick model and bootstrap re-sampling) and shows a strong positive correlation between the multiple elements ratios (Sr/Ca, R=0.96; Ba/Ca, R=097; and Mg/Ca, R=0.63). Therefore $PC1_{CR-1}$ is here used as a proxy for PCP/ICD variations in CR-1 records and the positive values indicates higher PCP/ICD with drier conditions, with fissures and secondary conduits ventilated during dry periods allowing

degasification and thus promoting calcite precipitation upstream the seepage flow pathway that leads to the enrichment of Sr, Ba and Mg relative to Ca. The opposite scenario is interpreted for negative values, were wetter conditions leads to fill the ventilate conduits with water, preventing the degasification and consequently the precipitation of calcite. The $PC2_{MFZ\text{-}N\text{-}1}$ accounts for 31% of the dataset variance with more than 95% of statistical significance as showed by broken-stick model and by confidence limits based on bootstrap re-sampling. This PC agrees with the prior aragonite precipitation described by Wassenburg et al. (2019), where positive correlations with U/Ca and Sr/Ca of 0.78 and 0.36 respectively, and negative correlations with Mg/Ca of 0.64 can be explained due to the partition coefficient with aragonite ($K_{Mg}<1$; $K_{sr}>1$;$K_{U}>>1$). Due to the consistency among the trace elements and with the stable isotope's records, $PC2_{MFZ\text{-}N\text{-}1}$ is used as a proxy for PAP, with negative values indicating drier conditions with low (high) ratios of U(Mg)/Ca due to the incorporations of the trace element in the prior aragonite precipitated, and positive values indicating high ratios of U(Mg)/Ca lead by wetter conditions. $PC2_{MFZ\text{-}N\text{-}1}$ negative correlation with $\delta^{13}C$ and $\delta^{18}O$ corroborate with this hypothesis since PAP can increase $\delta^{13}C$ by degasification such as PCP, and $\delta^{18}O$ is relate to changes in rainfall, indicating a hydrological feature controlling the trace elements variations.

The novel high-resolution trace element records from MFZ-N-1 are used here as a palaeohydrological indicator, allowing to access wetter/drier conditions, and together with the $\delta^{18}O$ record it is possible to identify whether shifts in $\delta^{18}O$ reflecting changes in the amount of moisture from monsoonal and extratropical sources are relate to changes in the amount of rainfall, as well as in previous studies performed in Southern Brazil (Cruz et al., 2007; Bernal et al., 2016). This multi-proxy approach is a powerful tool to understand how climate changes can affect the rainfall distribution and whether it can cause changes in the hydrological availability. In Figure 51 it is show a comparison between the $PC2_{MFZ\text{-}N\text{-}1}$ and the stable isotopes record.

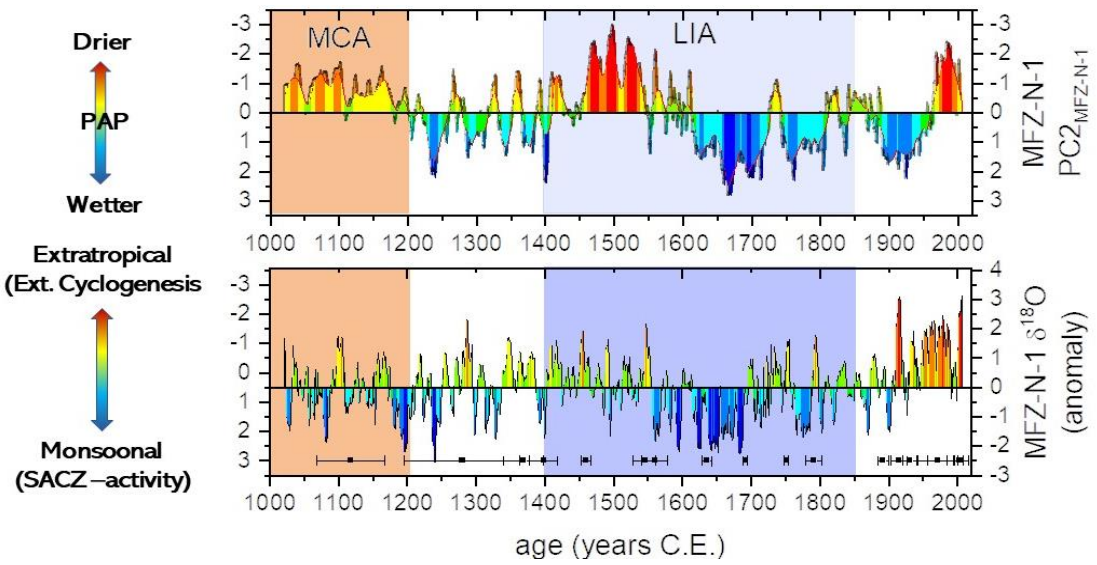

Figure 51 – MFZ-N-1 $\delta^{18}O$ and trace elements PC timeseries. Negative (positive) anomalies of $\delta^{18}O$ represent more contribution of monsoonal (extratropical) moisture by enhancement of SACZ (extratropical cyclogenesis) activity. $PC_{MFZ\text{-}N\text{-}1}$ positive (negative) values indicates more (less) prior-aragonite precipitation and drier (wetter) conditions.

The $\delta^{18}O$ variations shows consistency during some intervals like the negative anomaly between 1600-1723 C.E. where strong negatives anomalies of $\delta^{18}O$ are related to strong positive anomalies of $PC2_{MFZ\text{-}N\text{-}1}$, or like the period between 1400-1550 C.E. where positive anomalies of $\delta^{18}O$ are related to strong negative anomalies of $PC2_{MFZ\text{-}N\text{-}1}$. This variation may be caused by a strengthening (weakening) of SACZ activity represented by anomalous negative values of $\delta^{18}O$ that increased (decrease) the moisture availability resulting in wetter (drier) conditions as indicate by $PC2_{MFZ\text{-}N\text{-}1}$. Differences in the $\delta^{18}O$ and the PC may arise from the *moisture source effect* in the control of oxygen isotope composition of local rainfall. Following this reasoning decoupling periods, as observed between near 1870-1940 C.E., when trace elements suggest a marked increase in local rainfall while the $\delta^{18}O$ describes an positive trend (less moisture accordingly to the *amount effect*) may result from a strengthening of extratropical cyclone.

The same relation is observed for CR-1 with $\delta^{18}O$ and trace elements PCs. Periods of $\delta^{18}O$ strong negative anomalies as between 1550 and 1600 C.E. are accompanied by negative anomalies in $PC1_{CR\text{-}1}$, but also the strongest negative anomaly period of $PC1_{CR\text{-}1}$ are related to positive anomalies of $\delta^{18}O$ between 1800 and 1870 C.E. This relationship shows that changes in SAMS activity and in the extratropical cyclogenesis can significantly impact the moisture availability. Another relation observed in MFZ-N-1 and CR-1 is the anomalous negative period of $\delta^{18}O$ during MCA with drier conditions indicated by both trace elements PCs. This can be result by a weakening

of the extratropical cyclogenesis that leads to less extratropical moisture availability, decreasing the $\delta^{18}O$ not necessarily by a strengthening of SACZ, and resulting in drier conditions in both cave sites.

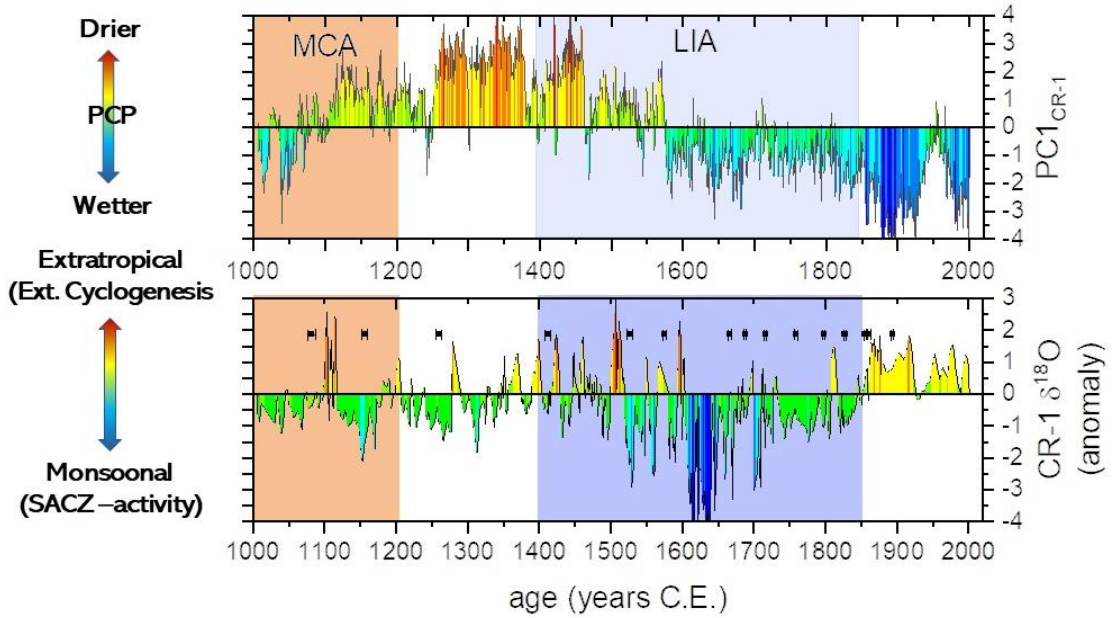

Figure 52 – CR-1 $\delta^{18}O$ and trace elements PC timeseries. Negative (positive) anomalies of $\delta^{18}O$ represent more contribution of monsoonal (extratropical) moisture by enhancement of SACZ (extratropical cyclogenesis) activity. $PC_{MFZ\text{-}N\text{-}1}$ positive (negative) values indicates more (less) prior-aragonite precipitation and drier (wetter) conditions.

8.2 Possible Links Between Speleothems Proxies from Southeast Brazil and SSTs From the Atlantic and Pacific Ocean

The $\delta^{18}O$ values from CR-1 and MFZ-N-1 are predominantly negative (positive) during AMO/AMV negative (positive) phases as indicated by comparisons with AMO/AMV reconstructions from Mann et al. (2009) (Fig. 53) and Wang et al. (2017) (Fig. 54). This relation between the δ18O records is also observed in the cross wavelet analysis with periodicities of 64 and 256 years observed with statistical significance above 95% in the period of 1300-1700 C.E. Trace elements PCs indicate drier (wetter) conditions during positive (negative) phases of AMO/AMV, where positive correlations with PC1CR-1 are of 0.45, and negative correlations with $PC2_{MFZ\text{-}N\text{-}1}$ of 0.3. These comparisons suggest that negative phases of AMO/AMV are related to a strengthening of SAMS/SACZ activity and to predominantly wetter conditions, with opposite conditions observed during positive phases of AMO/AMV.

Seager et al. (2010) shows through climate models forcing by SSTs that larger amounts of precipitation variability over southeast south America (SESA) are caused by changes in tropical SSTs. Also, the study shows that cold phases of tropical SSTs are related to an increase in rainfall

amount, while opposite conditions are observed for warm phases as the Pampas Dust Bowl drought in 1930 was forced by warm SST anomalies. Seager et al. (2010) posit that tropical Atlantic SST anomalies linked to SESA precipitation are the tropical components of AMO. Comparisons between modern SSTs from the Atlantic Ocean in different latitudes show that SSTs vary in phase in a multidecadal scale thought the Atlantic, reinforcing that the Atlantic Multidecadal Oscillation or Variability is an intrinsic variability mode for most of the Atlantic Ocean (Figure 53 and 54).

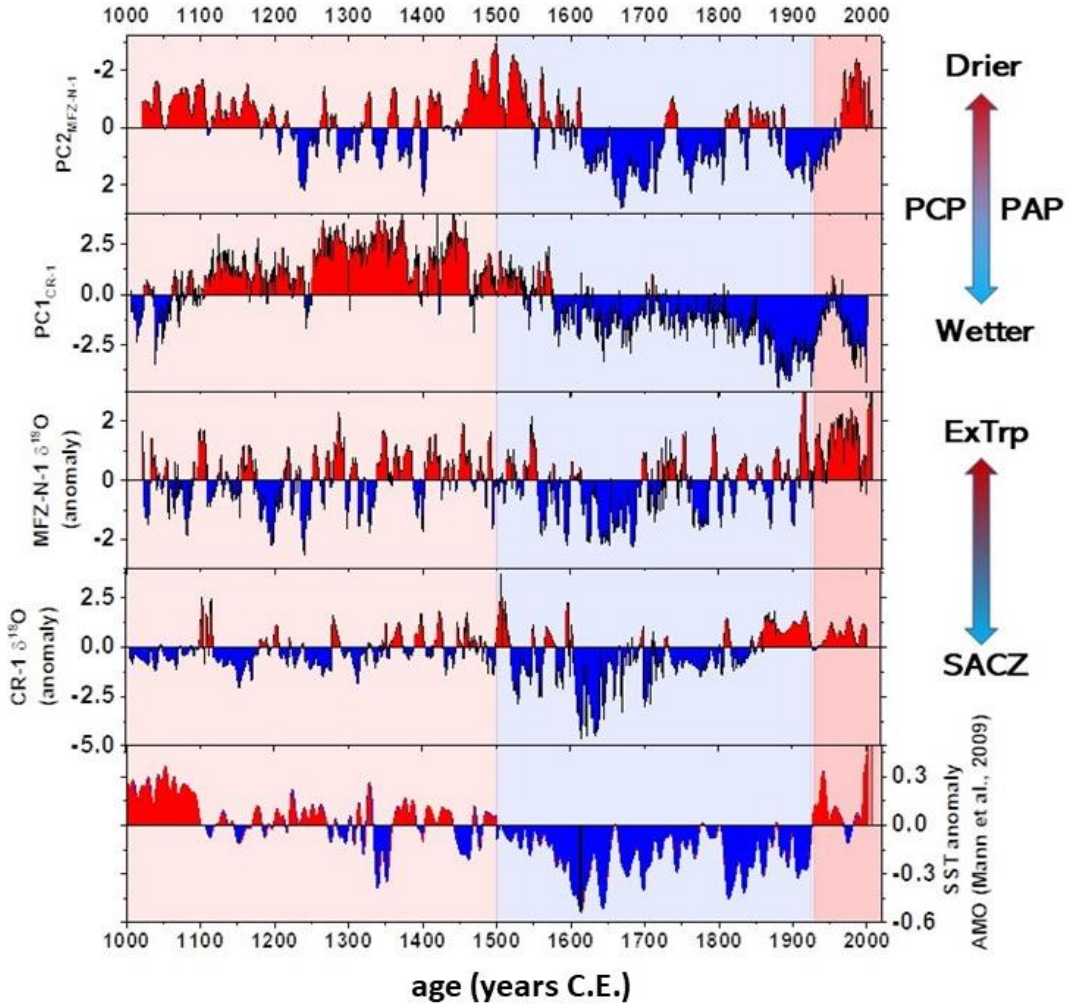

Figure 53 - Comparison between the δ18O records and trace elements PCs with AMO reconstructions from Mann et al. (2009). The light red(blue) boxes represent the positive(negative) phases of AMO.

The relations observed between the speleothems proxies and the AMO/AMV reconstructions may reflect the influence of tropical Atlantic SSTs in the precipitation variability over SESA, with cold (warm) phases related to increase (decrease) in rainfall precipitation over the study area. Comparisons with other $\delta^{18}O$ records showed in section **8.1** indicates that the variations in δ18O may be caused by shifts in SACZ axis position southward (northward) that leads to increase (decrease) of the monsoonal moisture in the study area. The relation between AMO/AMV with the $\delta^{18}O$ of MFZ-N-1 and CR-1 indicates that tropical Atlantic SSTs may play a role in the position of

SACZ axis, with cold (warm) SSTs resulting in a southward (northward) displacement of SACZ axis.

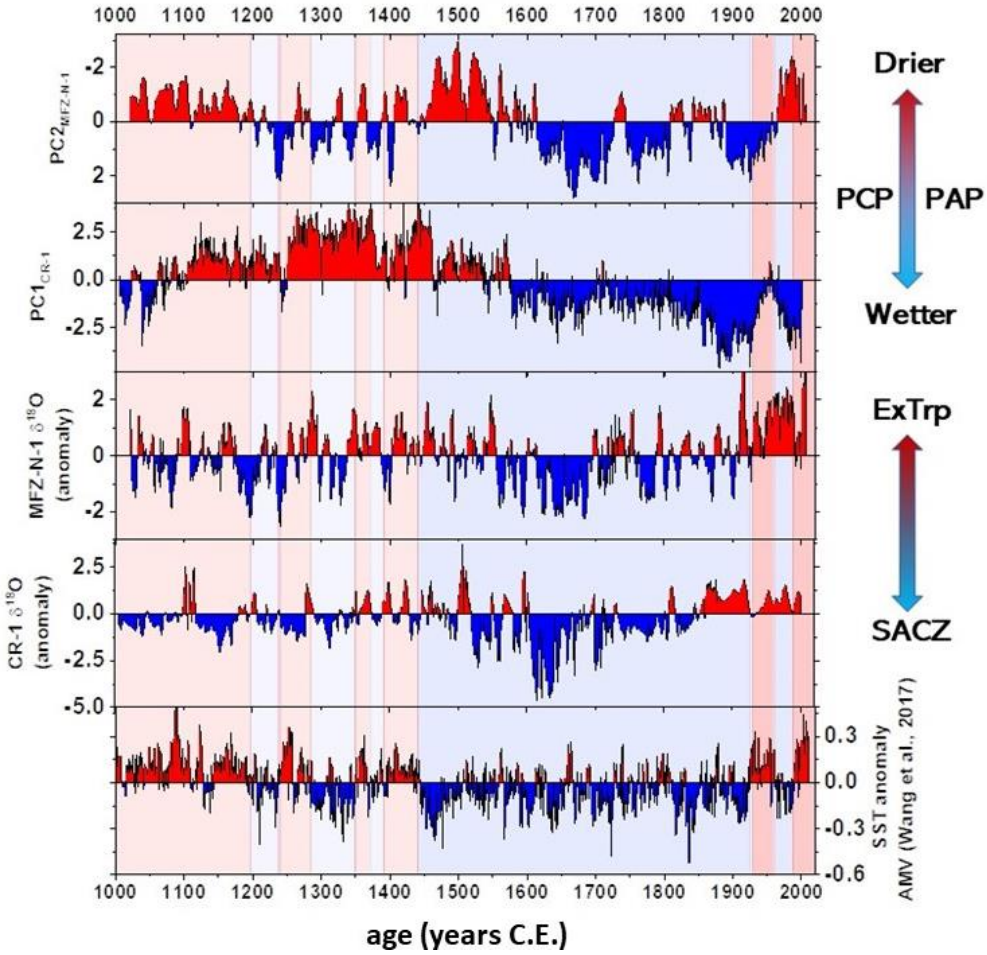

Figure 54 - Comparison between the δ18O records and trace elements PCs with AMV reconstructions from Wang et al. (2017). The light red(blue) boxes represent the positive(negative) phases of AMV.

The Pacific SSTs also play an important role in SESA precipitation variability. The reconstructed index for PDO from Biondi et al. (2001) does not show a clear correspondence with the speleothem's proxies, while the PDO index from Mann et al. (2009) has a correspondence between negative (positive) phases with wetter (drier) conditions evidenced by the trace elements PCs. This PDO index is complicated to use due to its extremely similarity with AMO index from Mann et al. (2009), which gives the comparison a bias in the interpretation of PDO influence in the rainfall variability of the study area. IPO only shows a weak positive correlation of 0.14 with MFZ-N-1 $\delta^{18}O$ record not showing a clear influence over the study region.

ENSO reconstruction based on Conroy et al. (2010) shows a strong positive correlation with $PC2_{MFZ\text{-}N\text{-}1}$ of 0.42 and a negative correlation with $PC1_{CR\text{-}1}$ indicating that El Nino/La Nina phases are related to wetter/drier conditions in the cave sites and positive correlations between CR-1 and

MFZ-N-1 δ18O of 0.37 and 0.15, respectively (Fig. 55). These relations observed agree with previous studies (Silva et al., 2011; Kayano and Andreoli, 2007) that correlate positive ENSO phases with an increase in precipitation over subtropical regions in South America. Positive phases of El Niño results of an intense positive SST anomaly over equatorial Pacific that leads to an increase in the ascending activity in this region and causing a divergence zone over northern Amazon, dislocating the moisture influx into the continent from the Atlantic Ocean towards the SESA region, which agrees with the speleothems proxies from Malfazido and Cristal caves. (Silva et al., 2011). Therefore, ENSO may be an important feature controlling the rainfall variability of the study area, where El Niño (La Niña) conditions are associated with an increase (decrease) in wetter (drier) conditions.

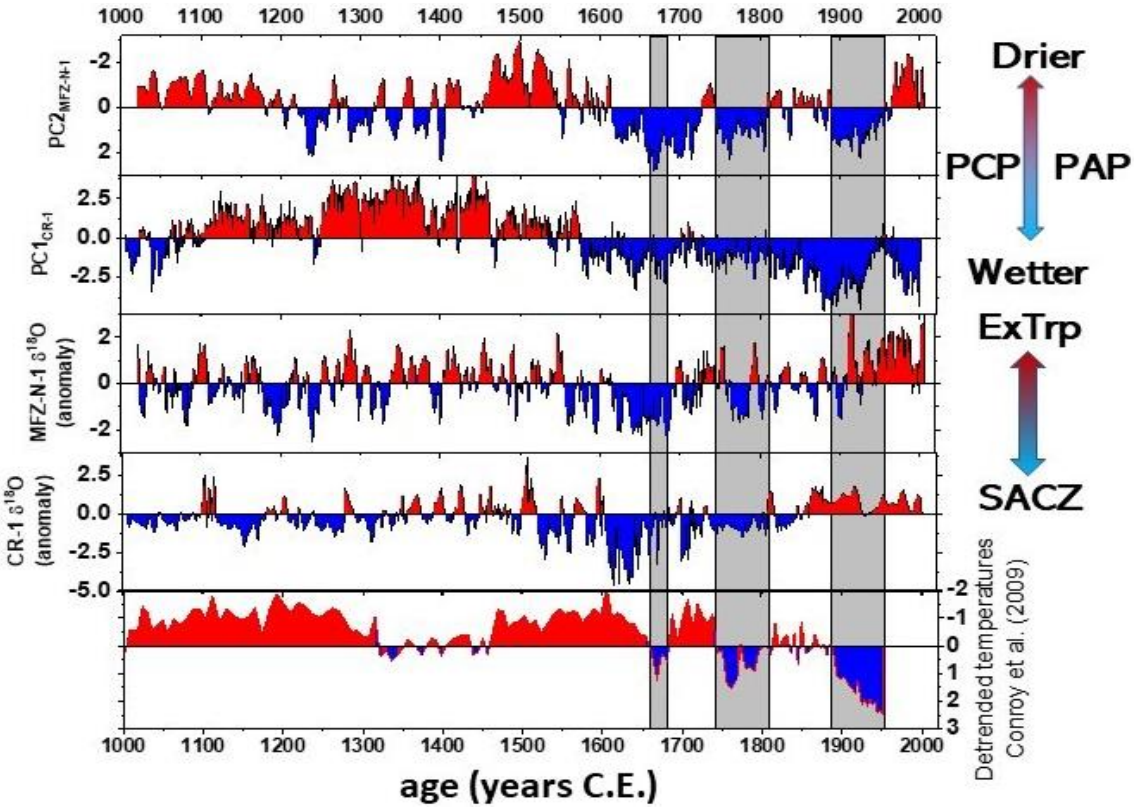

Figure 55 - Comparisons between the speleothem's proxies and Nino index from Conroy et al. (2010). The grey bars indicate positive phases of El Niño

Indo Pacific Warm Pool (IPWP) influence in the precipitation variability has not been widely studied for SESA, especially in a paleo scale. The SST reconstruction of the IPWP from Oppo et al. (2009) shows a high correlation with the trace element PCs with positive correlations of 0.6 with $PC1_{CR-1}$ and negative correlations with $PC2_{MFZ-N-1}$ of 0.33. These relations indicate that periods of negative anomalies of IPWP SSTs (cold SST) coincide with wetter conditions in southeast Brazil

(Fig. 56). Even though a directly relation between the SESA and this feature might not be clear, ENSO conditions are directly related with the SSTs from IPWP. Previous studies show that during El Niño phase over central eastern Pacific, the warm waters (fresh and low-density) from IPWP region moves towards the central equatorial pacific due to wind currents linked to ENSO activity, creating a slight cooling of SSTs (~1°C) in tropical western Pacific (Delcroix and Picaut, 1998; Gagan et al., 2004). Therefore, this relation between positive ENSO phases and negative IPWP SSTs anomalies can account for the correlations observed between the trace elements PCs and IPWP.

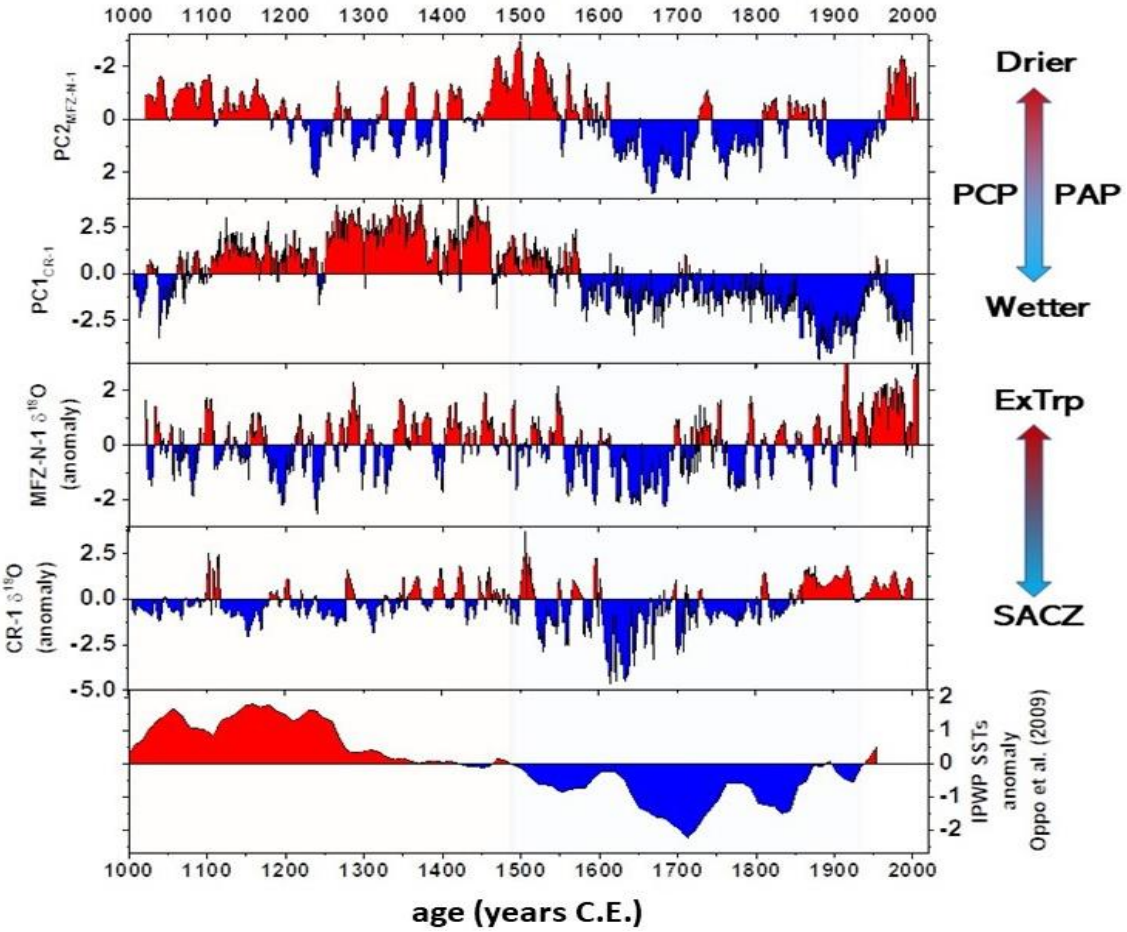

Figure 56 - Comparison between the δ18O records and trace elements PCs with IPWP reconstructions from Oppo et al. (2009). The light red(blue) boxes represent the positive(negative) anomalies of IPWP SSTs.

To summarize, SSTs variations from Atlantic Ocean are important climatic features for the precipitation patterns and intensity due to its influence in SACZ activity and displacement of its main axis over the study region. The Pacific Ocean also presents climatic features that influence the precipitation variability with El Niño/La Niña events as the main link between SSTs variations in the Pacific Ocean and precipitation variability over SESA.

8.3 Last Millennium Extreme Precipitation Frequency Reconstruction Based on a Speleothem Paleoflood Record of Malfazido Cave

Despite numerous works have documented evidence of flooding recorded by detrital layers within speleothems, few studies have developed paleoflood reconstructions in the last years using such samples. Malfazido speleothems have been identified in this study as potential for paleoflood reconstruction, since it is observed detrital layers within speleothems samples collected in the flood zones of Malfazido cave, and even though of the detrital layers commonly bearing detrital thorium (^{232}Th) the high concentration of uranium in this speleothem (1.5 ~ 6 ppm) associated with a simple stratigraphy allowed the acquisition of a well-resolved chronology for the last millennium. The cave context suggest that high travertine pools are flooded during heavy rainfall events as observed during a field work on June 3rd, where 100 mm of rainfall during two days on the previous week to the fieldwork flooded the travertine pools upstream the cave river, where the speleothems were collected. A remarkable feature of this sample is the fastest growth rate documented for the southeast Brazil, which enabled the speleothem to be used as a high-resolution archive of Malfazido cave floods.

The cave flood index reconstructed for Malfazido cave shows in general positive anomalies in decadal frequency associated with negative anomalies of δ^{18}O including the period with high recurrence of cave floods between 1640-1680 C.E (Fig 75). Despite of this relation observed, the most anomalous period of cave flood frequency (1760-1880 C.E.) is marked by a strong positive anomaly in δ^{18}O of CR-1 record and by increase in the variability of δ^{18}O in MFZ-N-1. The periods with predominance of positive anomalous decadal frequency are related to wetter conditions indicated by the trace elements PCs, with the period of 1640-1680 C.E. marked by most positive values of $PC2_{MFZ\text{-}N\text{-}1}$ and the highest frequency period (1760-1880 C.E.) marked by positive anomalies of $PC2_{MFZ\text{-}N\text{-}1}$ and for the most negative anomalies of $PC1_{CR\text{-}1}$ and consequently the wettest conditions recorded by CR-1 for the last millennium (Fig. 57).

These relations between the speleothems proxies (δ^{18}O and trace elements PCs) indicate that the periods with higher recurrence of events are related to enhancement of rainfall, and even though it is commonly related to increase in SAMS activity, the highest recurrence period observed in the last millennium seems to be related to enhanced extratropical cyclogenesis influence over southeast of Brazil.

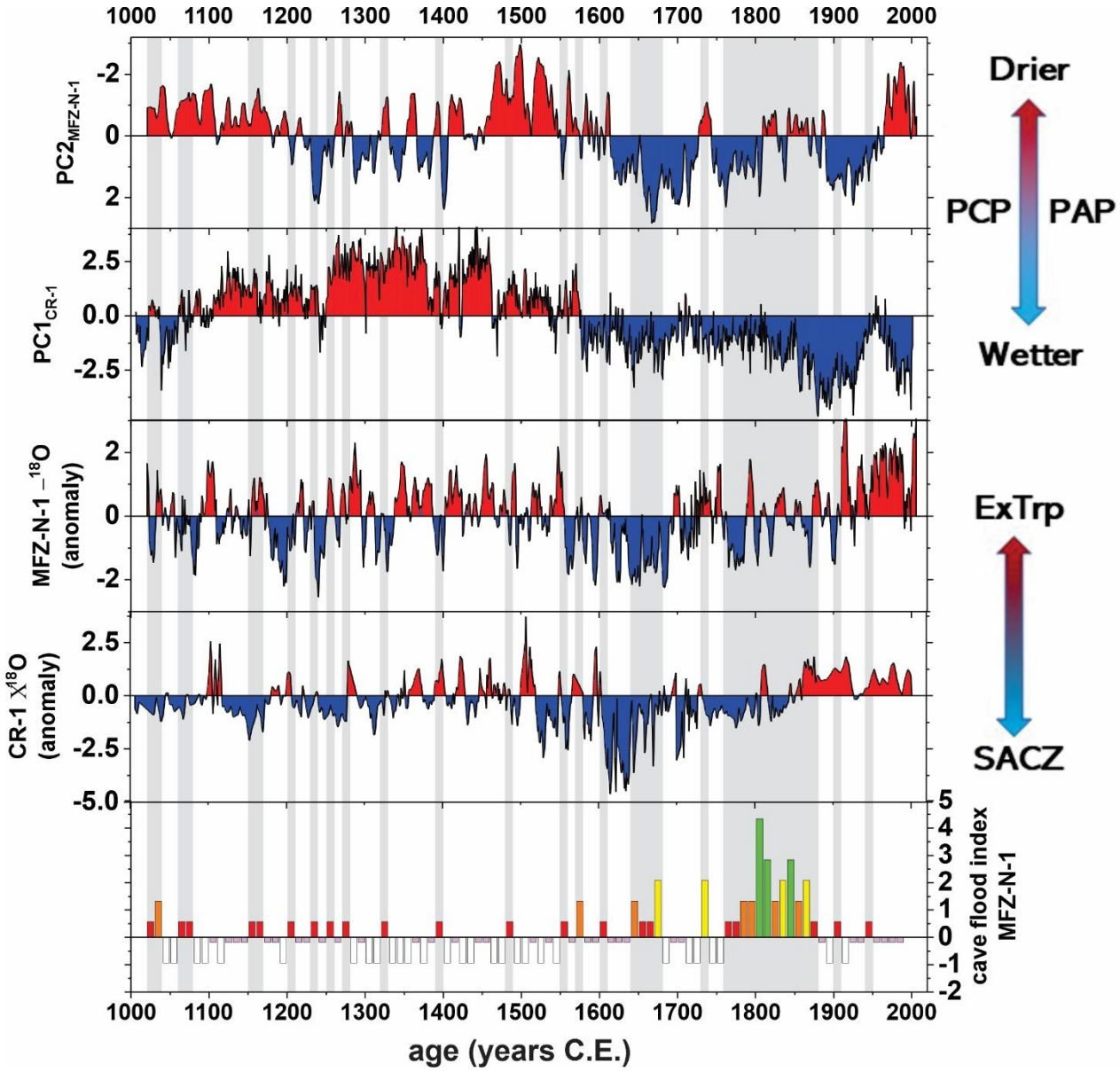

Figure 57 - Comparisons between the speleothems proxies (δ18O and trace elements PCs) with the cave flood index of MFZ-N-1. The grey bars indicate the periods with decadal frequency above the mean.

Extreme precipitation events occurring in Southeast Brazil are strongly related to variations in SSTs from both Atlantic and Pacific Ocean, and AMO and SACZ are recognized as one of the main climate indices affecting the extreme precipitation events (Pedron et al., 2016), and the speleothem dataset of MFZ-N-1 and CR-1 corroborate with these observations (Fig. 57 and 58).

For southern Brazil, the changes in the frequency of extreme rainfall events are generally consistent with changes in the total amount of monthly precipitation, and this pattern is also related to the ENSO phenomenon (Grimm and Tedeschi, 2009). El Niño enhances wet conditions, and the

result confirms the influence of El Niño/La Niña events on the rainfall and extreme events in southern Brazil (Grimm et al., 1998; Grimm et al., 2000).

Negative phases of AMO and negative anomalies in IPWP SST are observed during periods of higher frequency of cave floods events (1550-1680 C.E., 1760-1880 C.E.) and coincides with the most negatives AMO anomalies for the last millennium (Fig. 58). However, a period of cave flood frequency above the average observed during 1150-1280 C.E is associated with the most positive anomalies of IPWP and positive to neutral phases of AMO. ENSO positive anomalies (El Niño conditions) are related to periods of high frequency cave floods during 1640-1680 C.E. and 1750-1800 C.E, but negative ENSO phases are also associated with periods of high frequency of cave floods such as 1150-1280 C.E. and 1550-1640 C.E. Even though the periods with above average cave flood events can be associated with different indices, they occur mostly in the same periods of high volcanic activity.

Albeit the challenge to directly correlate the occurrence of cave flood events to these indices, their combination in phases that are related to extreme precipitation events and to enhancement of rainfall over southeast Brazil seem to be directly related to higher frequency of the cave floods. For instance, periods with positive ENSO (El Niño conditions), negative AMO and IPWP combined with high volcanic activity (1760-1880 C.E.) show the higher frequency of cave flood events observed for the last millennium (Fig. 58).

Knudsen et al. (2014) suggests that external forcing, such as volcanic activity, might be leading the pace of AMO variability, where a higher incidence of volcanic events can contribute to negative AMO conditions, which in turn results in more precipitation over southeast Brazil due to an enhancement of SAMS/SACZ activity. Previous studies also showed relations between volcanic forcing and changes in Pacific SSTs (Rodysill et al., 2013; Adams et al., 2003), where volcanic eruptions might also drive the ocean-atmosphere system towards more El Niño-like conditions. Also, Rodysill et al. (2013) showed that volcanic eruptions can directly decrease the IPWP SSTs, leading to reduced atmospheric convection over western Pacific and thus causing drought in the IPWP region. This mechanism is used to explain a severe multidecadal drought in East Java (IPWP region) in 1810 C.E ± 30 years. This drought event coincides with the period of highest cave flood frequency in Malfazido cave of the last millennium. As discussed in section 8.2, negative phases of IPWP may enhance the moisture influx in the study area by El Niño-like conditions, and so this

coincidence between both extreme events may be related to these climatic features that affect the precipitation in the study area (Fig. 58).

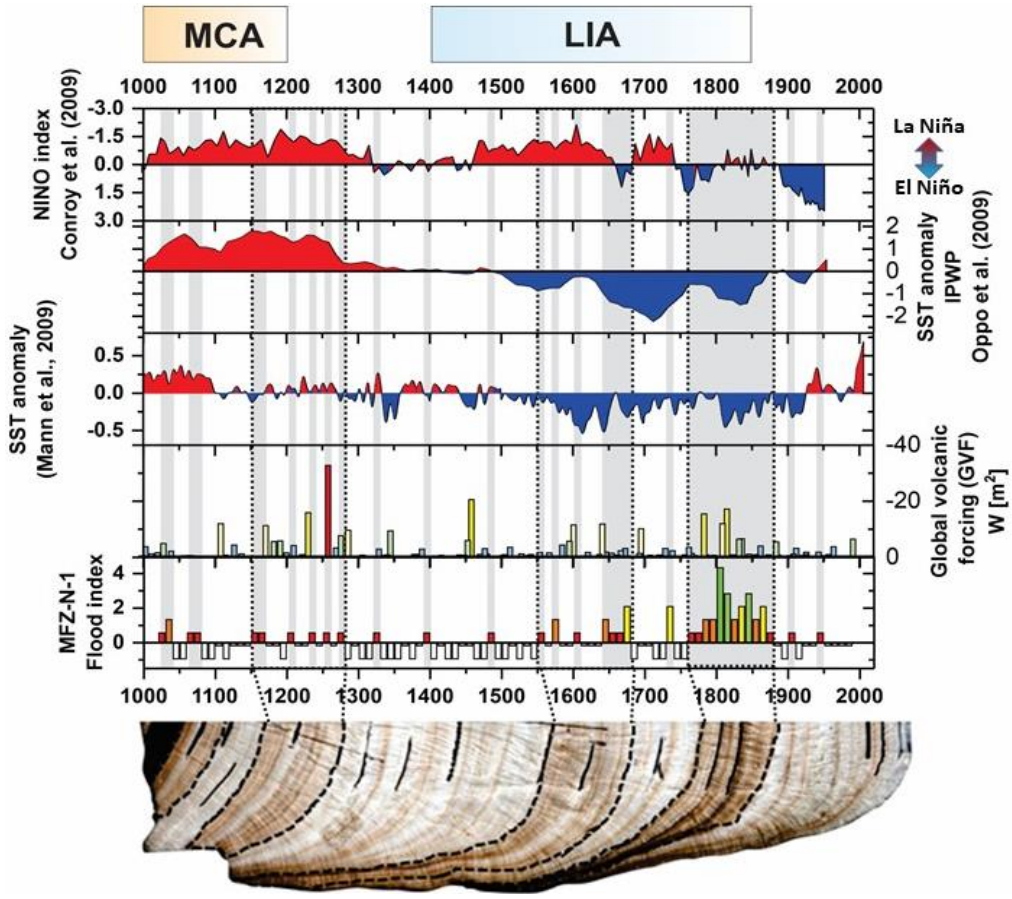

Figure 58 - Comparisons between MFZ-N-1 cave flood index with Global Volcanic Forcing and climatic indices from Atlantic and Pacific Ocean. From top to bottom: Niño 3.0 anomalies from Conroy et al. (2009); IPWP SSTs anomalies from Oppo et al. (2009); AMO reconstruction from Mann et al. (2009); Global Volcanic Forcing (GVF) from Sigl et al. (2015). The grey bars correspond to periods with decadal cave flood frequency above the mean and the pointed line correspond to periods with high recurrency of cave flood events. MFZ-N-1 scan showing the correspondence periods of high frequency of cave flood events marked by high concentration of mud layers within the speleothem.

Variations in SSTs may drive higher frequency of cave floods by enhancement of the SAMS/SACZ activity and by El Niño-like conditions. The volcanic forcing seems to be related to high frequency cave floods periods, thus this external forcing may influence the occurrence of extreme precipitation by its influence on climatic features such as AMO, ENSO and IPWP that are related to the rainfall variability of SESA.

8.4 Late and Middle Holocene Paleoflood Cave Frequency Based on Lage Branca Speleothems and Paleoclimate Reconstructions Based on Speleothem Records from PETAR Site, Southeast Brazil

As discussed in section 8.1, the variability of $\delta^{18}O$ in speleothems from Southeast Brazil is mainly related to a source effect, with monsoonal (extratropical) with depleted (enriched) $\delta^{18}O$ signatures, which indicates that $\delta^{18}O$ records can be used as a suitable proxy for changes in precipitation regimes from tropical-extratropical interactions over South America moisture source (Cruz et al, 2005). Trace elements records from CR-1 show a high correlation with themselves and their linear covariance of trace elements ratios indicates that prior calcite precipitation may control the trace element ratios with Ca. A similar relation is observed for speleothems from Botuvera cave, where Bernal et al. (2016) showed that prior calcite precipitation is controlling the trace elements ratios in the cave, thus Botuvera speleothem record can be used as a suitable proxy for reconstructing hydrological conditions (wetter/drier) above the cave. Bernal et al. (2016) described a high correlation between the trace elements and the $\delta^{18}O$, indicating that atmospheric circulation and SAMS intensity have been closely correlated during the Holocene, and that both are responding to solar precession.

The figure 59 shows the comparison between $\delta^{18}O$ records from PETAR site (LB1, CB-3 and TP-6) and with Botuvera cave speleothem (Btv21a). As discussed above, the $\delta^{18}O$ variations are interpreted as changes in moisture source contributions, and the trace element from BTV21a is interpreted as a hydrological proxy for wetter/drier conditions. A clear difference is observed between the Middle and Late Holocene in all the records, where Middle Holocene shows the most enriched $\delta^{18}O$ values, trace elements show the most positive values, and Late Holocene have the most depleted $\delta^{18}O$ and negative anomalies in trace element records of Btv21a (Fig. 59). Cruz et al. (2005) posit that increase in the influence of SAMS activity in southeast of Brazil is characterized by depleted $\delta^{18}O$ in speleothems, suggesting an enhancement in summer rainfall, but the study also alerts that this interpretation should be handled carefully once speleothem $\delta^{18}O$ cannot detect changes in paleorainfall amount, due to the source effect be the main control of $\delta^{18}O$ variations. However, the high correlations between trace elements ratios with Ca and $\delta^{18}O$ observed for Btv21a in Botuvera cave, and the correlations between $\delta^{18}O$ and trace elements from CR-1, where both share the same modulation, suggest that the $\delta^{18}O$ variations observed in speleothems may be directly related to an enhancement of summer rainfall activity with wetter conditions

observed during the Late Holocene in comparison with the Middle Holocene, with an inflexion point at about 4.2 ky BP, as indicated in other regions in Brazil such as Northeastern Brazil (Utida et al., 2020).

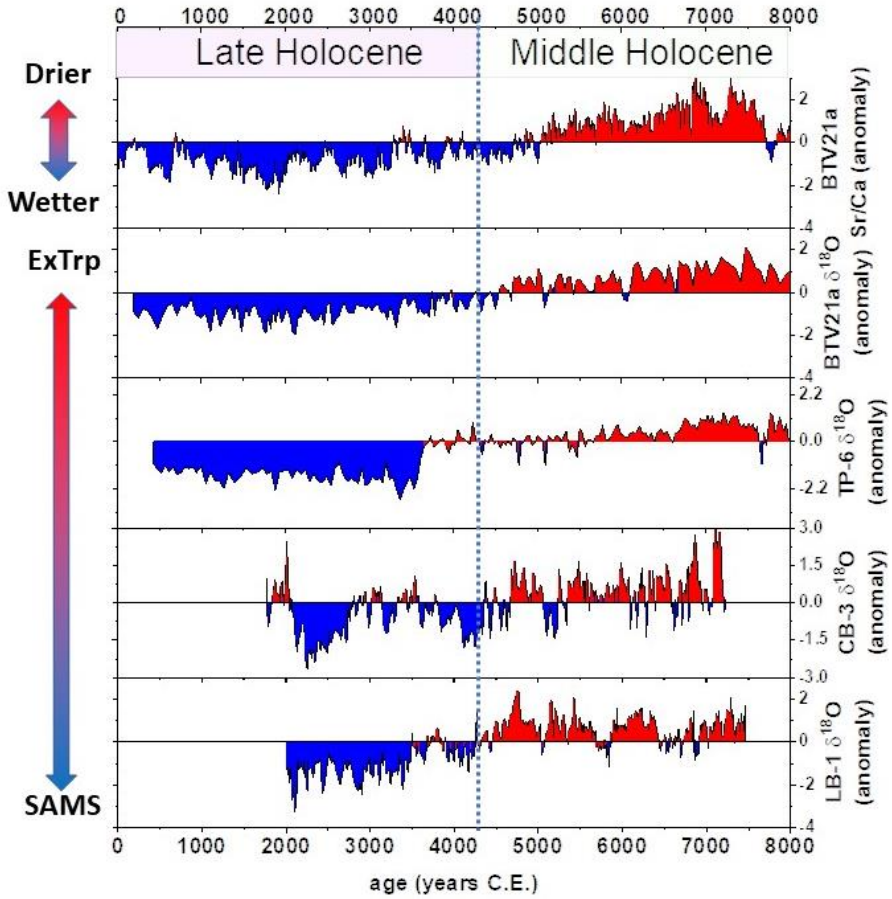

Figure 59 - Comparison between speleothems δ18O records from Southeast of Brazil and trace elements from Botuvera cave. From top to bottom: Btv21a – Sr/Ca anomaly and δ18O from Botuvera cave speleothem (Bernal et al., 2016); TP-6 - δ18O from Tapagem cave in PETAR site; CB-3 and LB-1 - δ18O records from Lage Branca cave.

Lage Branca speleothems present $\delta^{18}O$ records with a decadal resolution that can aid the interpretation for multidecal scale, allowing to assess the multidecadal variability of tropical-extratropical interactions over Southeast of Brazil. Due to the presence of detrital layers within the speleothem, LB-1 and CB-3 present a high potential for the reconstruction of paleocave flood events during Late and Middle Holocene, and the comparison with δ18O and trace elements records from PETAR site allow the assessment of paleoclimate conditions, in which changes in the frequency of paleoflood events in Lage Branca cave may occur. Figure 60 shows a comparison between paleoflood records of Lage Branca speleothems with $\delta^{18}O$ and trace elements from Botuvera cave. The difference between the recurrence of paleo flood events is also clear between the Late and Middle Holocene with an increase in the frequency after the transition between these

periods. These higher frequencies are associated with an enhancement o SAMS activity indicated by a regional negative anomaly of $\delta^{18}O$ in the speleothem's records. The transition between the middle and Late Holocene is marked by a strong negative anomaly of $\delta^{18}O$ in CB-3 record accompanied by an abrupt increase in the cave floods recorded in CB-3 and LB-1, with an abrupt change in the growth axis of CB-3 (related to the presence of thick detrital layers). A second period of increase in cave flood is observed from 2700-2000 C.E. and coincides with the strongest negative anomaly observed in CB-3 and LB-1. These relations suggest that an increase in SAMS activity over the study area may affect the recurrence of cave flood events in Lage Branca cave and that these events may be related to enhancement of summer rainfall in the Southeast of Brazil.

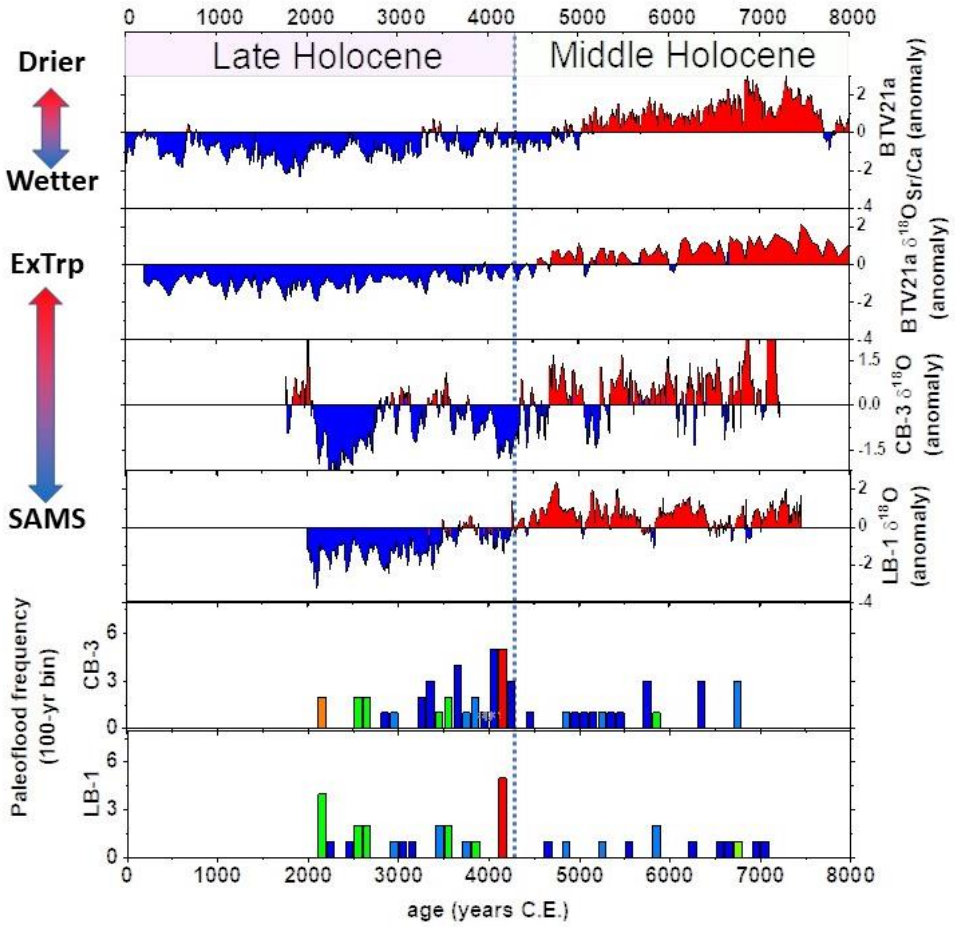

Figure 60 - Comparisons between the paleoflood frequency record of Lage Branca (CB-3 and LB-1) with δ18O and trace element records. From top to bottom: Btv21a – Sr/Ca anomaly and δ18O from Botuvera cave speleothem (Bernal et al., 2016); CB-3 and LB-1 - δ18O records from Lage Branca cave; paleoflood frequency record from Lage Branca speleothems.

The Late Holocene shows a trend towards negative values of δ18O anomalies from 4000-2000 B.P., and this trend is also observed for the PC1CR-1 that indicates wetter conditions in Cristal Cave site agreeing with the observed for Botuvera Cave with an increase in SAMS activity

leading to an enhancement of wetter conditions probably due to increase in the summer rainfall. The speleothems from Lage Branca stop to growth close to 2000 B.P. coinciding with the most depleted values of $\delta^{18}O$ in all the records and a strong negative anomaly in PC1CR-1. The hiatus in the speleothems is marked by a thick detrital layers, and the negative anomalies of $\delta^{18}O$ and trace elements indicate that the speleothems may have stopped to grow during the wetter conditions observed in Lage Branca cave site between the period of 2000 B.P. to 7200 B.P. This condition may increase the frequency of cave floods until the point that speleothems with slow growth rates such as CB-3 and LB-1 might have its deposition suppressed by constant exposition to flooded conditions.

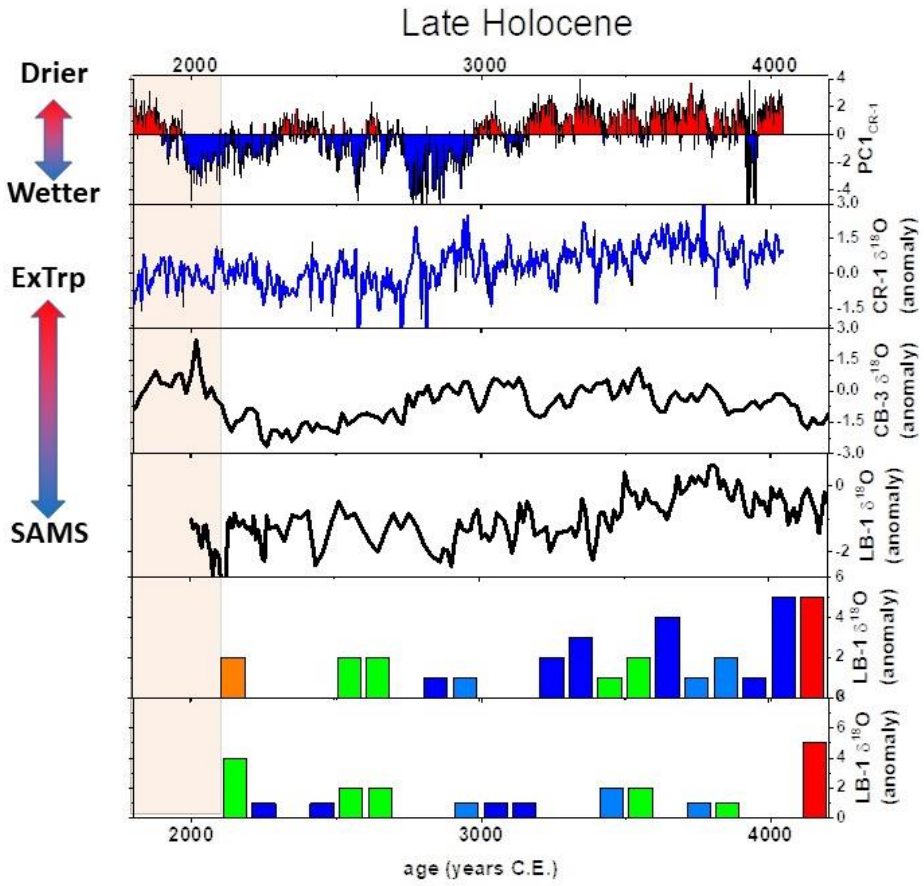

Figure 61 - Comparisons between the paleoflood frequency record of Lage Branca (CB-3 and LB-1) with δ18O and trace element records. From top to bottom: δ18O and PC1CR-1 of trace elements from Cristal cave; CB-3 and LB-1 - δ18O records from Lage Branca cave; paleoflood frequency record from Lage Branca speleothems.

9 CONCLUSIONS

The high-resolution paleoclimate reconstruction based on stable isotopes and trace elements from speleothems collected at Malfazido and Cristal cave sites contributed to the understanding of

the tropical-extratropical interactions and the paleoprecipitation variability during the last millennium in Southeastern and Southern Brazil.

The statistical analysis of the speleothem data revealed the main periodicities in the geochemistry data that suggest the most likely association between precipitation variability and the atmospheric circulation in the study area to SSTs anomalies in the Atlantic and Pacific Oceans. The correlation and covariance between speleothem's trace elements allowed to relate the variations in concentrations to prior-calcite precipitation for Cristal cave speleothem and prior-aragonite precipitation for Malfazido speleothem. Therefore, it is possible to conclude that changes in concentrations of trace element ratios over Ca are associated with variations in levels of recharge into the karstic aquifer, as such conditions lead to an influence in the volume of carbonate precipitated in the unsaturated zone above the cave, and so are mainly related to rainfall recharge over the cave site. These relationships confirm that these trace elements records may be used as hydrological proxies for wetter or drier conditions due to increase or decrease in the precipitation over the study area.

The comparison with paleoclimate indices help the understanding of the impact of climate changes on the occurrence of extreme events in the study area. Cave flood reconstructions based on high resolutions speleothem geochemical record from Malfazido cave produced in this study are used to assess the periods with higher recurrence of extreme precipitation events in Paraná State, as well as the changes in frequency of severe food events. The comparison between cave flood frequency and climate modes that operates on decadal to multi-decadal time scales suggest that SSTs from both Atlantic and Pacific Ocean may play a role in the increase of frequency of those events during periods of SSTs anomalies associated with the enhancement of SAMS activity over SESA or to El Niño-conditions. The high frequency of extreme floods is also correlated to periods with high volcanic activity during the Little Ice Age Period, and a possible link between this internal forcing is attested.

Therefore, the novel high-resolution records of Malfazido cave and Cristal cave contribute in an unprecedented manner to understand the frequency of extreme precipitation events related to cave floods, and in which atmospheric-circulation and hydrological conditions that these changes in frequency are observed. Relationship with SSTs and external forcing discussed here contribute to the understanding of how climate changes and consequently changes in SSTs from Atlantic and Pacific Ocean can impact the recurrence of extreme events over eastern Paraná.

New stable isotopes records with decadal resolution of Middle and Late Holocene were reconstructed using Lage Branca speleothems from PETAR site. This speleothems samples are also used as paleoflood cave records based on the presence of detrital layers within the speleothems. Even though the speleothems were collected in galleries at different heights and sensitivity to to be flooded, a consistent occurrence of these floods events proxy is observed between the samples especially for thick layers, showing that paleoflood events shows a good replicability between speleothems. The speleothem mud layers records showed an increase in the cave flood frequency from Middle to Late Holocene. These differences between the number of flood events per time periods are in agreement with the more negative δ18O values observed in the same speleothem records that indicate an enhancement of SAMS activity over Southeast Brazil during the last 4 ky B.P. Trace elements from Botuvera cave and Cristal cave showed that enhancement in the SAMS activity may be relate to increase in the summer rainfall indicated by wetter conditions in both cave sites. This paleoclimate scenario indicates that the frequency of paleoflood in Lage Branca cave may be directly affected by enhancement of SAMS activity and to increase in summer rainfall. A hiatus observed in both speleothems in 2000 B.P. characterized by a thick detrital layer may indicate the period when the frequency of floods suppressed the speleothems growth in the lowers galleries by frequent exposition to flooded conditions.

In summary, Lage Branca speleothems are present as novel paleoflood cave records covering the period between 2000 and 7200 B.P. This is an unprecedent record for all Southeast of Brazil and may help to understand of how low frequency cave flood can be affected by changes in the atmospheric circulation and in the summer rainfall.

10 REFERENCES

Abdi, H., Williams, L.J., 2010, Principal component analysis: Wires Computational Statistics, v. 2, p. 433-459, doi.org/10.1002/wics.101.

Adams, J.B., Mann, M.E., Ammann, C.M., 2003, Proxy evidence for an El Niño-like response to volcanic forcing: Nature, v. 426, p. 274-278, doi.org/10.1038/nature02101.

Alexander, M. A., Halimeda Kilbourne, K., & Nye, J. A. , 2014, Climate variability during warm and cold phases of the Atlantic Multidecadal Oscillation (AMO) 1871-2008: Journal of Marine Systems, v. 133, p. 14–26, doi.org/10.1016/j.jmarsys.2013.07.017

Amaya, D.J., 2019, The Pacific Meridional Mode and ENSO: a Review : Current Climate Changes Reports, v. 5, p. 296-307, doi.org/10.1007/s40641-019-00142-x.

Ampuero, A., et al., 2019, The Forest Effects on the Isotopic Composition of Rainfall in the Northwestern Amazon Basin: Journal of Geophysical Research: Atmospheres, v. 125, issue 4, doi.org/10.1029/2019JD031445.

Atkison, T.C., 1977, Carbon dioxide in the atmosphere of the unsaturated zone: An important control of groundwater hardness in limestones: Journal of Hydrology, v. 35, p. 111-113, doi.org/10.1016/0022-1694(77)90080-4.

Baldini, J.U.L., McDermott, F., Fairchild, I.J., 2002, Structure of the 8200 year cold event revealed by a speleothem trace element record: Science, v. 296, p. 2203-2206, doi: 10.1126/science.1071776.

Amundson, R., Stern, L., Baisden, T., Wang, Y., 1998, The isotopic composition of soil and soil-respired CO2: Geoderma, v. 82, p. 83-114, doi.org/10.1016/S0016-7061(97)00098-0.

Bernal, J. P., Cruz, F. W., Stríkis, N. M., Wang, X., Deininger, M., Catunda, M. C. A., Auler, A. S., 2016, High-resolution Holocene South American monsoon history recorded by a speleothem from Botuvera Cave, Brazil: Earth and Planetary Science Letters, v. 450, p.186–196, doi.org/10.1016/j.epsl.2016.06.008.

Biondi, F., Gershunov, A., Cayan, D.R., 2001, North Pacific Decadal Climate Variability since 1661: Journal of Climate, v. 14, p. 5-10, doi.org/10.1175/1520-0442(2001)014<0005:NPDCVS>2.0.CO;2.

Buckley, B.M., Ummenhofer, C.C., D'Arrigo, R.D., Hansen, K.G., Truong, L.H., Le, C.N., Stahle, D.K., 2019, Interdecadal Pacific Oscillation reconstructed from trans-Pacific tree rings: 1350–2004 CE: Climate Dynamics, v. 53, p. 3181–3196, doi.org/10.1007/s00382-019-04694-4.

Carvalho, L. M. V., Jones, C., & Liebmann, B. ,2002, Extreme precipitation events in southeastern South America and large-scale convective patterns in the South Atlantic covergence zone: Journal of Climate, v. 15, p. 2377–2394. doi.org/10.1175/1520-0442(2002)015<2377:EPEISS>2.0.CO;2.

Campos, J.L.P.S., Cruz, F.W., Ambrizzi, T., Deininger, M., Vuille, M., Novello, V.F., Strikis, N.M., 2019, Coherent South American Monsoon Variability During the Last Millennium Revealed Through High-Resolution Proxy Records: Geophysical Research Letters, v. 46, p. 8261-8270, doi.org/10.1029/2019GL082513.

Clark, I. D., Fritz, P., 1997, Environmental Isotopes in Hydrogeology, CRC Press, 328 p.

Conroy, J.L., Overpeck, J.T., Cole, J.E., El Niño/Southern Oscillation and changes in the zonal gradient of tropical Pacific sea surface temperature over the last 1.2 ka: Science Highlights: Open Science, v. 18, p. 32-34.

Cruz, F.W.; Burns, S.J., Karmann, I., Sharp, W.D., Vuille, M., Cardoso, A.O., Ferrari, J.A., Silva Dias, P.L., Viana, O. Jr., 2005a, Insolation-driven changes in atmospheric circulation over the

past 116 ky in subtropical Brazil: Nature, v. 434, p. 63-66, doi: 10.1038/nature03365.

Cruz, F.W., Karmann, I., Viana Jr. O., Burns, S. J., Ferrari, J. A., Vuille, M., Sial, A. N., Moreira, M.Z., 2005b, Stable isotope study of cave percolation waters in subtropical Brazil: Implications for paleoclimate inferences from speleothems: Chemical Geology, v. 220, p. 245-262, doi.org/10.1016/j.chemgeo.2005.04.001.

Cruz, F.W., Burns, S.T., Jercinovic, M., Karmann, I., Sharp, W.D., Vuille, M., 2007, Evidence of rainfall variations in Southern Brazil from trace element ratios (Mg/Ca and Sr/Ca) in a Late Pleistocene stalagmite: Geochimica et Cosmochimica Acta, v. 71, no. 9, p. 2250-2263, doi.org/10.1016/j.gca.2007.02.005

Dansgaard, W., 1964, Stable isotopes in precipitation: Tellus, v. 16, p. 436-468, doi.org/10.3402/tellusa.v16i4.8993.

Dasgupta, S., Saar, M. O., Edwards, R. L., Shen, C. C., Cheng, H., & Alexander, E. C. ,2010, Three thousand years of extreme rainfall events recorded in stalagmites from Spring Valley Caverns, Minnesota: Earth and Planetary Science Letters, v. 300, p. 46–54. doi.org/10.1016/j.epsl.2010.09.032

Debortoli, N. S., Camarinha, P. I. M., Marengo, J. A., & Rodrigues, R. R. , 2017, An index of Brazil's vulnerability to expected increases in natural flash flooding and landslide disasters in the context of climate change: Natural Hazards, v. 86, 557–582, doi.org/10.1007/s11069-016-2705-2.

Delcroix, T., Picaut, J., 1998, Zonal displacement of the western equatorial Pacific "fresh pool": Journal of Geophysical Research, v. 103, p. 1087-1098, doi.org/10.1029/97JC01912.

Denniston, R. F., & Luetscher, M., 2017, Speleothems as high-resolution paleoflood archives: Quaternary Science Reviews, v. 170, p. 1–13, doi.org/10.1016/j.quascirev.2017.05.006

Denniston, R. F., Villarini, G., Gonzales, A. N., Wyrwoll, K. H., Polyak, V. J., Ummenhofer, C. C., Cugley, J.,2015, Extreme rainfall activity in the Australian tropics reflects changes in the El Niño/Southern Oscillation over the last two millennia: Proceedings of the National Academy of Sciences of the United States of America, v. 112, p. 4576–4581. doi.org/10.1073/pnas.1422270112.

Desmarchelier, J.M., Malcolm, J.C., McCulloch, M.T., 2006, Rapid trace element analysis of speleothems by ELA-ICP-MS: Chemical Geology, v. 231, p. 102-117, doi.org/10.1016/j.chemgeo.2006.01.002.

Dorale, J. A., Lepley, S., & Edward, R. L. , 2005, The ultimate flood recorder: flood-deposited sediments preserved in stalagmites: EGU General Assembly 2005, v. 7, p.5–6.

Dreybrodt, W., 2008, Evolution of the isotopic composition of carbon and oxygen in a calcite precipitating H2O–CO2–CaCO3 solution and the related isotopic composition of calcite in

stalagmites: Geochimica et Cosmochimica Acta, v. 72, no. 19, p. 4712-4724, doi.org/10.1016/j.gca.2008.07.022.

Edwards, R.L., Chen, J.H., Wasserburh, G.J., 1986, 238U - 234U - 230Th - 232Th systemtics and the precise measurement of time over the past 500.000 years: Earth Planetary Science Letters, v. 81, p. 175-192, doi.org/10.1016/0012-821X(87)90154-3.

Fairchild, I. J.; Baker, A., 2012, Speleothem Science – From Process to Past Environments, Wiley-Brackwell, 416 p.

Fairchild, I.J., Borsato, A., Tooth, A.F., Frisia, S., Hawkeswirth, C.J., Huang, Y., McDermot, F., Spiro, B., 2000, Controls on trace element (Sr–Mg) compositions of carbonate cave waters: implications for speleothem climatic records: Chemical Geology, v. 166, p. 255-269, doi.org/10.1016/S0009-2541(99)00216-8.

Fairchild, I.J., McMillan, E.A., 2007, Speleothems as indicators of wet and dry periods: International Journal of Speleology, v. 36, p. 69-74, doi.org/10.5038/1827-806X.36.2.2.

Fairchild, I. J., Smith, C.l., Baker, A., Fuller, L., Spötl, C., Mattey, D., McDermott, F., E.I.M.F., 2006, Modification and preservation of environmental signals in speleothems: Earth-Science Reviews, v. 75, p. 105-153, doi.org/10.1016/j.earscirev.2005.08.003.

Fairchild, I.J., Treble, P.C., 2009, Trace elements in speleothems as recorders of environmental change: Quaternary Science Reviews, v. 28, p. 449-468, doi.org/10.1016/j.quascirev.2008.11.007.

Feinberg, J. M., Lascu, I., Lima, E. A., Weiss, B. P., Dorale, J. A., Alexander, E. C., & Edwards, R. L. , 2020, Magnetic detection of paleoflood layers in stalagmites and implications for historical land use changes: Earth and Planetary Science Letters, v. 530, doi.org/10.1016/j.epsl.2019.115946

Finné, M., Kylander, M., Boyd, M., Sundqvist, H. S., & Löwemark, L. , 2015, Can XRF scanning of speleothems be used as a non-destructive method to identify paleoflood events in caves? : International Journal of Speleology, v. 44, p. 17–23, doi.org/10.5038/1827-806X.44.1.2

Fohlmeister, J., Voarintsoa, N.R.G., Lechleitner, F.A., Boyd, M., Brandstätter, S., Jacobson, M.J., Oster, J.L., 2020, Main controls on the stable carbon isotope composition of speleothems: Geochimica et Cosmochimica Acta, v. 279, p. 67-87, doi.org/10.1016/j.gca.2020.03.042.

Folland, C. K., Colman, A. W., Rowell, D. P., Davey, M. K., 2001, Predictability of northeast Brazil rainfall and real-time forecast skill, 1987–1998: Journal of Climate, v. 14, p. 1937–1958, doi.org/10.1175/1520-0442(2001)014<1937:PONBRA>2.0.CO;2.

Folland, C., Palmer, T. & Parker, D., 1986, Sahel rainfall and worldwide sea temperatures, 1901–85: Nature, v. 320, p. 602–607, doi.org/10.1038/320602a0

Ford, D., Williams, P., 2007, Karst Hydrogeology and Geomorphology: Sussex, John Wiley & Sons, 562 p.

Frappier, A. B., Pyburn, J., Pinkey-Drobnis, A. D., Wang, X., Corbett, D. R., & Dahlin, B. H. , 2014, Two millennia of tropical cyclone-induced mud layers in a northern Yucatán stalagmite: Multiple overlapping climatic hazards during the Maya Terminal Classic "megadroughts." : Geophysical Research Letters, v. 41, p. 5148–5157, doi.org/10.1002/2014GL059882.

Gagan, M.K., Hendy, E.J., Haberle, S.G., Hantoro, W.S., 2004, evolution of the Indo-Pacific Warm Pool and El Niño-Southern oscillation: Quaternary International, v. 118-119, p. 127-143, doi:10.1016/S1040-6182(03)00134-4.

Grinsted, A., Moore, J. C., Jevrejeva, S., 2004, Application of the cross wavelet transform and wavelet coherence to geophysical time series: Nonlinear Processes in Geophysics, European Geosciences Union (EGU), v. 11, p. 561-566.

Gázquez, F., Calaforra, J. M., Forti, P., Stoll, H., Ghaleb, B., & Delgado-Huertas, A. ,2014, Paleoflood events recorded by speleothems in caves: Earth Surface Processes and Landforms, v. 39, p. 1345–1353, doi.org/10.1002/esp.3543.

Ghil, M., Allen, M. R., Dettinger, M. D., Ide, K., Kondrashov, D., Mann, M. E., Yiou, P. , 2002, Advanced spectral methods for climatic time series: Reviews of Geophysics, v. 40, p. 3-1-3–41. https://doi.org/10.1029/2000RG000092.

González-Lemos, S., Jiménez-Sánchez, M., & Stoll, H. M. , 2014, Sediment transport during recent cave flooding events and characterization of speleothem archives of past flooding: Geomorphology, v. 228, p. 87–100, doi.org/10.1016/j.geomorph.2014.08.029

González-Lemos, S., Müller, W., Pisonero, J., Cheng, H., Edwards, R. L., & Stoll, H. M. , 2015, Holocene flood frequency reconstruction from speleothems in northern Spain: Quaternary Science Reviews, v. 127, p. 129–140, doi.org/10.1016/j.quascirev.2015.06.002

Goldenberg, S.B., Landsea, W.C., Mestas-Nuñez, A.M., Gray, W.M., 2001, The recent increase in Atlantic Hurricane Activity: Causes and Implications: Science, v. 293, p. 474-479, doi:10.1126/science.1060040.

Grimm, A.M., Barros, V.R., Doyle, M.E., 2000, Climate Variability in Southern South America Associated with El Niño and La Niña Events: Journal of Climate, v. 13, p. 35-58, doi.org/10.1175/1520-0442(2000)013<0035:CVISSA>2.0.CO;2.

Grimm, A.M., Ferraz, S.E.T., Gomes, J., 1998, Precipitation Anomalies in Southern Brazil Associated with El Niño and La Niña Events: Journal of Climate, v. 11, p. 2863–2880, doi.org/10.1175/1520-0442(1998)011<2863:PAISBA>2.0.CO;2.

Grimm, A. M., & Tedeschi, R. G. ,2009, ENSO and extreme rainfall events in South America.: Journal of Climate, v. 22, p. 1589–1609, doi.org/10.1175/2008JCLI2429.1.

Hammer, Ø. ,2019,. Manual Past 3.25. Manual, 1999.

Hammer, Ø., Harper, D. A. T., & Ryan, P. D. , 2001, PAST : Paleontological Statistics Software Package for Education and Data Analysis : Palaeontologia Electronica,v. 4, p. 1–9.

Hanley, D. E., Bourassa, M. A., O'Brien, J. J., Smith, S. R., & Spade, E. R. , 2003, A quantitative evaluation of ENSO indices: Journal of Climate, v. 16, p, 1249–1258. doi.org/10.1175/1520-0442(2003)16<1249:AQEOEI>2.0.CO,2.

Huang, Y., Fairchild, I.J., 2001, Partitioning of Sr2+ and Mg2+ into calcite in karst-analogue experimental solutions: Geochimica et Cosmochimica Acta, v. 65, p. 47-62, doi.org/10.1016/S0016-7037(00)00513-5.

Hurrell, J. W., Kushnir, Y., Ottersen, G., Visbeck, M., 2003, An Overview of the North Atlantic Oscillation. Geophysical Monograph, v. 134.

Jamieson, R.A., Baldini, J.U.L., Frappier, A.B., Müller, W., 2015, Volcanic ash fall events identified using principal component analysis of a high-resolution speleothem trace element dataset: Earth and Planetary Science Letters, v. 426, p. 36-45, doi.org/10.1016/j.epsl.2015.06.014.

Johnson, K.R., Hu, C., Belshaw, N.S., Henderson, G.M., 2006, Seasonal trace-element and stable-isotope variations in a Chinese speleothem: the potential for high-resolution paleomonsoon reconstruction: Earth Planetary Science Letters, v. 244, p. 394-407, doi.org/10.1016/j.epsl.2006.01.064.

Karmann, I., 1994, Evolução e dinâmica atual do sistema cárstico do alto vale do rio Ribeira de Iguape, sudeste do Estado de São Paulo. [Tese de Doutorado]: São Paulo, Universidade de São Paulo, Instituto de Geociências.

Karmann, I., Cruz, F.W., Viana, O., Burns, S., Climate influence on geochemistry parameters of waters from Santana–Pérolas cave system, Brazil: Chemical Gelogy, v. 244, p. 232-247, doi:10.1016/j.chemgeo.2007.06.029.

Kayano, M. T. & Andreoli, R.V., 2007, Relations of South American summer rainfall interannual variations with the Pacific Decadal Oscillation: International Journal of Climatology, v. 27, p. 531-540, doi.org/10.1002/joc.1417.

Kayano, M. T. & Andreoli, R.V., 2006, Relationships between rainfall anomalies over northeastern Brazil and the El Niño–Southern Oscillation: Journal of Geophysical Research, v. 111, D13 , doi.org/10.1029/2005JD006142.

Kayano, M. T., & Capistrano, V. B. , 2014, How the Atlantic multidecadal oscillation (AMO) modifies the ENSO influence on the South American rainfall: International Journal of Climatology, v. 34, p. 162–178, doi.org/10.1002/joc.3674

Kerr, R. A., 2000, A North Atlantic climate pacemaker for the centuries. Science, v. 288, p. 1984–1985.

Knight, J. R., Folland, C. K., ScaifE, A. A., 2006, Climate impacts of the Atlantic Multidecadal Oscillation. Geophysical research letters, v. 33, L17706, doi:10.1029/2006GL026242.

Knudsen, M. F., Seidenkrantz, M. S., Jacobsen, B. H., & Kuijpers, A., 2011, Tracking the Atlantic Multidecadal Oscillation through the last 8,000 years: Nature Communications, v. 2 doi.org/10.1038/ncomms1186.

Lachniet, M., 2009, Climatic and environmental controls on speleothem oxygen-isotope values: Quaternary Science Reviews, v. 28, p. 412-432, doi.org/10.1016/j.quascirev.2008.10.021.

Lauritzen, S-E., Lundberg, J., 1999, Speleothems and climate: a special issue of The Holocene: The Holocene, v. 9, p. 643–647, doi.org/10.1191/095968399666229065.

Li, H.-C., Ku, T.-L., You, C.-F., Cheng, H., Edwards, R.L., MA, Z.-B., Tsai, W.-S., LI, M.-D., 2005, 87Sr/86Sr and Sr/Ca in speleothems for paleoclimate reconstruction in Central China between 70 and 280 kyr ago: Geochimica et Cosmochimica Acta, v. 69, p. 3933-3947, doi.org/10.1016/j.gca.2005.01.009.

Liebmann, B., Jones, C., & de Carvalho, L. M. V. , 2001, Interannual variability of daily extreme precipitation events in the state of Saõ Paulo, Brazil: Journal of Climate, v. 14, p. 208–218. doi.org/10.1175/1520-0442(2001)014<0208:IVODEP>2.0.CO,2

Lima, K. C., Satyamurty, P., & Fernández, J. P. R. , 2010, Large-scale atmospheric conditions associated with heavy rainfall episodes in Southeast Brazil: Theoretical and Applied Climatology, v. 101, p. 121–135, doi.org/10.1007/s00704-009-0207-9.

Locosselli, G.M., Brienen, R., De Souza Martins, V.T., Gloor, E., Boom, A., De Souza, E.P., Saldiva, P.H.N., Buckeridge, M.S., 2020, Intra-annual oxygen isotopes in the tree rings record precipitation extremes and water reservoir levels in the Metropolitan Area of São Paulo, Brazil: Science Of The Total Environment, v. 743, p. 140798, doi.org/10.1016/j.scitotenv.2020.140798.

Mann, M. E., Zhang, Z., Rutherford, S., Bradley, R. S., Hughes, M. K., Shindell, D., Ni, F. , 2009, Global signatures and dynamical origins of the little ice age and medieval climate anomaly: Science, v. 326, p. 1256–1260, doi.org/10.1126/science.1177303

Martineau, P., Nakamura, H., Kosaka, Y., Yamamoto, A., 2020, Importance of a vertically tilting structure for energizing the North Atlantic Oscillation: Scientific Reports, v. 10, article number 12617, doi.org/10.1038/s41598-020-69551-5.

MacDonald, G.M., Case, R.A., 2005, Variations in the Pacific Decadal Oscillation over the past millennium: Geophysical Research Letters, v. 32, article number 08703, doi:10.1029/2005GL022478.

McDermott, F., 2004, Palaeo-climate reconstruction from stable isotope variations in speleothems: a review: Quaternary Science Reviews, v. 23, no. 7-8, p. 901-918, doi.org/10.1016/j.quascirev.2003.06.021.

McMillan, E., I.J. Fairchild, Frisia, S., Borsato, A., McDermott, F., 2005, Annual trace element cycles in calcite-aragonite speleothems: evidence of drought in the western Mediterranean 1200–1100 yr BP: Journal of Quaternary Science, v. 20, p. 423-433, doi.org/10.1002/jqs.943.

Morse, J.W., Bender, M.L., 1990, Partition coefficients in calcite: Examination of factors influencing the validity of experimental results and their application to natural systems: Chemical Geology, v. 82, 265-277

Musgrove, M., Banner, J., 2004, Controls on the spatial and temporal variability of vadose dripwater geochemistry: Edwards Aquifer, central Texas: Geochimica et Cosmochimica Acta, v. 68, p. 1007-1020, doi.org/10.1016/j.gca.2003.08.014.

Novello, V.F. et al., 2019, Vegetation and environmental changes in tropical South America from the last glacial to the Holocene documented by multiple cave sediment proxies: Earth and Planetary Science Letters, v. 524, p. 115717, doi.org/10.1016/j.epsl.2019.115717.

Novello, V.F. et al., 2016, Centennial-scale solar forcing of the South American Monsoon System recorded in stalagmites: Scientific Reports, v. 6, issue 24762, doi:10.1038/srep24762.

Novello, V.F. et al., 2018, Two Millennia of South Atlantic Convergence Zone Variability Reconstructed From Isotopic Proxies: Geophysical Research Letters, v. 45, p. 5045-5051.

Pedron, I. T., Silva Dias, M. A. F., de Paula Dias, S., Carvalho, L. M. V., & Freitas, E. D. , 2017, Trends and variability in extremes of precipitation in Curitiba – Southern Brazil: International Journal of Climatology, v. 37, p. 1250–1264, doi.org/10.1002/joc.4773

Pessenda, L. C. R.; Goubeia, S. E. M.; Ribeiro, A. S.; Oliveira, P. E.; Aravena, R., 2010, Late Pleistocene and Holocene vegetation changes in northeastern Brazil determined from carbon isotopes and charcoal records in soils: Paleogeography, Palaeoclimatology, Paleoecology, v. 297, p. 597-608, doi.org/10.1016/j.palaeo.2010.09.008.

Richards, D. A., & Dorale, J. A. , 2003, Uranium-series chronology and environmental applications of speleothems:Uranium-Series Geochemistry, v. 52, p. 407–460, doi.org/10.2113/0520407.

Rodysill, J.,R., Russel, J.M., Crausbay, S.D., Bijaksana, S., Vuille, M., Edwards, R.L., Cheng, H., 2013, A severe drought during the last millennium in East Java, Indonesia: Quaternary Science Reviews, v. 80, p. 102-111, doi.org/10.1016/j.quascirev.2013.09.005.

Seager, R., Naik, N., Baethgen, W., Robertson, A., Kushnir, Y., Nakamura, J., Jurburg, S., 2010, Tropical oceanic causes of interannual to multidecadal precipitation variability in southeast South America over the past century: Journal of Climate, v. 23, p. 5517–5539, doi.org/10.1175/2010JCLI3578.1.

Schulz, M., & Mudelsee, M. ,2018, REDFIT : Estimating red-noise spectra directly from unevenly spaced paleoclimatic time series: Computers & Geosciences, v. 28, p. 421-426, doi.org/10.1016/S0098-3004(01)00044-9.

Shen, C. C., Lawrence Edwards, R., Cheng, H., Dorale, J. A., Thomas, R. B., Bradley Moran, S. Edmonds, H. N. , 2002, Uranium and thorium isotopic and concentration measurements by magnetic sector inductively coupled plasma mass spectrometry: Chemical Geology, v. 185, p. 165–178, doi.org/10.1016/S0009-2541(01)00404-1.

Silva, G.A.M., Drumond, A., Ambrizzi, T., 2011, The impact of El Niño on South American summer climate during different phases of the Pacific Decadal Oscillation: Theoretical and Applied Climatololy, v. 106, p. 307–319, doi.org/10.1007/s00704-011-0427-7.

Silva, L.C.R., S Ternberg, L., Haridasan, M., Hoffmann, W.A., Miralles-Wilhelm, F., F Ranco, A.C., 2008, Expansion of gallery forests into central Brazilian savannas: Global Change Biology, v. 14, p. 2108-2118, doi: 10.1111/j.1365-2486.2008.01637.x.

Sinclair, D. J. , 2011, Two mathematical models of Mg and Sr partitioning into solution during incongruent calcite dissolution. Implications for dripwater and speleothem studies: Chemical Geology, v. 283, p. 119–133, doi.org/10.1016/j.chemgeo.2010.05.022.

Sinclair, D.J., Banner, J.L., Taylor, F.W., Partin, J., Jenson, J., Mylroie, J., Goddard, E., Quinn, T., Jocson, J., Miklavic, B., 2012, Magnesium and strontium systematics in tropical speleothems from the Western Pacific: Chemical Geology, v. 294-295, p. 1-17, doi.org/10.1016/j.chemgeo.2011.10.008.

Souza, P., Cavalvanti, I. F. A., 2009, Atmospheric centers of action associated with the Atlantic ITCZ position. Royal Meteorological Society, v. 29, p. 2091-2105.

Taylor, B. L., 2014, A Speleothem-based- high resolution reconstruction of climate in Southern Brazil over the past 4,100 years [Tese de Doutorado], Amherst, University of Massachusetts Amherst, 108 p.

Timmermann, A., Okumura, Y., An, S. I., Clement, A., Dong, B., Guilyardi, E., Yin, J. , 2007, The influence of a weakening of the Atlantic meridional overturning circulation on ENSO: Journal of Climate, v. 20, p. 4899–4919, doi.org/10.1175/JCLI4283.1.

Tooth, A.F., Fairchild, I.J., 2003, Soil and karst aquifer hydrological controls on the geochemical evolution of speleothem-forming drip waters, Crag Cave, southwest Ireland: Journal of Hydrology, v. 273, p. 51-68, doi.org/10.1016/S0022-1694(02)00349-9.

Torrence, C., Compo, G. P., 1998, A practical guide to Wavelet Analysis: Bulletin of the American Meteorological Society, v. 29, no. 1, p. 61-78.

Treble, P. Shelley, J.M.G., Chappell, J., 2003, Comparison of high resolution sub-annual records of trace elements in a modern (1911–1992) speleothem with instrumental climate data from

southwest Australia: Earth and Planetary Science Letters, v. 216, no. 1-2, p. 141-153, doi.org/10.1016/S0012-821X(03)00504-1.

Trouet, V., Esper, J., Graham, N.E., Baker, A., Scourse, J.D., Frank, D.C., 2009, Persistent Positive North Atlantic Oscillation Mode Dominated the Medieval Climate Anomaly: Science, v. 324, p. 78-80, doi: 10.1126/science.1166349.

Utida, G., et al., 2020, Climate changes in Northeastern Brazil from deglacial to Meghalayan periods and related environmental impacts: Quaternary Science Reviews, v. 250, p. 106655, doi.org/10.1016/j.quascirev.2020.106655.

Vasconcellos, F. C., & Cavalcanti, I. F. A., 2010, Extreme precipitation over Southeastern Brazil in the austral summer and relations with the Southern Hemisphere annular mode: Atmospheric Science Letters, v. 11, p.21–26, doi.org/10.1002/asl.247.

Verheyden, S., Keppens, E., Fairchild, I.J., McDermott, F., Weis, D., 2000, Mg, Sr and Sr isotope geochemistry of a Belgian Holocene speleothem: implications for paleoclimate reconstructions: Chemical Geology, v. 169, p. 131-144, 10.1016/S0009-2541(00)00299-0.

Vuille M., Burns S. J., Taylor, B. L., Cruz, F. W., Bird, B.W., Abbott, M. B., Kanner, L.C., Cheng H., V.F. Novello., 2012, A review of the South American monsoon history as recorded in stable isotopic proxies over the past two millennia: Climate Of The Past Discussions, v. 8, p. 637-668, doi:10.5194/cpd-8-637-2012.

Vuille, M., Werner, M., Stable isotopes in precipitation recording South American summer monsoon and ENSO variability: observations and model results: Climate Dynamics, v. 25, p. 401-413, doi 10.1007/s00382-005-0049-9.

Wang, R., and H. Ren, 2020, Understanding Key Roles of Two ENSO Modes in Spatiotemporal Diversity of ENSO: Journal of Climate, v. 33, p. 6453–6469, doi.org/10.1175/JCLI-D-19-0770.1.

Wang, J., Yang, B., Ljungqvist, C., Luterbacher, J., Osborn, T. J., Briffa, K. R., Zorita, E., 2017, Internal and external forcing of multidecadal Atlantic climate variability over the past 1,200 years. Nature geoscience, v. 10, p. 512-518.

Wang, W., S. Saha, H. Pan, S. Nadiga, and G. White, 2005, Simulation of ENSO in the New NCEP Coupled Forecast System Model (CFS03): Monthly Weather Review, v. 133, p. 1574-1593, doi.org/10.1175/MWR2936.1.

Wassenburg, J.A., et al., 2019, Calcite Mg and Sr partition coefficients in cave environments: Implications for interpreting prior calcite precipitation in speleothems: Geochimica et Cosmochimica Acta, v. 269, p. 581–596, doi.org/10.1016/j.gca.2019.11.011.

Wassenburg, J.A., et al., 2016, Determination of aragonite trace element distribution coefficients from speleothem calcite–aragonite transitions: Geochimica et Cosmochimica Acta, v. 190,p.

347-367, doi.org/10.1016/j.gca.2016.06.036.

Wei, W., & Lohmann, G. ,2012, Simulated Atlantic multidecadal oscillation during the Holocene: Journal of Climate, v. 25, p. 6989–7002, doi.org/10.1175/JCLI-D-11-00667.1.

Wilhelm, B., Ballesteros Cánovas, J. A., Macdonald, N., Toonen, W. H. J., Baker, V., Barriendos, M., … Wetter, O. , 2019, Interpreting historical, botanical, and geological evidence to aid preparations for future floods: Wiley Interdisciplinary Reviews: Water, v. 6, doi.org/10.1002/wat2.1318.

Zhang, R., Delworth, T. L., 2005, Simulated tropical response to a substantial weakening of the Atlantic thermohaline circulation: J. Clim., v. 18, p. 1853-1860, doi:10.1175/JCLI3460.1.

Zhang, W., Li, S., Jin, F., Xie, R., Liu, C., Stuecker, M. F., Xue, A., 2019, ENSO Regime Changes Responsible for Decadal Phase Relationship Variations Between ENSO Sea Surface Temperature and Warm Water Volume: Geophysical Research Letters, v. 46, p. 7546-7553, doi.org/10.1029/2019GL082943.

UNIVERSIDADE DE SÃO PAULO
INSTITUTO DE GEOCIÊNCIAS

Paleoclimate reconstruction based on high-resolution multiproxy geochemistry of speleothems from Paraná and São Paulo states, Brazil

JULIO CAUHY RODRIGUES

Orientador: Prof. Dr. Francisco William da Cruz Júnior

Dissertação de Mestrado

Nº 864

COMISSÃO JULGADORA

Dr. Francisco William da Cruz Júnior

Dr. Juan Pablo Bernal Uruchurtu

Dra. Marília Harumi Shimizu

SÃO PAULO
2020